UNIVERSIDADE FEDERAL DO RIO DE JANEIRO

Fernanda Freire Tovar Moll

NEUROPLASTICIDADE NA DISGENESIA DO CORPO CALOSO: IMAGEM DO TENSOR DE DIFUSÃO POR RESSONÂNCIA MAGNÉTICA

Rio de Janeiro
2007

Fernanda Freire Tovar Moll

NEUROPLASTICIDADE NA DISGENESIA DO CORPO CALOSO: IMAGEM DO TENSOR DE DIFUSÃO POR RESSONÂNCIA MAGNÉTICA

Tese de Doutorado apresentada ao Programa de Pós-Graduação em Ciências Morfológicas, Instituto de Ciências Biomédicas, Universidade Federal do Rio de Janeiro, como parte dos requisitos necessários à obtenção do título de Doutor em Ciências Morfológicas

Orientador: Professor Roberto Lent

Rio de Janeiro
2007

Tovar-Moll, Fernanda Freire
Neuroplasticidade na agenesia do corpo caloso: imagem do tensor de difusão por ressonância magnética / Fernanda Freire Tovar Moll. Rio de Janeiro, 2007.
xv, 106f. : il.;

Tese (doutorado) -
Universidade Federal do Rio de Janeiro, Instituto de Ciências Biomédicas, 2007.

Orientador: Roberto Lent

1. Corpo caloso / anormalidades. 2. Imagem por ressoância magnética. 3. Plasticidade neuronal – Tese. I. Lent, Roberto (Orient.). II. Universidade Federal do Rio de Janeiro. Instituto de Ciências Biomédicas. Pós-graduação em Ciências Morfológicas III. Título.

CDD: 658.4

Fernanda Freire Tovar Moll

NEUROPLASTICIDADE NA DISGENESIA DO CORPO CALOSO:
IMAGEM DO TENSOR DE DIFUSÃO POR RESSONÂNCIA MAGNÉTICA

Rio de Janeiro, _____ de _____ de 2_____.

_____
(Professor Roberto Lent, UFRJ)

_____
(Professora Ana Martinez, UFRJ)

_____
(Professor Emerson L. Gasparetto, UFRJ)

_____
(Professor Jorge Marcondes, UFRJ)

AGRADECIMENTOS

Muitas pessoas, de forma direta ou indireta, contribuíram para a realização deste trabalho. Para cada uma, o meu imenso carinho. Muito obrigada.

Agradeço antes de tudo, aos meus pais Ana e Ricardo, exemplos de dedicação e profissionalismo. Incentivadores, espelhos e alicerces de toda a minha formação pessoal e profissional.

Ao meu orientador e amigo professor Roberto Lent, exemplar cientista, por guiar meus passos neta tese e, mais ainda, por ter me feito acreditar e mergulhar neste trabalho.

Aos queridos professores e pesquisadores Vivaldo Moura Neto e José Garcia Abreu Júnior, por suas orientações científicas ao longo dos seis anos do curso de medicina e dos dois anos de mestrado. Responsáveis pelo meu início e permanência no horizonte da ciência básica e relacionada à clínica.

Aos meus sogros Jorge e Alice Moll, por terem possibilitado a realização deste trabalho no Labs e por me estimularem e apoiarem sempre com muito carinho, tanto na carreira radiológica, como científica.

Aos meus amigos Ricardo de Oliveira Souza e Ivanei Bramati pela fundamental participação e crucial contribuição neste trabalho.

Aos doutores Leonardo Azevedo e Elaine Gerk por permitirem o acesso aos pacientes do Hospital Fernandes Figueira, Fiocruz.

À doutora Maria Beatriz Gonzaga pelo carinho e suporte com os pacientes.

Aos amigos doutores Pedro Ângelo e Ricardo Pinheiro (Tche), pelo exemplo profissional, de conhecimento e carinho.

Aos colegas médicos, técnicos e auxiliares da Rede Labs – D'Or, por todo apoio.

À amiga Débora Oliveira Lima, pela inestimável ajuda e dedicação.

Aos amigos e colegas do Laboratório de Neuroplasticidade, e em especial à professora Daniela Uziel, pelas trocas de idéias e ajuda durante a tese.

Aos pacientes e seus familiares pela disponibilidade e dedicação.

Aos colegas e amigos do NIH, em especial aos doutores Henry McFarland e Kristina Simonyan.

Aos meus irmãos Paula e Ricardo e aos meus avós, pelo apoio e paciência com que me aturaram nos momento mais estressantes.

Aos queridos amigos e parentes, não aqui mencionados um a um, mas importantes e que sempre me deram força, suporte e carinho.

Ao meu amigo e admirado marido, Gito (Jorge Moll), exemplo de vida, pesquisador, homem e pai, por tudo que me tem apoiado, estimulado e proporcionado durante estes dez anos de convivência e, principalmente, por ter feito estes meus anos muito mais felizes.

Aos meus amadíssimos filhotes Francisco e Eduardo, por terem preenchido minha vida e por compreenderem e apoiarem, ainda que do jeitinho deles, minhas ausências e minha jornada profissional.

RESUMO

A disgenesia do corpo caloso (DCC) é observada em várias patologias cerebrais do desenvolvimento. Entretanto, ainda que diversos estudos realizados em animais tenham contribuído para o entendimento desta patologia, os mecanismos subjacentes envolvidos na DCC ainda são obscuros. Neste estudo, aplicamos imagem do tensor de difusão e fascigrafia para investigar a presença e as características de circuitos anômalos nestes pacientes. Nossos principais achados foram: (1) nos casos de disgenesia parcial do corpo caloso (CC) (com remanescente caloso) ou de hipoplasia do CC, as fibras calosas conectam, em sua maioria, as regiões neocorticais esperadas; (2) o remanescente caloso e o CC hipoplásico possuem arranjo topográfico de fibras semelhante ao CC normal; (3) ao menos dois feixes anômalos robustos formam identificados nos pacientes com DCC: o conhecido feixe de Probst (FP) e um feixe ainda não descrito que denominamos feixe sigmóide; (4) enquanto o FP é topograficamente organizado com fibras dispostas em U e de conexão ipslateral, o feixe sigmóide é um feixe comissural assimétrico e heterotópico, que conecta região pré-frontal com o córtex occipito-parietal contralateral. Estes resultados sugerem que, frente a situações de impedimento de cruzamento da linha média durante o desenvolvimento do cérebro humano, algumas propriedades das fibras calosas são mantidas (como a organização topográfica) enquanto outras são dramaticamente alteradas, levando à formação de feixes aberrantes da substância branca.

ABSTRACT

Callosal dysgenesis (CD) is observed in many neurodevelopmental conditions, but its subjacent mechanisms are unknown, despite extensive research on animals. Here we employ magnetic resonance diffusion tensor imaging and tractography in human CD, to reveal the aberrant circuitry of these brains. We searched particularly for evidence of plasticity. Four main findings are described: (1) in presence of a callosal remnant or of a hypoplastic corpus callosum (CC), fibers therein largely connect the expected neocortical regions; (2) callosal remnants and hypoplastic CCs display a fiber topography similar to normal; (3) at least two long abnormal tracts are formed in patients with defective CC: the well-known Probst bundle (PB), and a so far unknown sigmoid, asymmetrical aberrant bundle connecting the frontal lobe with the contralateral occipito-parietal cortex; (4) while the PB is topographically organized and has an ipsilateral U-connectivity, the sigmoid bundle is a long, heterotopic commissural tract. These observations suggest that when the developing human brain is confronted with factors that hamper CC fibers to cross the midline, some properties of the miswired fibers are maintained (such as side-by-side topography), while others are dramatically changed, leading to the formation of grossly abnormal white matter tracts.

LISTA DE ILUSTRAÇÕES

LISTA DE ABREVIAÇÕES

AVC	Acidente Vascular Cerebral
BPF	“Brain Parenchimal Fraction”
CA	Comissura Anterior
CC	Corpo Caloso
CDA	Coeficiente de Difusão Aparente
CI	Cápsula Interna
D	Tensor de Difusão
DCC	Disgenesia do Corpo Caloso
DTI	Imagem do Tensor de Difusão (“Diffusion Tensor Imaging”)
EDSS	“Expanded Disability Status Scale”
EEG	Eletro Encefalograma
EM	Esclerose Múltipla
FA	Anisotropia Fracional
FACT	“Fiber Assignment by Continuous Tracking”
FP	Feixe de Probst
GIG	Glia do Indusium Grisium
GMZ	Glia Mediana de Zíper
IPD	Imagem Ponderada em Difusão
MD	Difusibilidade Média
NIH	Institutos Nacionais de Saúde (“National Institutes of Health”)
PASAT	“Paced Auditory Serial Addition Task”

RM	Ressonância Magnética
RMf	Ressonância Magnética Funcional
ROI	Região de Interesse
SB	Substância Branca
SC	Substância Cinzenta
SE	Spin-eco
SNC	Sistema Nervoso Central
TBSS	“Tract-based Spatial Statistics”
TIH	Transferência Interna Hemisférica
ΔT	Intervalo de Tempo

SUMÁRIO

1. INTRODUÇÃO

A reorganização do sistema nervoso central em resposta a condições adversas é conhecida desde invertebrados a humanos, podendo variar em complexidade, tanto a nível micro como macroscópico (ELBERT et al., 2002; NORDEEN e NORDEEN, 2004; BLITZ et al., 2004). Evidências clínico-patológicas sugerem que cérebros imaturos possuem maior capacidade de reorganização em comparação aos cérebros adultos (BENARSCONI et al., 2000; VILLABLANCA e HOVDA, 2000). Este fenômeno foi denominado “efeito Kennard” em homenagem à pesquisadora que originalmente o descreveu (KENNARD, 1934; FINGER e WOLF, 1988).

Um dos modelos mais bem-sucedidos e explorados para o estudo da neuroplasticidade em diversas espécies animais diz respeito a observações e manipulações experimentais do corpo caloso (CC) em diferentes estágios de formação e desenvolvimento pré e pós-natal. Nosso estudo representa uma vertente desta vasta linha de pesquisa, centrada, mais particularmente, na neuroplasticidade do CC e de estruturas e feixes a ele relacionados, como revelado por imagens anatômicas obtidas do cérebro humano *in vivo*, tanto normal como doente.

Diversos mecanismos moleculares e celulares estão envolvidos na formação e no desenvolvimento do CC. A possibilidade de comprometimento destes mecanismos em diferentes graus, aliada à capacidade peculiar de cada cérebro em reagir e se adaptar a condições adversas pode explicar, em parte, a diversidade de alterações anatômicas do CC: agenesia (ausência do CC), disgenesia parcial (persistência de um pequeno remanescente do CC), ou hipoplasia (redução moderada do CC). Supõe-se

que essa diversidade anátomo-patológica explicaria as diversas apresentações clínicas (LASSONDE et al., 2003) dos pacientes com disgenesias[1] do CC (DCC). Tais pacientes podem ser assintomáticos, apresentar sintomas de leve retardo mental, crises convulsivas ou pequenas alterações motoras, ou apresentar deficiências mentais e somáticas graves. Desta forma, a investigação de pacientes com DCC representa oportunidade única para investigação da neuroplasticidade humana.

Ainda que a DCC tenha sido extensamente investigada em modelos animais, os mecanismos subjacentes às alterações do CC humano ainda são pouco compreendidos. A maioria dos estudos se baseou em descrições anatômicas *post-mortem* de pequenos grupos de pacientes e, mais recentemente, em investigações *in vivo* por métodos de imagem, como tomografia computadorizada e ressonância magnética (RM) convencional (MEYER et al., 1998a; KUKER et al., 2003).

Sinais de plasticidade em pacientes com DCC foram primeiramente descritos por Probst (PROBST, 1901 *apud* LEE, 2004), que caracterizou o feixe longitudinal que hoje leva seu nome (“feixe de Probst”, FP), como produto da reorganização de axônios comissurais calosos que falharam em cruzar a linha média. Os FP foram reproduzidos e explorados em modelos animais (LENT, 1982; 1983; OZAKI et al., 1987; OZAKI e SHIMADA, 1988; OZAKI et al., 1989), entretanto sua capacidade funcional e topografia exata permanecem indeterminadas.

Mais recentemente, técnicas avançadas de neuroimagem vieram a permitir a delimitação e reconstrução mais precisa dos principais feixes de substância branca (SB)

[1] Utilizaremos o termo genérico *disgenesia* do corpo caloso (DCC) para englobar todas as alterações congênitas que repercutem sobre a forma do CC.

em humanos *in vivo* (MORI et al., 1999). Tais técnicas foram aplicadas com sucesso no estudo da anatomia do CC normal e de pacientes com DCC (LEE et al., 2004), e mais recentemente também de animais acalosos (REN et al., 2007).

1.1 FORMULAÇÃO DA TESE

Na presente Tese, utilizamos uma nova técnica de ressonância magnética (RM) denominada “Imagem do Tensor de Difusão” (*diffusion tensor imaging*, DTI) e “fascigrafia” por RM (SHRAGER e BASSER, 1998; BASSER et al., 2000) para investigação das características anatômicas de pacientes com DCC. A técnica de DTI se baseia na mensuração da difusibilidade direcional das moléculas de água no tecido cerebral, resultante do movimento browniano. Devido à propriedade dos axônios em dificultar a difusibilidade da água transversalmente e favorecer a movimentação ao longo do seu eixo maior, a movimentação das moléculas nos feixes de SB é marcadamente direcional (ou *anisotrópica*), ocorrendo predominantemente no sentido das fibras. Utilizando medidas de anisotropia da difusão das moléculas da água, métodos de computação gráfica podem reconstruir a trajetória de conjuntos de fibras axonais. Este desdobramento da técnica chama-se Fascigrafia (do inglês *“tractography”*), e representa o primeiro método capaz de rastrear as fibras da SB no cérebro humano *in vivo* (BASSER et al., 1994). Tais foram os métodos utilizados neste trabalho para caracterizar os principais feixes de SB e investigar possíveis circuitos aberrantes em humanos com DCC.

Resumindo, o objetivo da presente Tese foi buscar evidências de neuroplasticidade de grandes vias no sistema nervoso central, investigando a

organização estrutural da SB em pacientes com diferentes tipos de DCC. Focalizamos os seguintes aspectos: (I) presença, trajetória e conectividade dos FP; (II) circuitos aberrantes até então não descritos nestes pacientes; (III) trajetória e conectividade de fibras calosas remanescentes em pacientes com DCC parcial; (IV) características topográficas internas dos feixes investigados.

1.2 SÍNTESE DA TESE

A estrutura desta Tese pode ser resumida da seguinte forma:

No **capítulo 2,** fazemos uma revisão da literatura sobre estrutura, desenvolvimento e formação do CC, enfatizando aspectos da anatomia da maior comissura cerebral, presente apenas em mamíferos placentários, e mencionando as teorias sobre fatores envolvidos na sua gênese e desenvolvimento.

No **capítulo 3,** introduzimos o leitor às malformações do CC. Classificamos os tipos de disgenesias do CC em humanos, síndromes neurológicas associadas, diversidades de apresentação clínica e possíveis candidatos a fatores causais. Comentamos como as alterações disgenéticas do CC podem ter efeitos à distância, levando a modificações da forma e da estrutura do cérebro como um todo. As evidências de reorganização da estrutura cerebral nas DCC em modelos animais e em humanos constituem o substrato fundamental para a formulação da presente Tese.

No **capítulo 4,** relatamos o método utilizado para a investigação das questões desta Tese. Nos subitens deste capítulo, relatamos as bases fundamentais do método

de imagem do tensor de difusão por ressonância magnética e fascigrafia, e descrevemos a validação do método em algumas patologias cerebrais.

No **capítulo 5,** resumimos a metodologia aplicada especificamente para a investigação da presente Tese. Descrevemos as etapas de recrutamento e investigação clínica dos pacientes e controles e detalhamos os protocolos de aquisição e pós-processamento dos dados de imagem.

No **capítulo 6**, resumimos os principais achados desta Tese. Descrevemos a estrutura e a trajetória das fibras do CC nos indivíduos do grupo controle investigado, bem como as principais alterações anatômicas encontradas nos pacientes com disgenesias do CC pelo método de DTI e fascigrafia. Detalhamos a conformação da trajetória do remanescente caloso dos pacientes com agenesia parcial do CC. Identificamos a reorganização estrutural da substância branca em pacientes com disgenesia do CC, descrevendo a trajetória do feixe anômalo de Probst e a evidência adicional, recentemente descrita, de neuroplasticidade: o Feixe *Sigmóide*.

No **capítulo 7** discutimos os resultados. Correlacionamos nossos achados com conceitos envolvendo a formação e a estrutura do CC normal e anormal e com conceitos de plasticidade cerebral, formulando hipóteses de possíveis explicações para as alterações encontradas nos pacientes estudados.

Nos **capítulos 8 e 9**, resumimos as conclusões da Tese. Conferimos também visões críticas ao nosso trabalho, mencionando pontos importantes que, por uma razão ou outra, não foram abordados e, finalmente, descrevemos estudos ora em curso e algumas perspectivas para o futuro.

Nos **capítulos 10 e 11** encontram-se as referências e anexos da Tese, respectivamente.

1.3 O CORPO CALOSO

1.3.1 ESTRUTURA DO CORPO CALOSO

Entende-se por “comissuras” os feixes antiparalelos de SB que contêm axônios que conectam os hemisférios cerebrais, podendo suas fibras fazer conexão entre regiões similares (homotópicas) ou não similares (heterotópicas) dos hemisférios cerebrais. São comissuras cerebrais: a comissura anterior, a comissura hipocampal, a comissura posterior (intercolicular), a comissura habenular, a aderência intertalâmica e o CC (HEIMER, 1983; LENT et al., 2001) (**Figura 1**). O CC, descrito por Reil (1812), é a maior comissura cerebral em mamíferos placentários e conecta regiões homólogas dos lobos cerebrais (HOFER et al., 2006). O CC contém 200 a 300 milhões de fibras no homem, representando 1,2% dos neurônios corticais (AZEVEDO et al., 2008); 56 milhões de fibras no macaco *Rhesus* (LAMANTIA e RAKIC, 1990), correspondendo a 7,4% (HERCULANO-HOUZEL et al., 2007); 23 milhões no gato (BERBEL e INNOCENTI, 1988); e 7 milhões de fibras no camundongo (KAMNASARAN, 2005), chegando a quase 50% dos neurônios corticais (HERCULANO-HOUZEL et al., 2006). Devido à sua complexidade de desenvolvimento estrutural e funcional, como também à diversidade de alterações estruturais e funcionais relacionadas à sua mal-formação, o CC tem exercido enorme fascínio como objeto de estudo por mais de cem anos (KAMNASARAN, 2005).

Figura 1: Comissuras cerebrais

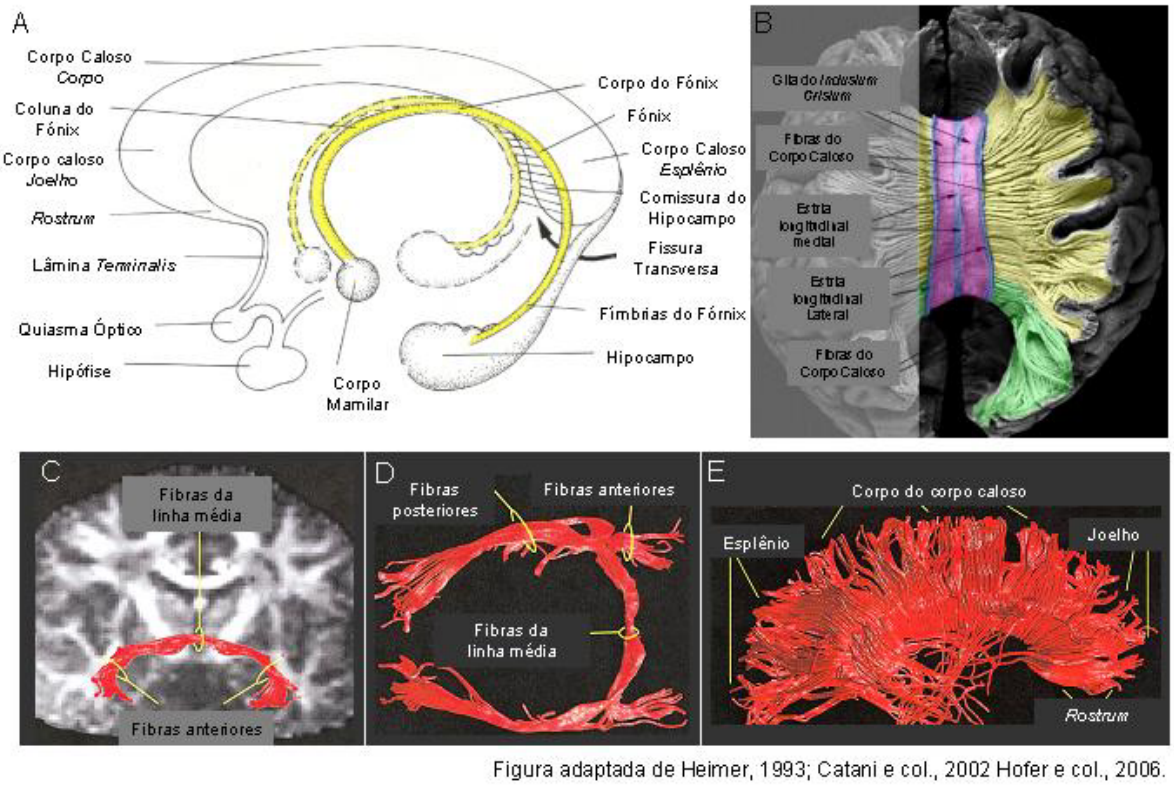

Figura adaptada de Heimer, 1993; Catani e col., 2002 Hofer e col., 2006.

Figura 1: A. Esquema tridimensional ilustrando as relações entre o CC, fórnix e comissura do hipocampo. **B**. Esquema de representação das fibras do corpo caloso e estruturas da linha média. **C**. Reconstrução por fascigrafia de fibras da comissura anterior (CA) projetadas em imagem de FA (FA, do inglês *Fractional Anisotropy*) no plano coronal. **D.** Fibras da CA reconstruídas por fascigrafia (em visão axial). **E.** Fibras do CC reconstruídas por fascigrafia (em visão sagital).

O CC está envolvido em diversas funções motoras, sensoriais e visuais, como controle motor bimanual, fusão dos campos visuais, lateralização de sons e discriminação visual de objetos em movimento rápido (HOUZEL et al., 2002; ABOITIZ e MONTIEL, 2003). Acredita-se que o surgimento do CC tenha permitido a transferência de informações entre os hemisférios cerebrais de forma mais rápida e eficaz. Entretanto, seu valor adaptativo e evolutivo, bem como seu papel na determinação das

assimetrias inter-hemisféricas do adulto, ainda se encontram em debate (ABOITIZ e MONTIEL, 2003).

A morfologia do CC está relacionada a sexo, preferência manual e dominância hemisférica para a linguagem falada, encontrando-se alterada em diversas patologias, como esquizofrenia e epilepsia (DEQUARDO, 1996; INNOCENTI, 2003; WESTERHAUSEN, 2003; DOUAUD, 2007).

Em 1995, Witelson propôs um modelo de segmentação topográfica do CC em três partes: i) o terço mais anterior (o **joelho**) contém fibras que conectam regiões pré-frontais; ii) o terço médio (o **corpo**) interconecta regiões motoras, sômato-sensitivas e auditivas; e iii) o terço mais posterior é subdividido em duas porções: a mais anterior (o **istmo**) conecta regiões temporais superiores e parietais, e a mais posterior, o **esplênio**, contém fibras associadas a regiões têmporo-parietais e occipitais (visuais) (WITELSON, 1995; ABOITIZ et al., 2003) (**Figura 2**).

Figura 2: Esquema da estrutura do corpo caloso no plano sagital mediano

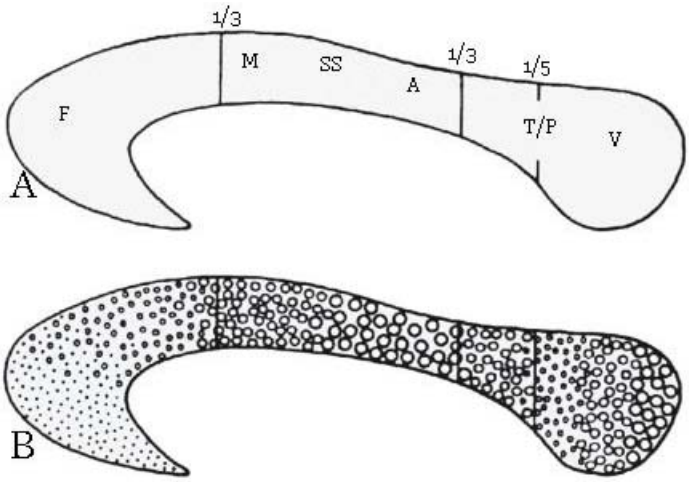

Figura 2: A. A – fibras auditivas; F – frontais; M – motoras; SS – somato-sensitivas; T/P – fibras têmporo-parietais; V – fibras visuais. **B.** Representação das diferenças regionais da composição de fibras em cada região. Círculos maiores indicam fibras de maior diâmetro. (Adaptado de ABOITIZ e MONTIEL, 2003).

Em primatas, esta segmentação topográfica é acrescida de um segundo fator, relacionado ao diâmetro dos axônios que compõem o CC. À microscopia óptica, as fibras do CC variam de 0,4 a 15 μm de diâmetro, a maioria variando entre 0,6 e 1,0 μm. A maioria das fibras (~95%) é mielinizada, mesmo na região do joelho, onde as fibras não-mielinizadas chegam a 16% (ABOITIZ et al., 1992; OLIVARES et al., 2001). Dependendo da região do CC, as diferenças ocorrem de modo que as fibras que ligam regiões frontais e têmporo-parietais, presentes no joelho, são fibras de condução lenta, de menor diâmetro, e pouco (ou nada) mielinizadas, enquanto as fibras do corpo e do esplênio são fibras de condução rápida, grande diâmetro (> 3 μm) e mielinizadas. Tais diferenças estruturais corroboram uma das explicações sobre a vantagem evolutiva do CC, que teria permitido mais rapidez de integração entre regiões motoras e sensitivas homólogas. A condução inter-hemisférica rápida não seria tão crucial em regiões de maior complexidade intrínseca, onde o tempo de processamento interno deve ser naturalmente maior, como é o caso das regiões pré-frontais, que se acham conectadas por fibras calosas finas e de condução lenta (ABOITIZ e MONTIEL, 2003; MIHRSHAHI, 2006).

Estudos recentes de RM têm trazido novas luzes à anatomia e à conectividade do CC em humanos. Recentemente, HOFER e colaboradores (2006) descreveram a anatomia e a trajetória das fibras calosas estudadas em humanos *in vivo* por DTI, e compararam seus resultados com dados da conectividade de CC até então baseados

em primatas não-humanos. Os resultados daquele estudo sugerem, por exemplo, que, ao contrário do que se acreditava, um número maior de fibras calosas parece estar relacionado (ou conectando) as áreas pré-motora e motora suplementar em humanos (HOFER et al., 2006).

1.3.2 EVOLUÇÃO DO CORPO CALOSO

O CC é uma estrutura exclusiva de mamíferos placentários (*Eutheria*). Sua emergência evolutiva e a ausência de equivalente morfológico nas espécies não-placentárias são vistos como verdadeira inovação evolutiva (MIHRSHAHI, 2006).

Em mamíferos acalosos, muitas das funções do CC são conduzidas pela comissura anterior (CA) e, em menor grau, pela comissura do hipocampo. Acredita-se que o CC tenha surgido evolutivamente como comissura mais eficaz, reduzindo a distância e aumentando a velocidade de transmissão de informações entre os hemisférios. O córtex motor primário, presente mesmo nos eutérios mais primitivos e de pequeno porte, é conectado por fibras calosas. Segundo esta hipótese, do ponto de vista evolutivo, o CC surgiu suprindo a necessidade de comunicação mais rápida e eficaz para funções motoras mais especializadas e complexas, que podem estar relacionadas (I) ao fato de os mamíferos placentários, como os camundongos, exibirem maior complexidade manual se comparados a marsupiais de mesmo porte (IVANCO et al., 1996; MIHRSHAHI, 2006), como também (II) ao fato de certas atividades motoras ou visuais, por exemplo, serem perdidas ou lentificadas em animais e humanos após secção calosa (SHALOMON e WAHLSTEN, 2002; LASSONDE et al., 1995).

Outras evidências suportam a relação entre as funções desencadeadas pela CA e pela comissura hipocampal em mamíferos não placentários e as funções do CC em mamíferos eutérios. Ao contrário do que ocorre em répteis (cuja representação topográfica sensorial se dá ao nível do mesencéfalo), uma representação sensorial telencefálica organizada topograficamente surge nos mamíferos. Em marsupiais, por exemplo, a integração destas áreas corticais é feita principalmente ventralmente por uma robusta CA, enquanto nos eutérios, tal integração é feita pelo CC (mais dorsal) (SHANG et al., 1997). Se comparada ao CC, a conexão via CA possui a desvantagem de conferir um percurso mais longo à suas fibras (e, portanto, de transmissão inter-hemisférica mais lenta). Desta forma, pode-se inferir que se evolutivamente as fibras comissurais permitiram a integração de hemi-representações corticais sensoriais nos mamíferos, a dorsalização de fibras inter-hemisféricas neocorticais com a formação do CC nos mamíferos eutérios, garantiu a redução do tempo de transmissão e uma comunicação inter-hemisférica mais eficaz (ABOITIZ e MONTIEL, 2003). Tais correlações sugerem certa ligação filogenética entre estas comissuras cerebrais.

1.3.3 FORMAÇÃO DO CORPO CALOSO

Durante o desenvolvimento do sistema nervoso (SN), os neurônios, guiados por estruturas de células gliais ou moleculares, emitem seus prolongamentos axonais através de trajetos seletos a fim de estabelecerem conexões precisas com seus alvos, muitas vezes bem distantes de seus corpos celulares. Este processo é denominado axogênese, durante a qual o cone de crescimento, extremidade distal de um axônio capaz de discernir entre moléculas atrativas ou repulsivas, guia o crescimento neurítico

(KOLODKIN, 1996; LI et al., 1996, GARCIA-ABREU et al., 1996). Tais moléculas normalmente secretadas por alvos intermediários ou definitivos podem ser solúveis, associadas a membranas celulares, ou componentes da matriz extracelular, bloqueando ou servindo de substrato-suporte para o crescimento neurítico. Este é um fenômeno complexo que ocorre, por exemplo, nas várias etapas do desenvolvimento do CC, quando axônios, em sua maioria derivados de neurônios das camadas corticais II-III e V, percorrem longas distâncias até alcançarem seus alvos no lado oposto do cérebro (revisto por LINDWALL et al., 2007).

O CC se forma em humanos ao redor da 12^{a} semana de gestação (RAKIC e YAKOVLEV, 1968) e acredita-se seguir um padrão bem definido de desenvolvimento, obedecendo a um gradiente tanto ântero-posterior, como ventro-dorsal (KIER and TRUWIT, 1996; 1997). De acordo com esta teoria, o joelho é formado inicialmente, seguido do corpo e, por fim, do esplênio. O rostro, anterior ao joelho, é o último segmento a se desenvolver. Entretanto, alguns autores defendem a idéia de que o CC tem origem bicêntrica, os segmentos rostrais se originando na *lamina terminalis*, os segmentos mais caudais na comissura do hipocampo (OZAKI et al., 1992; DEAZEVEDO et al., 1997, RICHARDS et al., 2004). Os mecanismos que precedem o surgimento do joelho, estrutura de formação precoce, são fundamentais para o desenvolvimento normal do CC.

Desta forma, uma vez formadas as vesículas telencefálicas a partir do prosencéfalo, os hemisférios cerebrais precisam se unir na linha média, dorsalmente, provendo substrato para o cruzamento dos axônios comissurais. Evidências indicam que tal fusão na linha média seja proporcionada por moléculas secretadas por células

gliais locais (*glia mediana de zíper - GMZ*), por volta do 14-15º dia de gestação em camundongos (SHU e RICHARDS, 2001).

Modelos animais contribuíram muito para a formulação de hipóteses sobre os mecanismos e os fatores envolvidos na formação do CC, enquanto a maioria das evidências sobre a existência de mecanismos semelhantes em humanos decorre de poucos estudos mais recentes (LENT et al. 2005; REN et al., 2006). Acredita-se que a projeção inicial dos axônios calosos das camadas corticais em direção à SB seja ocasionada por polaridade intrínseca destes neurônios, associada a gradientes de moléculas solúveis, como semaforinas, efrinas e netrinas (BAGNARD et al., 1998; POLLEUX et al., 1998; UZIEL et al., 2006), o que atrai os axônios para a superfície ventricular e depois os faz defletir na zona intermediária em direção à linha média. Além disso, muitos axônios calosos bifurcam na SB, emitindo um ramo lateral e outro medial, eliminando depois o primeiro para a permanência do segundo (GARCEZ et al., 2007). De um modo ou de outro, esta “deflexão” para a linha média diferencia os axônios calosos de axônios subcorticais que vão prosseguir em sentido lateral e inferior pela cápsula interna (SERAFINI et al., 1995; BAGNARD et al., 1998; HU et al., 2003; UZIEL et al., 2006). Em seqüência, próximo à linha média, células gliais parecem ser as responsáveis pelo cruzamento e direcionamento dos axônios calosos para o hemisfério oposto, são elas: *glia mediana de zíper (GMZ)*, a *cunha glial* e a *glia do indusium griseum* (GIG). A GMZ parece ter um papel primordial possibilitando a fusão dos hemisférios. A cunha glial é uma estrutura bilateral localizada ventralmente ao CC no ângulo medial dos ventrículos laterais, e formada por células da glia radial, enquanto a GIG tem localização dorsal na margem do sulco inter-hemisférico. A cunha glial e a

GIG, em conjunto, secretam fatores repulsivos, como Slit e Wnt, que mantêm os axônios calosos em crescimento confinados em um “corredor glial” através da linha média, conduzindo-os em direção ao hemisfério contralateral (SHU e RICHARDS, 2001; RICHARDS, 2002; RICHARDS et al., 2004; LENT et al., 2005; KEEBLE e COOPER, 2006). Outros fatores, como receptores de fator de crescimento de fibroblasto (FGFr1), Nfia e Nfib, e a proteína 43 associada ao crescimento (GAP43), parecem estar envolvidos na formação desta estruturas gliais ou desempenham papel de sinalizadores diretos para axônios calosos (SMITH et al., 2006; SHU et al., 2003; STEELE-PERKIN et al., 2005; SHEN et al., 2002). Feixes axonais propriamente ditos também estão envolvidos na formação do CC, como é o caso de neurônios pioneiros do feixe do cíngulo, apontados como os primeiros a cruzar a linha média e servir de molde para o cruzamento subseqüente das projeções calosas (KOESTER e O’LEARY, 1994; RASH e RICHARDS, 2001; mas veja-se também OZAKI e WAHLSTEN, 1998). Quanto ao hemisfério contralateral, pouco se sabe sobre os fatores que determinam o ponto de chegada dos axônios calosos, *i.e.*, seus alvos homotópicos. O amadurecimento das projeções calosas ocorre por intensa arborização sináptica e pela eliminação seletiva de projeções transitórias e extranumerárias (HEDIN-PEREIRA et al., 1999; INNOCENTI e PRICE, 2005). Tal processo é corroborado por evidências de redução perinatal do CC em modelos animais, bem como, mais recentemente, por estudos de RM em humanos (CLARKE et al., 1989; THOMPSON et al., 2000; KESHAVAN et al., 2002).

RICHARDS et al. propuseram uma organização dos mecanismos moleculares e celulares envolvidos no desenvolvimento do CC, estabelecendo divisão arbitrária do

percurso dos axônios calosos em seis etapas, ou “pontos de decisão”, exemplificados na **Figura 3** a seguir (RICHARDS et al., 2004).

Figura 3: Desenvolvimento do Corpo caloso em seis etapas (1- 6)

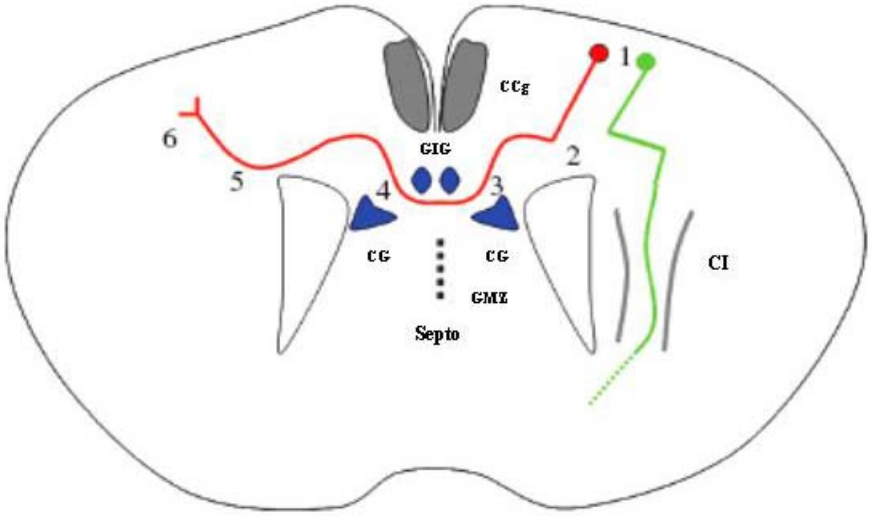

Figura 3: Representação de um neurônio caloso, em vermelho, enquanto em verde está representado um neurônio com projeção para a cápsula interna (CI). CCg, córtex do cíngulo; GIG, glia do indusium griseum; CG, cunha glial; GMZ, glia mediana de zíper. *(Adaptado de RICHARDS et al., 2004).*

1.3.4 A FUNÇÃO DO CORPO CALOSO – CALOSOTOMIA E DISGENESIA DO CORPO CALOSO

Ainda existem controvérsias relacionadas à natureza funcional das conexões calosas, se excitatórias ou inibitórias. Entretanto, a maior parte dos estudos sobre transferência inter-hemisférica (TIH) se baseou em ligações excitatórias ente os hemisférios cerebrais por axônios calosos (BLOOM, 2005). Destes estudos, a grande maioria foi desenvolvida ao se acompanhar e analisar pacientes submetidos a

calosotomia cirúrgica como tratamento para epilepsia refratária ao tratamento farmacológico. SPERRY e seus colaboradores observaram que estes pacientes, conhecidos como “split-brains”, desenvolviam uma síndrome de desconexão inter-hemisférica no pós-operatório (SPERRY, 1970; GAZANIGA, 1995, 2005). A síndrome de desconexão é caracterizada pela falta completa de transferência inter-hemisférica, com conseqüente ausência de integração entre os hemisférios se informações sensitivas são apresentadas individualmente a um dos hemisférios (SPERRY, 1970; GAZZANIGA, 1995, 2005; PAUL et al., 2007). Estas deficiências na transferência de informações sensoriais e de coordenação motora bimanual, por exemplo, são acompanhadas de alterações sutis de comportamento. Desta forma, quando todo o CC é seccionado, ocorre o bloqueio inter-hemisférico de informações motoras, sensoriais e práxicas. Tais evidências contribuíram para o entendimento da especialização hemisférica, e de como os hemisférios interagem para conservar a unidade da consciência subjetiva (GAZZANIGA et al., 1987). Outros estudos mostraram que funções como a transferência visuomotora inter-hemisférica, ainda que lenta em pacientes com calosotomia total, não está totalmente abolida, e sugerem que vias alternativas têm papel importante na transferência inter-hemisférica na ausência do CC (BERLUCCI et al., 1995; SAVAZZI et al., 2007).

Por outro lado, a secção parcial ou lesões adquiridas do CC, como isquemia focal, traumas ou neoplasias, permitiram o estudo de funções de segmentos específicos do CC, fortalecendo o conceito de segmentação também topográfica da função dessa comissura (RISSE et al., 1989, CORBALLIS et al., 2001).

Além dos pacientes submetidos à calosotomia cirúrgica, pacientes com distúrbios do desenvolvimento do CC também têm contribuído para o entendimento de sua função. Entretanto, pacientes com ausência total ou parcial do CC vêm intrigando médicos e pesquisadores por décadas porque, curiosamente, não apresentam a síndrome de desconexão inter-hemisférica. De maneira geral, pacientes com DCC parecem manter a capacidade de transferência inter-hemisférica em alguns testes de estímulos simples. O mesmo não ocorre quando os testes requerem transferência ou integração de processos cognitivos complexos, requerem processamento mais rápido e não são influenciados por experiências prévias (BROWN et al., 1999). Estes achados sugerem um importante envolvimento do CC quando integrações inter-hemisféricas rápidas são necessárias, o que acompanha o aumento em complexidade das ações em jogo (PAUL et al., 2007).

Abaixo são listados alguns sintomas da síndrome de desconexão por calosotomia completa (KAMNASARAN, 2005):

- Apraxia unilateral - Incapacidade de resposta a comando verbal utilizando a mão esquerda;
- Agrafia unilateral - Incapacidade de escrita com a mão esquerda;
- Anosmia verbal - Incapacidade de identificar odores expostos à narina direita;
- Impedimento do processamento verbal - Informação verbal percebida superiormente à direita;
- Hemianopsia dupla - Incapacidade de identificar estímulos visuais nos hemicampos direito ou esquerdo com a mão contralateral;

- Apraxia de construção unilateral - Incapacidade de processamento espacial requerido pelo hemisfério direito;
- Anomia unilateral - Incapacidade de identificar objetos palpados pela mão esquerda;
- Mão alienígena - Ausência de coordenação dos movimentos das mãos;
- Perda de memória – Moderada;
- Alexitimia - Muito freqüente.

1.4 MALFORMAÇÃO DO CORPO CALOSO

1.4.1 CLASSIFICAÇÃO E EPIDEMIOLOGIA DAS DISGENESIAS DO CORPO CALOSO

Como relatado no capítulo anterior, vários fatores estão envolvidos na formação do CC. Alterações estruturais, celulares ou moleculares em qualquer destas etapas podem impedir a formação do CC no todo ou em parte. Etapas primordiais do desenvolvimento do sistema nervoso, como a formação dos hemisférios, são cruciais para o surgimento de comissuras como o CC. O prosencéfalo originará as vesículas telencefálicas, que originam os hemisférios cerebrais. É intuitivo concluir que o não desenvolvimento de hemisférios cerebrais acarreta a não formação de estruturas que os ligariam. Isto, de fato, é o que ocorre no distúrbio do desenvolvimento denominado “holoprosencefalia” (RICHARDS et al., 2004). Indivíduos portadores de tal alteração, por defeito da formação individualizada dos hemisférios cerebrais, não possuem CC (entre outras malformações), entretanto não são os únicos a apresentarem ausência total (agenesia) ou parcial do CC. Desta forma, a expressão disgenesia do CC (DCC) aplica-se a variáveis graus de sua malformação, desde a ausência total até a mínima deficiência no seu desenvolvimento (KENDALL, 1993), como a hipoplasia.

Dados de material de autópsia apontam para incidência das DCC na população geral de 1/19.000 (BLUM et al., 1990). Ainda, estima-se que a incidência seja de 0,0005-0,7% em crianças, 2-3% na população com comprometimento mental e de cerca de 47% em pacientes com anomalias do sistema nervoso central.

1.4.2 ACHADOS DE IMAGEM CARACTERÍSTICOS DAS DISGENESIAS DO CORPO CALOSO

Os achados de imagem variam de acordo com o grau de acometimento do CC. Na disgenesia total (agenesia) ou parcial, os ventrículos laterais estão separados e não-convergentes. Nos cortes axiais de tomografia computadorizada e RM, os ventrículos laterais são paralelos, apresentando cornos frontais pequenos e de bordas mediais côncavas, associados a aumento desproporcional dos cornos occipitais (colpocefalia). A colpocefalia está associada, em 40% dos casos, à disgenesia do CC (MONTANDON et al., 2003) (**Figura 4**).

Nas imagens sagitais, observa-se ausência parcial ou total do CC e os sulcos e giros corticais da face medial dos hemisférios irradiam a partir do terceiro ventrículo (estenogiria). O giro do cíngulo encontra-se evertido, o que é bem observado em planos coronais. Aspecto peculiar das DCC é a presença dos feixes de Probst (FP). Estes feixes são formados por fibras presumivelmente comissurais que não conseguiram cruzar a linha média e estabeleceram-se ipsilateralmente assumindo disposição longitudinal paralela aos ventrículos laterais em cada hemisfério cerebral. Os cornos anteriores dos ventrículos laterais encontram-se mais separados e com menor diâmetro. O terceiro ventrículo comumente é dilatado e em situação mais cranial, o septo pelúcido normalmente ausente (MONTANDON et al., 2003; KAMNASARAN, 2005).

Em estudo retrospectivo com 63 pacientes portadores de DCC, 30 pacientes apresentaram ausência total do CC e 33 apresentaram ausência parcial (BEDESCHI et al., 2006). A partir da época do insulto e dos eventos que culminam com a disgenesia

do CC, os métodos de imagem podem classificá-la nas seguintes formas: tipo I, ou agenesia, em que o CC está completamente ausente; tipo II, ou disgenesia parcial (ou hipogenesia), cujo CC apresenta graus variados de encurtamento (normalmente esplênio, ou corpo + esplênio ausentes); e tipo III, ou hipoplasia, em que o CC é completamente formado, porém apresenta redução em seu tamanho, podendo ser focal ou difusa, e estar associada a alterações evidentes do córtex (JINKINS et al., 1989; UTSUNOMIYA et al., 1997). Devido ao gradiente crânio-caudal de formação do CC, em casos de disgenesia parcial o remanescente do CC geralmente ocupa a topografia do joelho ou do joelho e do corpo.

Figura 4: Principais características anatômicas dos pacientes com DCC

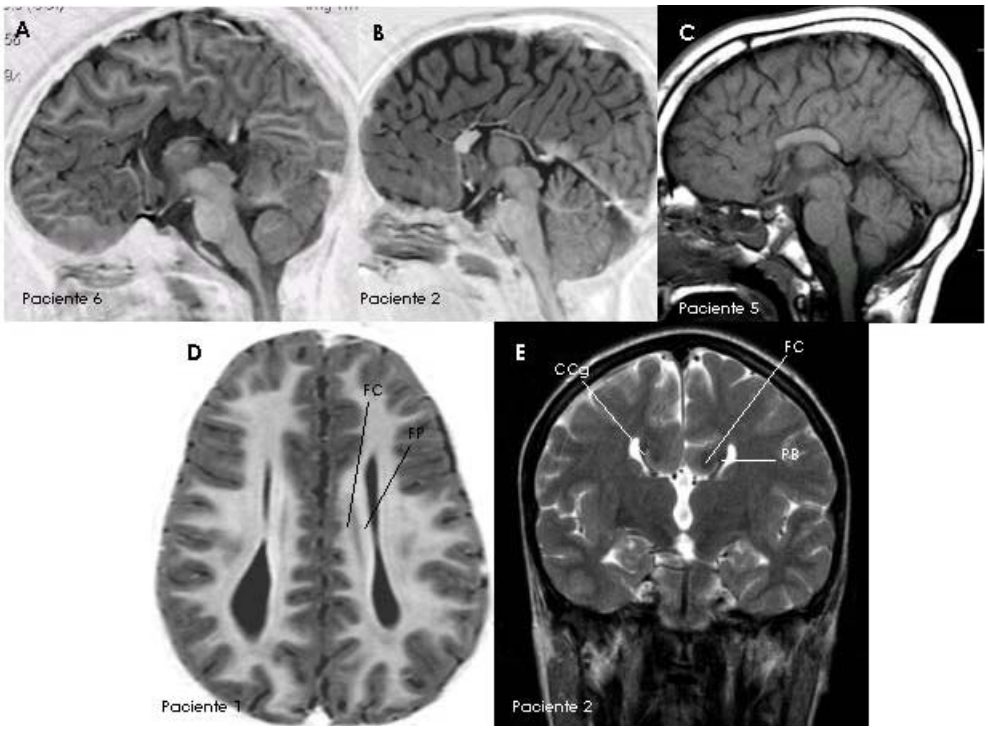

Figura 4: A-C. Imagens de ressonância magnética (RM) ponderada em T1 no plano sagital de pacientes com agenesia do corpo caloso (CC) (**A**), disgenesia parcial do CC (**B**) e hipoplasia do CC (**C**); **D**. Imagem de RM ponderada em T1 no plano axial de paciente com disgenesia parcial do CC. Note o paralelismo dos ventrículos laterais e presença do feixe de Probst (FP) paralelo ao feixe do cíngulo (FC). **E.** Imagem de RM ponderada em T2 no plano coronal de paciente com disgenesia parcial do CC. Note o córtex do cíngulo (CCg) evertido e, o FP e o FC evidentes neste plano.

1.4.3 MANIFESTAÇÕES CLÍNICAS

DCC pode se apresentar como síndrome isolada ou associada a outras malformações do SNC. Cerca de 85% das DCC se acompanham de outras anomalias do SNC e, nestes casos, convulsões, alterações motoras ou retardamento metal são as manifestações mais freqüentes. BEDESCHI et al. (2006) descreveram, em 63 pacientes analisados retrospectivamente, a associação com outras alterações do SNC em 14 pacientes portadores de disgenesia parcial de CC e em 10 pacientes com agenesia.

Entre as anomalias do SNC mais freqüentes associadas a DCC estão (ARIBANDI et al., 2004; KUKER et al., 2003):

- Cisto de Dandy Walker
- Cisto Inter-hemisférico
- Hidrocefalia
- Lipoma da linha média
- Malformação de Arnold-Chiari
- Encefalocele de linha média
- Prosencefalia
- Holoprosencefalia
- Hipertelorismo e fenda mediana

- Polimicrogiria
- Heteretopia de substância cinzenta
- Anomalias cardiovasculares, gênito-urinárias e gastrointestinais

Surpreendentemente, a ausência congênita do CC parece ter impacto limitado nas habilidades cognitivas de muitos pacientes com DCC. Os pacientes podem até ter QI normal, porém suas pontuações se encontram mais freqüentemente abaixo do normal. São constantes o comprometimento da capacidade de generalização, de fluência categórica (denominação de vários itens pertencentes à mesma categoria, por exemplo, nomes de frutas), e de resolução de problemas. Distúrbios de linguagem, como dificuldades de compreensão de sintaxe, prosódia e narrativas de humor, estão presentes. Tais alterações são relacionadas à deficiência de compreensão da linguagem não literal e de prosódia, fundamentais para a comunicação social. Existem evidências de lateralização da linguagem, em que: i) sintaxe e semântica são funções do hemisfério esquerdo, e ii) prosódia, do direito. A falta de integração entre estas funções poderia explicar esta deficiência nos pacientes com DCC (PAUL et al., 2003; ECKSTEIN e FRIEDERICI, 2006; PAUL et al., 2007).

Em testes de transferência inter-hemisférica, os pacientes com DCC apresentam tempos de reação prolongados. Entretanto, ao contrário dos calotomizados, pacientes com agenesia do CC não apresentam a síndrome de desconexão clássica. Uma possível explicação para tal diferença em relação aos pacientes submetidos à calosotomia cirúrgica, seria relacionada à maior possibilidade adaptativa do cérebro no caso dos pacientes com DCC. Supostamente, o cérebro acaloso, ainda em desenvolvimento, teria a possibilidade de compensar a ausência da principal comissura

cerebral através de mecanismos de neuroplasticidade (KAMNASARAN, 2005). Pacientes com DCC não apresentam, por exemplo, dificuldades em testes taquistoscópicos simples ou envolvendo reconhecimento verbal de objetos apresentados a um dos hemisférios (SAUERWEIN e LASSONDE, 1994). Estes pacientes falham, contudo, em testes mais complexos de comparação entre os campos visuais, o que indica a preservação de transferência inter-hemisférica em certo grau, mas que é dependente da realização de estímulos simples e não complexos.

Outras evidências tornam intrigante o estudo de pacientes com DCC. Em termos de sintomatologia, pacientes portadores (mesmo de ausência total do CC) podem levar vida relativamente normal, com pouca ou nenhuma interferência em atividades diárias, enquanto outros, com alterações anatômicas muito semelhantes, podem apresentar graves limitações, como um severo retardo mental. Estas diferenças apontam para graus diferentes de reorganização cerebral, o que pode até mesmo estar diretamente relacionado à causa específica da DCC, uma vez que diferentes fatores causais podem estar envolvidos em cada caso. Outra possibilidade é que tais alterações anatômicas consideradas semelhantes por análise *post-mortem* ou métodos de imagem como RM convencional, não sejam exatamente idênticas. Deste modo, outras alterações anatômicas poderiam se encontrar fora da capacidade de resolução ou detecção dos métodos classicamente usados. No caso da RM, avanços tecnológicos possibilitando o desenvolvimento de métodos específicos para o estudo da SB têm sido bastante promissores para o entendimento das DCC (LEE et al., 2004; GAZZANIGA, 2005).

A maior parte dos estudos clínicos e prognósticos dos pacientes com DCC foi realizada em número limitado de pacientes ou com base em curto período de tempo de

acompanhamento. Estudos mais recentes mostram que o comprometimento de habilidades cognitivas em pacientes com DCC varia com a idade e sugerem a necessidade de acompanhamento por tempo mais prolongado para que se tenha a real estimativa do prognóstico destes pacientes (MOUTARD et al., 2003).

1.4.4 ALTERAÇÕES GENÉTICAS ASSOCIADAS

Dados de prevalência da disgenesia do CC variam devido à inconstância dos recursos diagnósticos e de amostra populacional entre os estudos. Em geral, é reportada prevalência de 3-7 em 1000 na população geral e, de 2-3 em 100 em crianças com anomalias do desenvolvimento. A DCC está associada a mais de 50 síndromes genéticas. Mecanismos como mutação mendeliana de gene único, mutação esporádica de gene único ou até alterações genéticas complexas envolvendo tanto mutações hereditárias como esporádicas parecem estar envolvidas na gênese das DCC, com evidências relatadas de mais de 20 mutações cromossômicas autossômicas ou ligadas ao X (DOBYNS, 1996).

Somente cerca de 30-45% dos casos de DCC possuem causas conhecidas, em que 20-35% dos casos possuem síndrome genética conhecida e 10%, alterações cromossômicas mapeadas. Considerando-se somente os casos de ausência total do CC, somente 10-15 % têm causa conhecida (BEDESCHI et al., 2006; PAUL et al., 2007).

Com base nos mecanismos de desenvolvimento do CC, pode-se dividir a malformação do CC em dois tipos: **a.** axônios formados a partir do córtex de cada um dos hemisférios são impossibilitados de cruzar a linha média e formam os feixes de

Probst (FP); **b.** axônios calosos não são emitidos a partir do córtex. O tipo **a** deve ocorrer em todas as DCC em que os FP estão presentes. Em modelos animais, é o que ocorre também com modelos de camundongo mutante Balb (WAHLSTEN, 1994) e em animais submetidos a transecção mediana perinatal (LENT, 1981; 1982). O tipo **b** pode ocorrer em concomitância com alterações corticais como a lisencefalia, como na síndrome de Walker-Warburg, e também parece estar associado a anomalias como HSAS ligada ao X (hidrocefalias com estenose do aqueduto de Sylvius), MASA (retardo mental, adução do polegar, espasticidade e afasia). Estas últimas têm como causa uma mutação na molécula de adesão celular L1CAM (glicoproteína envolvida em sinalização e crescimento axonal) (Dobyns, 1996; Paul et al., 2007).

Exemplo de mutação mendeliana ocorre na patologia denominada lisencefalia com agenesia de CC ligada ao X, cuja mutação encontra-se no gene ARX. Exemplos de mutações esporádicas em gene único são as alterações no gene da L1CAM descritas acima.

Na síndrome autossômica recessiva de Andermann, mais prevalente em uma região de Quebec, Canadá, que se acompanha de DCC, alterações cognitivas, psicose e neuropatia periférica, a mutação encontra-se no gene do co-transportador de KCl (KCC3). Tal mutação não parece ter o mesmo efeito em camundongos. Outras mutações em humanos que levam à DCC, quando reproduzidas em animais, também não exibem o fenótipo esperado. O inverso também ocorre (DUPRÉ et al., 2003; SMITH et al., 2006; PAUL et al., 2007).

Além de incidência familiar rara e de grande parte dos casos não ter causa hereditária identificada, evidências como o risco aumentado da incidência de DCC em

gestações de mulheres acima dos 40 anos, contribuem para uma origem a partir de mutações esporádicas em grande parte dos casos.

O envolvimento de múltiplos genes nas DCC, evidências de que a penetração destas mutações nem sempre é a mesma (DUPRÉ et al., 2003) e de que alterações genéticas concomitantes podem estar presentes em alguns casos, sugerem mecanismos multifatoriais envolvidos nos genes das DCC, o que vai ao encontro aos múltiplos mecanismos e processos envolvidos na formação do CC normal.

1.5 IMAGEM DO TENSOR DE DIFUSÃO E FASCIGRAFIA: DESENVOLVIMENTO DO MÉTODO E VALIDAÇÃO EM PATOLOGIAS CEREBRAIS

1.5.1 DIFUSIBILIDADE DA ÁGUA E PRINCÍPIOS DA IMAGEM DO TENSOR DE DIFUSÃO

Quando observamos um recipiente contendo água, por exemplo, um copo d'água sobre uma mesa estável, tendemos a inferir um estado também estável do conteúdo no interior deste continente, no caso, o copo. Entretanto, as moléculas de água estão longe da "calmaria" mesmo que no interior de um copo imóvel. Na verdade, as moléculas da água, como a de qualquer outro fluido, estão em constante movimento randômico, o movimento browniano, descrito inicialmente por Robert Brown, no início do século XIX (BROWN, 1828 *apud* BEHRENS, 2004), ao observar o movimento de partículas de pólen na água. Similarmente, as moléculas de um outro fluido, quando adicionadas à água, se difundem através das moléculas de água seguindo rotas randômicas com resultantes radiais, normalmente de acordo com um gradiente de concentração. A difusão randômica da água em si é chamada de "self-diffusion" ou difusão própria. Este processo de difusão própria obedece às mesmas leis de difusão e o termo "difusão própria" e somente "difusão" se confundem. Matematicamente, entretanto, o primeiro tratamento teórico do movimento browniano foi provido por Albert Einstein em 1905 (EINSTEIN, 1956 *apud* BEHRENS, 2004).

As características microscópicas do meio são fundamentais na determinação do efeito macroscópico da difusão a ser observado, ou seja, o movimento molecular é afetado pelo meio em que ele ocorre, o que no caso de tecidos biológicos depende

diretamente da estrutura e arquitetura dos mesmos. Neste caso, podemos imaginar, por exemplo, um meio em que uma barreira de mielina hidrofóbica restringe a difusão das moléculas da água através da mesma. Neste meio, a difusão não ocorre igualmente em todas as direções, exibindo propriedade anisotrópica, diferentemente de um meio isotrópico, em que não existe restrição alguma e em que as moléculas se deslocam igualmente em todas as direções, como ocorre com o líqüor presente no interior dos ventrículos cerebrais (**Figura 5**).

Figura 5: RM anatômica e ponderada em difusão

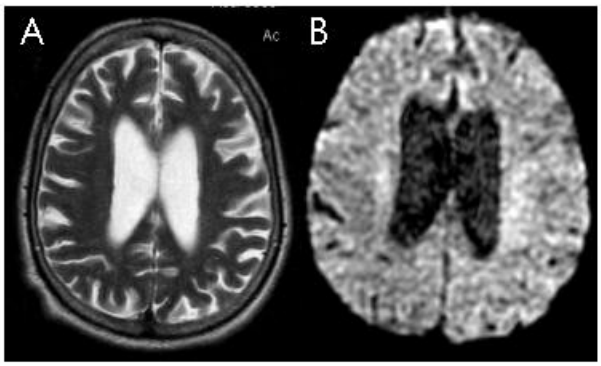

Figura 5: RM estrutural anatômica, ponderada em T2 (**A**) e ponderada em difusão (**B**), no plano axial de indivíduo normal.

No tecido cerebral, a restrição do movimento das moléculas ocorre em diversos níveis, como membranas celulares, macromoléculas, fibras axonais, etc. Nos grandes feixes de substância branca, por exemplo, este movimento é altamente anisotrópico e corre preferencialmente em direção paralela aos feixes axonais, em detrimento do movimento perpendicular a eles. Ainda que outras estruturas também sejam responsáveis pelas propriedades anisotrópicas da difusão na SB, uma vez que existem evidências de anisotropia em nervos não mielinizados (BEAULIEU et al., 1998) ou no

cérebro de neonatos (MCKINSTRY et al., 2002), a mielina é considerada a principal responsável pela direcionalidade da difusão nos feixes centrais.

De uma maneira simplista, podemos descrever o movimento de uma molécula de água em um intervalo de tempo (∆T), iniciado em t1=0 até T2=∆. A molécula exibirá um movimento randômico, mas se deslocará uma distância resultante vetorial “r”, como observado na **Figura 6** abaixo, adaptada de HAGMANN et al. (2006).

Figura 6*:* Movimento randômico das moléculas de água no tempo e no espaço

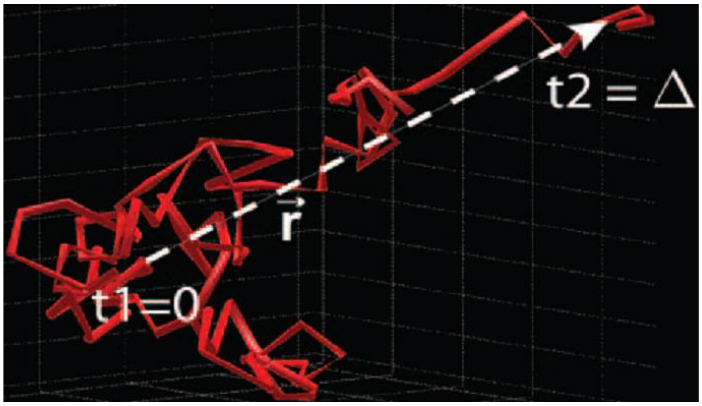

Figura 6: O processo de difusão da água livre em função do tempo pode ser representado por vetores e somas vetoriais, e ocorre igualmente em todas as direções (difusão isotrópica). A difusão anisotrópica, por sua vez, ocorre diferencialmente em direções preferenciais, e pode ser modelada através de formas elipsóides simples ou superpostas, refletindo características complexas da organização de tecidos como o músculo ou os feixes de substância branca. Adaptado de HAGMANN et al.,2006.

1.5.2 A IMAGEM DA DIFUSÃO POR RESSONÂNCIA MAGNÉTICA

Para que possamos medir difusibilidade por ressonância magnética (RM), o deslocamento das moléculas deve estar relacionado à intensidade de sinal medida pela RM. HAHN, em 1950, observou que o movimento de spins (ou próton de hidrogênio da água) em presença de campo magnético heterogêneo, causa um decremento na intensidade de sinal, ou seja, reduz a amplitude do spin eco. Em 1965, Stejskal e

Tanner, utilizando uma seqüência de pulso gradiente spin eco (SE), pela primeira vez mediram difusão com um experimento de RM, baseados no conceito de que os spins, movendo-se na direção do gradiente do campo magnético, são expostos a diferentes intensidades de campo magnético dependendo da posição em que ocupam ao longo do eixo de um gradiente (**Figura 7**). A seqüência de pulso gradiente SE difere da clássica seqüência SE por ter adicionalmente dois pulsos de gradientes de difusão. O resultante desta estrutura de seqüência permite a coleta de informações qualitativas e quantitativas (por quantidade de sinal lido) sobre spins estacionários e em movimento. Deste modo, o decaimento de sinal na RM será proporcional ao grau de movimento dos spins ao longo da direção do eixo do gradiente aplicado.

Figura 7: Esquema de seqüência spin-eco do modelo proposto por Stejskal-Tanner

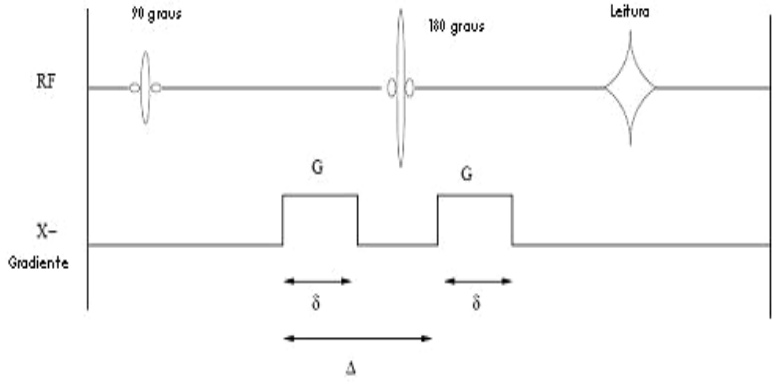

Figura 7: A seqüência de pulso clássica de Stejskal-Tanner, sensível à difusão da água, caracteriza-se por aplicação de um "lobo" de gradiente (G) após um pulso de 90 graus, para causar uma perda de fase dos spins dos núcleos de hidrogênio da água (defasagem ou "*dephasing*"). Em seguida, um pulso de 180 graus é aplicado, e um novo "lobo" de gradiente, de polaridade inversa, é aplicado para colocar os spins estacionários em fase novamente (recuperação de fase ou "*rephasing*"). É feita então a leitura do sinal, que será tanto menor quanto maior tenha sido o deslocamento das moléculas de água no ambiente. Adaptado de STEJSKAL e TANNER, 1965.

Um gradiente de difusão pode ser representado por um vetor 3D em que sua direção é a mesma da difusão e que seu comprimento corresponde à intensidade do gradiente aplicado. A intensidade do gradiente (ou ponderação em difusão) é normalmente expressa por um valor b (que é proporcional ao produto do quadrado do gradiente aplicado pelo intervalo de tempo de difusão).

Coeficiente de difusão aparente (CDA) - Em um meio homogêneo, as moléculas se movimentam normalmente a curtas distâncias e somente algumas realmente se distanciam, tipicamente obedecendo a uma função gaussiana (em forma de sino). Esta distribuição, por sua vez, dependendo do meio, dos seus limite e temperatura, pode ser mais ou menos estreita. Desta forma, esta distribuição gaussiana seria determinada por um coeficiente de difusão (***D***) e pelo intervalo de tempo (ΔT) do fenômeno observado (tempo de difusão). O coeficiente de difusão representa a viscosidade do meio e está relacionado ou dependente da estrutura do meio em que as moléculas difundem. O ***D*** da água a 37 ^{o}C, por exemplo, é de ***D***= 3 . 10^{-9} m^2/s.

A difusão absolutamente gaussiana, entretanto, não corresponde à realidade dos tecidos biológicos, em que várias estruturas como membranas semipermeáveis ou fibras mielinizadas vão determinar uma difusão não-gaussiana. Ainda assim, de forma aproximada, a imagem ponderada em difusão (IPD), assume o princípio de que em cada volume (ou voxel da imagem) existe difusão livre ou gaussiana. Nas IPDs, a medida quantitativa de difusão corresponde a uma aproximação de ***D***, denominada “coeficiente de difusão aparente” (CDA). O CDA é dependente da intensidade (*b*) e direção dos gradientes aplicados para a seqüência específica da IPD. Para o cálculo de CDA e obtenção da imagem correspondente aos valores do mesmo, são necessárias

duas aquisições, sendo uma aquisição ponderada em difusão com intensidade específica de um valor *b* e uma imagem de referência sem ponderação em difusão (*b*=0).

Como o CDA é muito dependente da direção do gradiente de difusão aplicado, é comum a aquisição de imagens ponderadas em difusão em três direções ortogonais seguidas do cálculo da média, o que permite uma melhor aproximação do coeficiente de difusão.

A primeira grande aplicação da imagem ponderada em difusão (IPD) veio da observação de que a difusão se alterava consideravelmente na área isquêmica em modelos experimentais de infartos em animais. A alteração da difusão determinava alteração de sinal (por difusão restrita ou redução do CDA) na imagem ponderada em difusão em poucos minutos após o evento isquêmico, na ausência de qualquer alteração nas imagens de RM convencionais (o que só acontece horas depois, em função do acúmulo de água no tecido extracelular). Hoje, a IPD é de extrema importância na prática clínica, no diagnóstico precoce e tratamento de acidentes vasculares isquêmicos (KIDWELL et al. 2003, SCHAEFER et al., 2005).

Imagem do tensor de difusão por ressonância magnética - A forma como ***D*** é construído e interpretado na IPD mascara qualquer efeito da orientação do tecido na propagação da difusão, o que ocorre em situações em que a difusão não é verdadeiramente isotrópica, e sim anisotrópica. Peter Basser, em 1994 (BASSER et al., 1994), propôs um modelo para medir a difusão anisotrópica em tecidos com tais estruturas, ao considerar portanto que a difusão nos mesmos não seria igual em todas as direções. Os princípios da Imagem do Tensor de Difusão (DTI) consideram que a difusão pode ser gaussiana, mas que também pode ser anisotrópica, podendo ser

representada por uma elipsóide, mas também por uma esfera (quando isotrópica). A distribuição gaussiana anisotrópica possui seis (no mínimo) graus de liberdade, e não somente um. Para isto, de cada ponto (ou voxel do tecido ou da imagem), obtém-se informação de ponderações de difusão em, no mínimo, seis diferentes direções (com $b \neq 0$) e uma direção não ponderada em difusão ($b=0$). Normalmente o valor do gradiente de difusão aplicado é de $b=1000$ s/mm^2. A informação resultante é um tensor de difusão e não um coeficiente de difusão (***D***). O tensor de difusão (também denominado ***D***) é uma matriz (como 3x3), que caracteriza a difusão no espaço 3D, podendo ser representado por uma elipsóide com eixo na direção da distribuição da difusão preferencial (**Figura 8**).

Figura 8: Representações do tensor de difusão

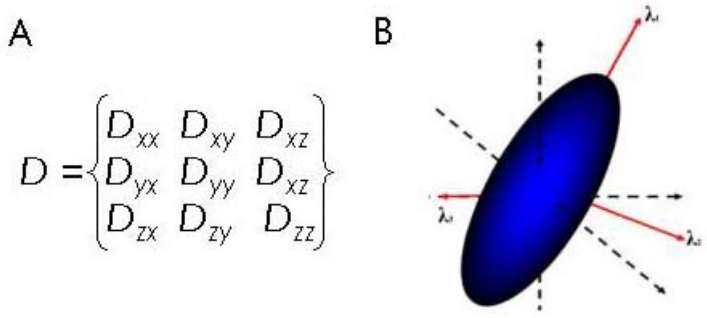

Figura 8: A. Esquema da matriz para o cálculo do tensor (D); **B.** Representação do tensor em elipsóide, com eixo principal na direção do maior componente da difusão (λ1).

O cálculo matemático do tensor permite a extração de várias medidas escalares. Para cada tensor estimado, é possível construir um sistema de coordenadas ortogonais no qual os componentes da difusão são decompostos. Desta forma pode-se determinar três coeficientes de difusão aparente independentes (um em cada eixo ortogonal), as

difusibilidades principais. As direções principais do tensor podem ser representadas por estes eixos ortogonais principais, conhecidos por *eigenvectors* (ϵ1, ϵ2, ϵ3). As difusibilidades principais são os componentes da difusão (ou a magnitude da difusão) ao longo de cada *eigenvector* e correspondem aos *eigenvalues* (λ1, λ2, λ3). *Eigenvectors* e *eigenvalues* descrevem as propriedades do tensor, e as propriedades relacionadas à difusibilidade geral e /ou anisotropia podem ser determinadas. Desta forma, *TRACE* (T) é a medida da difusibilidade geral do tecido, independente de direção. T= λ1 + λ2 + λ3. O mapa de difusibilidade em um corte axial de um cérebro humano normal é representado na **Figura 9B**. Difusibilidade média (DM), índice de difusibilidade bastante utilizado, é definida como T/3.

A anisotropia mede o quanto a difusão em uma das direções é preponderante em relação às outras. Existem vários índices de anisotropia, sendo Anisotropia Fracional (FA, do inglês *Fractional Anisotropy*) o índice mais comumente usado. O mapa de FA em um corte axial de um cérebro humano normal é representado na **Figura 9C**.

$$\mathrm{FA} = \frac{\sqrt{3}}{\sqrt{2}} \frac{\sqrt{(\lambda_1 - \lambda)^2 + (\lambda_2 - \lambda)^2 + (\lambda_3 - \lambda)^2}}{\sqrt{\lambda_1^2 + \lambda_2^2 + \lambda_3^2}}$$

Onde: $\lambda = \frac{\lambda_1 + \lambda_2 + \lambda_3}{3}$

FA, portanto, varia entre 0 e 1. A maior FA possível (FA=1), corresponde à situação em que (λ1 > 0 e λ2 = λ3 = 0). FA é nula em um meio isotrópico, em que (λ1 = λ2 = λ3).

A FA de cada voxel pode ainda ser unida à informação da direção do principal *eigenvector* de cada voxel e ser representado em um mapa de cores (PAJEVIC e PIERPAOLLI, 1999). São os chamados mapas de FA, codificados em cores segundo a orientação dos feixes. A convenção mais usada é a que representa em azul quando o principal vetor se encontra na direção do eixo supero-inferior (eixo z), em verde quando o principal vetor se encontra na direção do eixo ântero-posterior (eixo y) e, em vermelho quando o principal vetor se encontra na direção látero-lateral (eixo x). O mapa de FA codificado em cores segundo o principal *eigenvector* em um corte axial de um cérebro humano normal é representado na **Figura 9D**.

Figura 9: Mapas derivados da Imagem do Tensor de Difusão

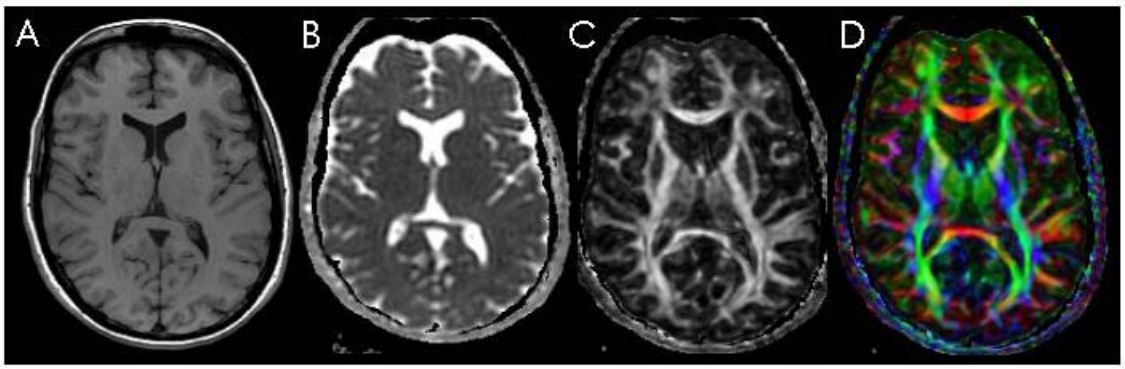

Figura 9: Imagens de ressonância magnética (RM) de indivíduo-controle no plano axial de mesma localização. **A**. RM ponderada em T1; **B**. mapa de difusibilidade Trace; **C**. mapa de anisotropia fracional (FA); **D**. mapa de FA codificado em cores segundo orientação dos feixes: fibras em disposição látero-lateral em vermelho, fibras em disposição ântero-posterior em verde e fibras em disposição supero-inferior em azul.

Comparando mapas, o mapa de FA informa somente sobre a magnitude da anisotropia, enquanto o mapa de FA colorido confere informação sobre a magnitude e a direcionalidade da anisotropia do tecido.

Estes mapas de FA denotam de maneira bastante acurada a anatomia dos grandes feixes de substância branca. Entretanto, quando um determinado voxel contém segmento de dois ou mais sistemas de feixes cruzando (ou simplesmente muito próximos), o modelo pode falhar por não discriminar mais de um sistema de fibras presente dentro de um mesmo voxel. Técnicas e modelos mais recentes para o cálculo do tensor de difusão surgiram em uma tentativa de minimizar esta limitação, como a difusão angular ou espectral (HAGMANN et al., 2006).

1.5.3 FASCIGRAFIA

A fascigrafia, como um desmembramento da DTI, permite a construção, por computação gráfica, de linhas que representam os feixes de SB *in vivo*. Tais linhas são construídas obedecendo à difusão predominante voxel a voxel. O princípio básico da fascigrafia pode ser resumido em decifrar matematicamente as características da arquitetura do tecido ao integrar as vias que possuam a maior coerência de difusão possível. Nesta concepção, por métodos computacionais de pós-processamento de DTI, certos *softwares* possuem algoritmos que utilizam informações como FA e o vetor principal de um voxel (ponto de partida) para determinar que outro voxel, dentre os adjacentes, possui maior probabilidade de representar continuidade com o ponto de início. Este estratégia é chamada FACT (*Fiber Assignment by Continuous Tracking*). O traçado começa em um voxel selecionado, e é interrompido quando encontra um voxel com FA menor ou o ângulo de deflexão maior do que foi estipulado pelo usuário como limite (*"threshold"* ou limiar) (**Figura 10**).

Figura 10: Vetor principal e algoritmo de fascigrafia

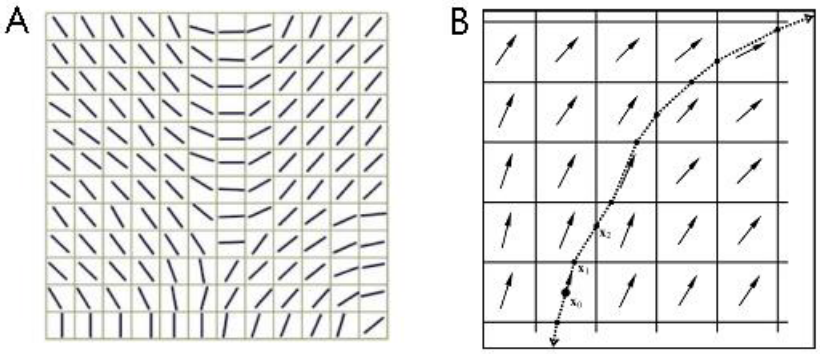

Figura 10: A. Representação do vetor principal em cada voxel (quadrados correspondentes ao volume de tecido examinado); **B.** Algoritmo de fascigrafia. Cada quadrado representa um voxel. As setas representam o vetor principal (*eigenvector*), o que o corresponde ao eixo principal da elipsóide que representa o tensor em cada voxel.

Uma outra estratégia, chamada “força-bruta”, permite maior abrangência do feixe selecionado. Esta técnica permite a identificação de bifurcações, mas requer operações de seleção de feixes em várias etapas, utilizando múltiplas regiões de interesse (ROI) (**Figura 11**).

Figura 11: Esquema representando a utilização de múltiplas regiões de interesse

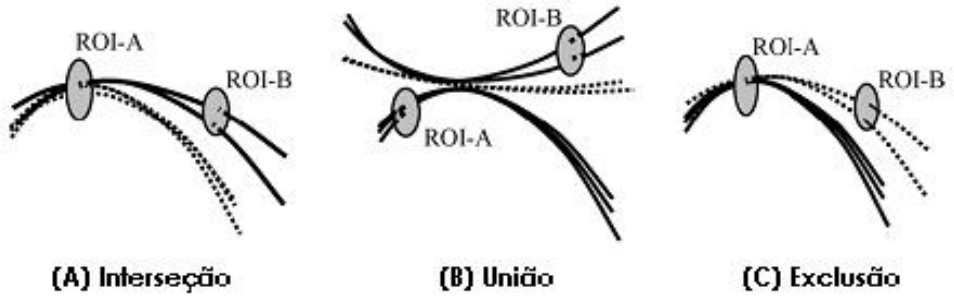

Figura 11: As fibras selecionadas são representadas por linhas contínuas. **A.** Operação booleana de tipo **Interseção**: o feixe selecionado deve passar por ambas as regiões de interesse (ROI): ROI-A **e** ROI-B; **B.** Operação de tipo **União**: o feixe selecionado deve passar pela ROI-A **ou** o ROI-B; **c.** Operação de tipo **Exclusão**: o feixe selecionado deve passar pela ROI-A e não deve passar pela ROI-B. (Adaptado de JIANG et al., 2006).

1.5.4 VALIDAÇÃO DO MÉTODO COM BASE EM MODELOS PATOLÓGICOS – IDENTIFICAÇÃO DA DESESTRUTURAÇÃO DO TECIDO CEREBRAL POR DTI

Nas seções abaixo, são descritos três estudos (utilizando DTI e estratégias de fascigrafia) desenvolvidos em paralelo à presente tese. São estudos clínicos em que a montagem de protocolos de investigação clínica e aquisição e processamento de dados de imagem contribuíram para a verificação e refinamento dos métodos utilizados nesta tese.

a) Aplicação do estudo por DTI na investigação da doença desmielinizante - Esclerose Múltipla: uma patologia de substância branca? [V. Anexo 1]

Como discutido anteriormente, a DTI nos possibilita quantificar o grau de organização do tecido cerebral *in vivo*. Desta forma, através de medidas quantitativas de FA e difusibilidade média (DM), o grau de alteração em diversas patologias também pode ser mensurado (FILIPPI et al., 2001; BRIELLMANN et al., 2003; SALAT et al., 2005; GE et al., 2005). A técnica é sensível o suficiente para detectar alterações sutis, muitas vezes não evidentes em técnicas de RM convencionais (CICCARELI et al., 2001). Estudamos o tecido aparentemente normal do tálamo de pacientes portadores de esclerose múltipla e em controles pareados para sexo e idade com DTI. Nesse estudo estabelecemos desenho do protocolo de investigação clínica e de imagem. Aplicamos técnicas de pós-processamento para cálculo do tensor de difusão, com criação de mapas de FA e DM, e estabelecemos a sistemática para a quantificação destes parâmetros nos sujeitos estudados, bem como suas relações com parâmetros clínicos. Um resumo dos objetivos e metodologia do estudo é descrito a seguir.

Resumo: A RM revolucionou o diagnóstico e acompanhamento de pacientes com esclerose múltipla (EM), ao possibilitar a precisa detecção e quantificação das lesões focais de substância branca (SB) *in vivo*. A presença e volume de tais lesões, entretanto, somente se correlaciona moderadamente com os sintomas apresentados por pacientes acometidos pela doença (BARKHOF et al., 1999; MCFARLAND et al., 2002). Baseados no reconhecimento das limitações das técnicas convencionais de RM e nos crescentes avanços dos conhecimentos em neuroimunologia e patologia da EM, vários autores têm direcionado sua atenção para o estudo da substância branca (SB) e cinzenta (SC) aparentemente normais, numa tentativa de melhor explicar a sintomatologia dos pacientes (BAGNATO et al., 2003).

Apesar de classicamente considerada uma patologia de SB, estudos *post-mortem* e *in vivo* demonstraram que a SC também se encontra acometida na EM. Lesões focais e acometimento difuso microscópico em tecido aparentemente normal foram demonstrados no córtex e na SC profunda destes pacientes (CIFELLI et al., 1998; KUTZELNIGG et al. 2005). Lesões talâmicas, em particular, são críticas devido à importância funcional do tálamo, podendo ser relacionadas ao comprometimento de funções motoras e cognitivas (ALEXANDER et al., 1986). Ainda, uma vez que os axônios talâmicos conectam estruturas subcorticais a regiões específicas no córtex, atravessando a SB, é possível que tanto lesões diretas como indiretas, induzidas por degeneração axonal secundária a lesões de SB, estejam presentes no tálamo de pacientes com EM.

Técnicas avançadas de RM, como procedimentos de alta resolução, espectroscopia e difusão, foram utilizadas para estudar o envolvimento do tálamo na EM (RICHERT et al., 1998; GRIFFIN et al., 2001; SHARMA et al., 2006; IGLESE et al.,

2004; GEURTS et al., 2006). Tais estudos, entretanto, demonstraram resultados inconstantes e o grau de acometimento do tálamo e sua correlação com a apresentação clínica em pacientes permanecem obscuros. Em estudo conduzido no departamento de neuroimunologia dos Institutos Nacionais de Saúde (NIH), em Bethesda (Maryland/EUA), investigamos a sensibilidade da técnica de Imagem do Tensor de Difusão em detectar alterações do tecido talâmico aparentemente normal em pacientes com EM. Alterações nos parâmetros derivados de DTI, a FA e a DM foram correlacionadas com alterações clínicas dos pacientes, medidas através de escalas validadas: EDSS (*Expanded Disability Status Scale*) e escala de avaliação cognitiva (*Paced Auditory Serial Addition Task - PASAT*). Para investigar a correlação das alterações talâmicas com lesões focais presentes na SB e com atrofia cerebral, os valores de FA e DM também foram correlacionados, respectivamente, com volume de lesões focais presentes em imagens de RM convencional ponderadas em T1 e T2 e com medidas de volume cerebral (*Brain Parenchimal Fraction – BPF*). A metodologia e principais resultados do estudo são resumidos no Anexo 1.

b) Identificação da desestruturação do tecido cerebral por DTI: comparação baseada em voxel – disfonia espasmódica **[Anexo 2]**

O estudo da estrutura do tecido por DTI em casos individuais, por região de interesse (ROI), tem sido explorada em diferentes patologias cerebrais (O'SULLIVAN et al., 2004; PIERPAOLI et al., 2001). Este procedimento, entretanto, além de dispender tempo considerável e muito trabalho manual, possui a desvantagem de introduzir a possibilidade de erro dependente de operador. Mais recentemente, técnicas de pós-processamento foram desenvolvidas possibilitando a análise de parâmetros derivados do tensor de difusão, como FA ou DM, baseados em voxel. Tal técnica permite a

comparação estatística de estruturas cerebrais entre grupos de maneira automática através de *softwares* que garantem um registro fidedigno das imagens anatômicas e dos mapas derivados da DTI (SMITH et al., 2006). A metodologia, conhecida como TBSS (*tract-based spatial statistics*), tem se mostrado eficaz na identificação de alterações estruturais e tem contribuído para o entendimento da fisiopatologia de diversas patologias (DOUAUD et al., 2007; KARLSGODT et al., 2007). Estudamos pacientes portadores de disfonia espasmódica, patologia cujas bases anátomo-patológicas ainda se encontram obscuras. Pacientes e controles foram estudados pelo método de DTI, e os dados foram analisados através de ROIs e TBSS. A metodologia e resultados do estudo são descritos no Anexo 2, artigo aceito para publicação na revista *Brain*. A mesma metodologia era aplicada a outras patologias com o intuito de identificar alterações comuns entre os pacientes quando comparados aos indivíduos-controles (DOUAUD, 2007). Como mencionado no capítulo 8, a expertise nesta técnica revelou-se útil na análise de alterações estruturais de vários feixes de SB em pacientes com DCC.

c) Fascigrafia - Identificação do deslocamento ou degeneração dos feixes de substância branca por fascigrafia **[Anexo 3]**

A fascigrafia permite a reconstrução *in vivo* de linhas correspondentes aos grandes feixes de SB (MORI et al., 1999). É possível identificar o deslocamento e/ou degeneração dos feixes por um tumor (**Figura 12**) ou o acometimento e possível degeneração walleriana do feixe por acidente vascular cerebral (AVC) (JELLISON, 2004; FIELD, 2004; TOVAR-MOLL et al., 2007).

O estabelecimento eficaz da estratégia de reconstrução dos feixes por fascigrafia pelo método FACT e força-bruta requer a sistematização do procedimento utilizado e a

validação da identificação dos feixes pelo operador (que deve obter um coeficiente de variabilidade satisfatório). Os parâmetros de qualidade necessários adquiridos garantem a confiabilidade das estruturas mapeadas, sejam feixes de SB normais ou anômalos.

Como um exemplo adicional, um estudo de degeneração do feixe piramidal em pacientes com lesões isquêmicas em vários níveis anatômicos é reportado no Anexo 3, artigo publicado na revista *NeuroReport*.

A fascigrafia, em conjunto com os mapas de FA, foi base para a caracterização dos feixes normais e para a investigação de possíveis feixes anômalos nos pacientes com DCC analisados nesta tese. Por meio de reconstruções sucessivas, detalhamos o percurso dos feixes, o que tornou possível sugerir a conectividade dos mesmos. A metodologia específica da tese e os resultados dos feixes analisados encontram-se descritos nos capítulos 5 e 6.

Figura 12: Imagem do Tensor de Difusão e Fascigrafia

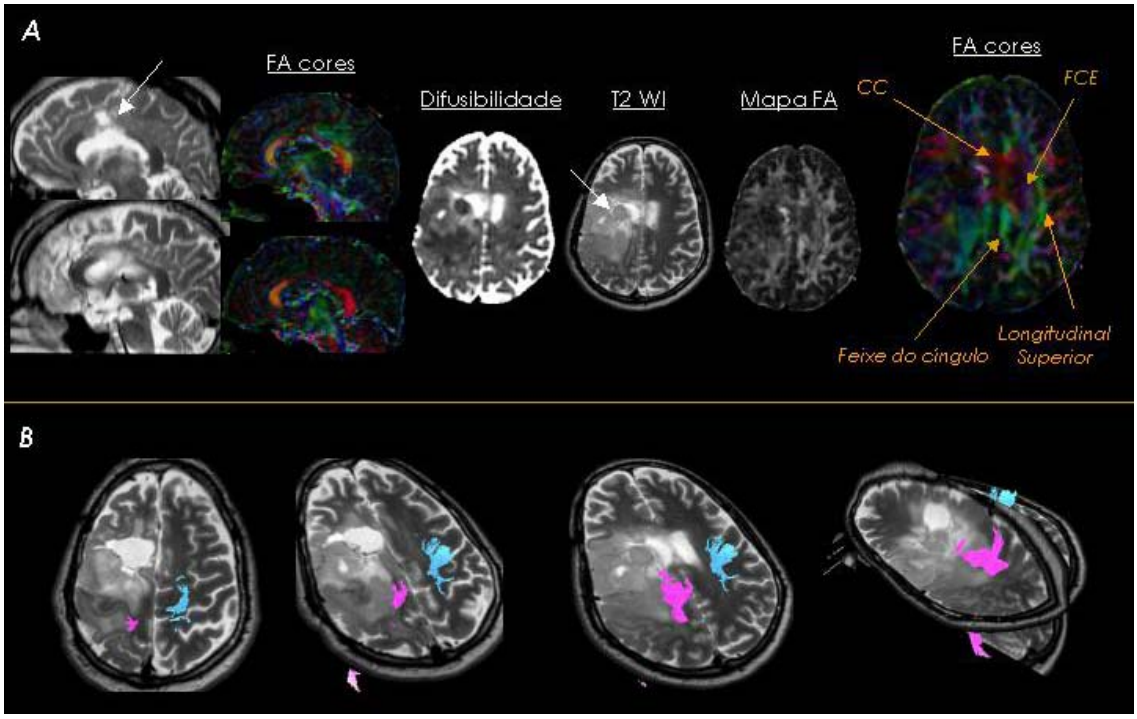

Figura 12: Paciente do sexo masculino, 29 anos, portador de recidiva de astrocitoma grau II. Acometimento dos feixes córtico-espinhal (FCE) e longitudinal superior no hemisfério cerebral esquerdo e no corpo caloso (CC) pela lesão tumoral (setas brancas). **A.** Mapas de anisotropia fracional (FA), FA codificada em cores, difusibilidade e imagem ponderada em T2 (TSE-T2) nos planos axial e sagital; **B.** Reconstrução dos feixes córtico-espinhais direito (azul) e esquerdo (rosa). Feixes projetados em cortes axiais e sagitais de imagens TSE-T2.

2 OBJETIVOS

O objetivo geral desta tese pode ser resumido em estudar a organização estrutural da substância branca na DCC em humanos e investigar evidências de neuroplasticidade presentes nestes indivíduos.

Mais precisamente, no presente estudo, utilizamos a técnica de DTI e fascigrafia para explorar as questões específicas resumidas e enumeradas a seguir:

(i) investigar a anatomia e a trajetória das fibras calosas no grupo controle;

(ii) estudar a anatomia de pacientes com DCC e investigar presença e trajetória dos FP nestes pacientes;

(iii) investigar existência de circuitos aberrantes até então não descritos nos pacientes com DCC;

(iv) estudar trajetória e conectividade de fibras do remanescente caloso em pacientes com DCC parcial.

3 METODOLOGIA

Seleção de pacientes e controles

Exame retrospectivo de prontuários e banco de dados do Hospital Fernandes Figueira resultou em listagem inicial de 48 pacientes com diagnóstico provável de disgenesia do CC, nascidos entre os anos de 1990 e 2002. Após confirmação de endereços e efetuados os respectivos contatos, 11 pacientes com provável DCC foram estudados prospectivamente. Um paciente (Paciente 4), incluído depois, era pai de dois pacientes da coorte inicial (Pacientes 2 e 3).

Todos os indivíduos ou respectivos responsáveis, no caso dos menores de 18 anos, foram informados e consentiram livremente com o procedimento (DECLARAÇÃO DE HELSINKI, 2000). Um paciente submetido ao protocolo de investigação foi posteriormente excluído do estudo porque seu CC se encontrava normal ao exame à RM.

O grupo controle constituiu-se de indivíduos normais sem história de distúrbios neurológicos (idade variando de 10 a 40 anos).

Pacientes e controles foram investigados por meio de:

1. Exame clínico e neurológico: todos os participantes foram submetidos a exame neurológico convencional. O exame neurológico se deteve na acuidade visual e auditiva, na preferência manual, no perímetro cefálico, peso e altura, na capacidade de sentar, levantar e andar de maneira independente, e no exame do equilíbrio dinâmico (observado durante a locomoção natural) e do equilíbrio estático (aferido pela pesquisa do sinal de Romberg e pelo “teste do empurrão”). A compreensão verbal e o uso de objetos e utensílios comuns foram

atentamente observados durante todo o período de interação com os examinadores, com o objetivo de se detectar distúrbios afásicos, apráxicos e agnósicos de magnitude suficiente para interferir nas atividades cotidianas. Atenção particular foi igualmente emprestada a malformações da cabeça, tronco ou membros, e a possíveis antecedentes familiares de doenças neurológicas e neuropsiquiátricas. Finalmente, história e duração gestacionais foram colhidas, com ênfase para intercorrências no primeiro trimestre, assim como para as condições do feto no momento do parto e nos dias que o precederam e sucederam de imediato.

2. Exame de RM de encéfalo em alto campo (1,5 Tesla), realizada no Serviço de Radiodiagnóstico do LABS – Exames Complementares em Medicina.

Protocolo de neuroimagem

1. Imagens anatômicas obtidas com as seguintes seqüências de pulso: spin-eco ponderada em T1 (TR / TE / Matriz /FOV = 550ms / 20ms / 256x256 / 240mm), turbo spin-eco ponderada em T2 (TR / TE / Matriz / FOV = 3500ms / 90ms / 256x256 / 256mm), seqüência ponderada em T1 com pulso de inversão-recuperação (IR) (TR / TE / TI / Matriz / FOV = 3000ms / 30ms / 300ms / 256x256 / 256mm), e FLAIR (TR / TE / TI / Matriz / FOV = 9000ms / 100ms / 2300ms / 256x256 / 256mm). Todas as seqüências adquiridas com cortes axiais contínuos de 5mm de espessura.

2. Imagens ponderadas em difusão (IPD) com seqüência eco-planar *single-shot* adquiridas em planos axial e sagital: (i) Axial: TR/TE = 4000/110ms, FOV = 256mm, matriz = 112x128, cortes contínuos de 5mm de espessura; (ii) Sagital: TR/TE =

4491/121ms, FOV = 256mm, matriz = 112x128, cortes contínuos de 5mm de espessura. Gradientes de difusão são aplicados em seis direções não-colineares (x, y, z, xy, yz, xz) (b=800 sec/mm²) e as imagens pós-processadas utilizando-se *software* de fascigrafia (Plataforma PRIDE, Fiber Track 4,1/Philips Medical Systems).

Descrição mais detalhada da metodologia utilizada se encontra no Anexo 4.

4 RESULTADOS: NEUROPLASTICIDADE NA DISGENESIA DO CORPO CALOSO EM HUMANOS [ANEXO 4]

Os seguintes tópicos de resultados citados abaixo são detalhados e discutidos no artigo em anexo (Anexo 4), publicado na revista *Cerebral Cortex:*

1. **Descrição anatômica e alterações em pacientes com DCC**. Imagens anatômicas de RM convencional revelaram anomalias tipicamente encontradas na DCC, incluindo paralelismo dos ventrículos laterais com colpocefalia, eversão do giro do cíngulo e formação dos FP. As características clínicas e principais achados de imagem dos pacientes se encontram sumariados na Figura 1 do artigo em anexo (Anexo 4).

2. **Organição topográfica de fibras calosas em indivíduos normais**. No presente estudo, demonstramos por DTI/fascigrafia uma organização topográfica crânio-caudal de fibras calosas em indivíduos normais, reproduzindo resultados recentemente publicados por outros grupos (XU et al., 2002; ABE et al., 2004; DE LACOSTE et al., 1985). Demonstramos também evidências de distribuição dorso-ventral das fibras no CC normal, que se relaciona com a origem medial ou lateral dos axônios que se projetam em direção à linha média e a cruzam através do CC.

3. **Organização topográfica de fibras calosas em pacientes com agenesia parcial ou hipoplasia do corpo caloso**. Demonstramos que em pacientes com agenesia parcial ou hipoplasia do CC, o remanescente caloso parece manter a organização crânio-caudal do CC normal, contendo fibras de regiões anatômicas esperadas, se comparados a segmentos a que se correspondem em corpos calosos normais.

4. **Feixes de Probst**. Os FP foram encontrados em cinco pacientes, dois com disgenesia total e três com disgenesia parcial do CC. Os FP atingiram alvos corticais

semelhantes aos das fibras calosas de indivíduos normais. Evidenciou-se, também, organização topográfica das fibras nos FP, relacionada às regiões corticais por estas conectadas.

5. **Evidências adicionais de neuroplasticidade**. Além do FP, em 4 dos 7 pacientes com agenesia parcial do CC foi evidenciado um feixe anômalo ligando o lobo frontal ao córtex occipital contralateral através do remanescente caloso. Este feixe **'sigmóide'** provou-se fortemente assimétrico, não sendo identificado, ou apresentando dimensões reduzidas, no lado oposto do cérebro. Este achado sugere que o cérebro de indivíduos com DCC pode sofrer extensa neuroplasticidade, incluindo a formação de feixes anômalos, compactos e longos, conectando regiões corticais distantes. As implicações clínicas destes feixes, assim como dos FP, são desconhecidas.

5 DISCUSSÃO

O CC é o maior feixe comissural no cérebro humano. Em adultos, lesões do CC, em especial a sua transecção cirúrgica, levam à clássica síndrome de desconexão inter-hemisférica (SPERRY, 1970). Pacientes com agenesia do CC, no entanto, usualmente não apresentam a síndrome clássica de desconexão inter-hemisférica (LASSONDE et al., 1991). Em contrapartida, a expressão clínica da DCC, mesmo isolada, pode variar da ausência total de manifestações a graves alterações cognitivas (LASSONDE et al., 2003). É interessante que esta variabilidade clínica não parece ser fortemente correlacionada com as características anatômicas macroscópicas do cérebro desses pacientes, sugerindo que as alterações críticas se dão em nível mais sutil, inacessível às técnicas empregadas até então. Apesar de a DCC ter sido extensamente explorada em animais, estudos em humanos têm se limitado a descrições anatômicas *post-mortem* ou em imagens de RM convencional. Mais recentemente, a DTI e a fascigrafia proporcionaram método eficaz para caracterizar alterações mais sutis na estrutura da SB *in vivo*. Como pudemos observar, este método permitiu a identificação de alterações plásticas associadas à formação de feixes aberrantes no cérebro humano.

Durante o desenvolvimento, os axônios do CC crescem percorrendo grandes distâncias até alcançarem seus destinos. Saindo do córtex de origem, cruzam a linha média guiados por mecanismos intrínsecos, células específicas e gradientes moleculares atrativos ou repulsivos, seguindo mecanismo integrado que garante a formação integral da comissura (POLLEUX et al., 1998, SERAFINI et al., 1995; BAGNARD et al., 1998; HU et al., 2003; UZIEL et al., 2006; SHU e RICHARDS, 2001;

RICHARDS, 2002; RICHARDS et al., 2004; LENT et al., 2005). O processo inicial de busca e cruzamento da linha média parece ser feito por axônios “pioneiros” originários no córtex do cíngulo (KOESTER e O’LEARY, 1994; RASH e RICHARDS, 2001; OZAKI e WAHLSTEN, 1998), enquanto a massa dos axônios comissurais calosos presumivelmente seguem os pioneiros em seqüência ordenada. Os mecanismos que regulam a sinalização e o crescimento dos axônios calosos no hemisfério contralateral são pouco conhecidos. Sabe-se que os axônios atingem seus alvos majoritariamente homotópicos, e que o estabelecimento do padrão maduro de projeções calosas envolve o crescimento transitório de axônios supranumerários, seletivamente eliminados mais tarde (INNOCENTI e PRICE, 2005) (*para detalhes rever o capítulo 3*). Intensamente explorados em modelos animais, estes mecanismos foram somente indiretamente descritos em humanos. Envolvimento de estruturas celulares e fatores da linha média no processo de formação do CC foram descritos em fetos humanos (LENT et al., 2005). Em coerência com modelos animais, a redução perinatal do volume de conexões calosas também foi sugerida em humanos, através de estudos da redução da área seccional do CC (CLARKE et al., 1989) ou de medidas do córtex ou CC por RM (KESHAVAN et al., 2002; THOMPSON et al., 2000).

Ainda que teorias clássicas descrevam um gradiente rostro-caudal de formação do CC (em que o segmento do joelho se formaria inicialmente ao redor da 11-12^{a} semana de gestação) (RAKIC e YAKOVLEV, 1968), outra teoria propõe a origem bicêntrica do CC, com o setor mais rostral formando-se a partir da lâmina terminal (“*terminalis”*), e uma região mais caudal aparecendo simultaneamente sobre a comissura hipocampal (KIER e TRUWIT, 1996; 1997). Em casos de disgenesia parcial do CC, em que um remanescente caloso está presente, este normalmente encontra-se

na posição topográfica do joelho, o que favorece a teoria de um gradiente rostro-caudal e não bi-cêntrico de desenvolvimento (RICHARDS et al., 2004). Nestes casos de DCC, os fatores envolvidos na gênese dos segmentos rostrais do CC estariam preservados, como por exemplo, o cruzamento de axônios pioneiros do cíngulo ou moléculas envolvidas particularmente nestas porções. Isto poderia ser explicado se diferentes fatores estivessem envolvidos na formação dos diferentes segmentos do CC. Ainda de acordo com o gradiente rostro-caudal de formação do CC, um evento patológico poderia bloquear o cruzamento axonal após a formação do joelho, garantindo a formação deste segmento, em detrimento do cruzamento de fibras dos segmentos mais posteriores.

Ainda que não chegando a seus alvos finais de maneira correta, existem várias evidências de que os neurônios do CC sobrevivem em casos de DCC, projetando, entretanto, axônios para alvos normais (remanescente caloso) ou anormais (FP) (**Figura 13**). Assim, os feixes reconstruídos a partir da DTI e fascigrafia, podem contribuir para o entendimento sobre o possível grau de reorganização cerebral na DCC. O fato de que um CC hipoplásico existe em alguns casos, enquanto um pequeno remanescente está localizado rostralmente em outros, levanta a questão de se as fibras contidas nestes feixes menores manteria o padrão usual de conectividade, observado em indivíduos normais (rigidez), ou teriam seu território de conectividade aumentado (plasticidade), ocupando regiões que foram deixadas “vazias” pela ausência de fibras calosas normais. Com base em nossos resultados, a primeira hipótese parece ser mais provável, uma vez que a maior parte das fibras nos remanescentes rostrais realmente parecem conectar os lobos frontais de uma forma muito específica e focalizada (**Figura 14**), e não parecem invadir outros territórios, exceto em certas situações particulares,

comentadas a seguir. Achados semelhantes têm sido relatados em modelos de camundongos com DCC (OLAVARRIA et al., 1988).

Figura 13: Conformação do feixe de Probst

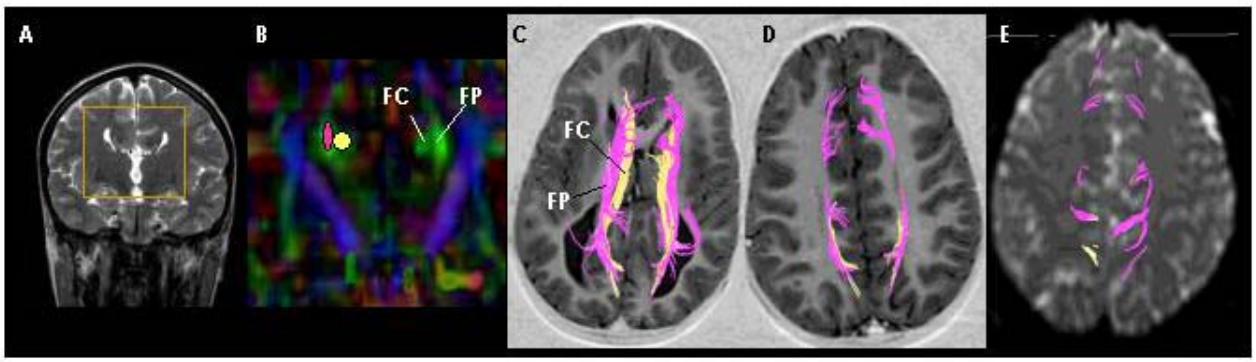

Figura 13: A. Imagem de RM ponderada em T2 no plano coronal. Detalhe (quadrado) indica região correspondente à de maior aumento em **B**. **B**. Mapa de FA codificada em cores segundo orientação dos feixes no plano coronal, com feixe do cíngulo (**FC**) e feixe de Probst (**FP**) codificados em verde. ROIs coloridos foram posicionados no FC (amarelo) e no FP (rosa) à esquerda para fascigrafia. **C-E**. Fibras dos FC (amarelo) e FP (rosa) reconstruídas bilateralmente e projetadas em imagens de RM ponderadas em T2 no planos axial.

Figura 14: Disposição das fibras do remanescente caloso

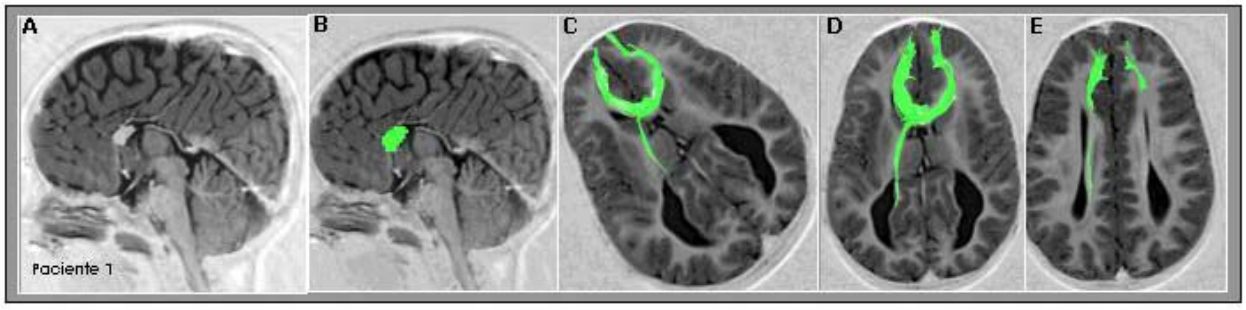

Figura 14: A. Ressonância magnética (RM) ponderada em T1 no plano sagital (linha média) de paciente com disgenesia parcial do corpo caloso (CC). **B.** Região de interesse (ROI) em verde utilizada para a reconstrução das fibras do remanescente caloso. **C-E.** Fibras do remanescente reconstruídas por fascigrafia (fibras em verde).

A topografia no CC normal tem sido demonstrada em animais (BARBAS e PANDYA, 1984; CIPOLLONI e PANDYA, 1985; ROCKLAND e PANDYA, 1986; OLAVARRIA et al., 1988; NAKAMURA e KANASEKI, 1989; MATSUNAMI et al., 1994) e em humanos (XU et al., 2002; ABE et al., 2004; DE LACOSTE et al., 1985). Como descrito no capítulo 2, existe um gradiente rostro-caudal de distribuição topográfica das fibras do CC. Assim, por exemplo, as regiões pré-frontais estão conectadas através do joelho, as parietais através do corpo, e as occipitais pelo esplênio (**Figura 16**). Além disso, uma topografia dorso-ventral das fibras calosas pode ser identificada, em que fibras mediais corticais cruzam dorsalmente dentro do CC, enquanto axônios mais laterais ocupam os setores ventrais do CC (**Figura 15**).

Figura 15: Segmentação topográfica do CC normal

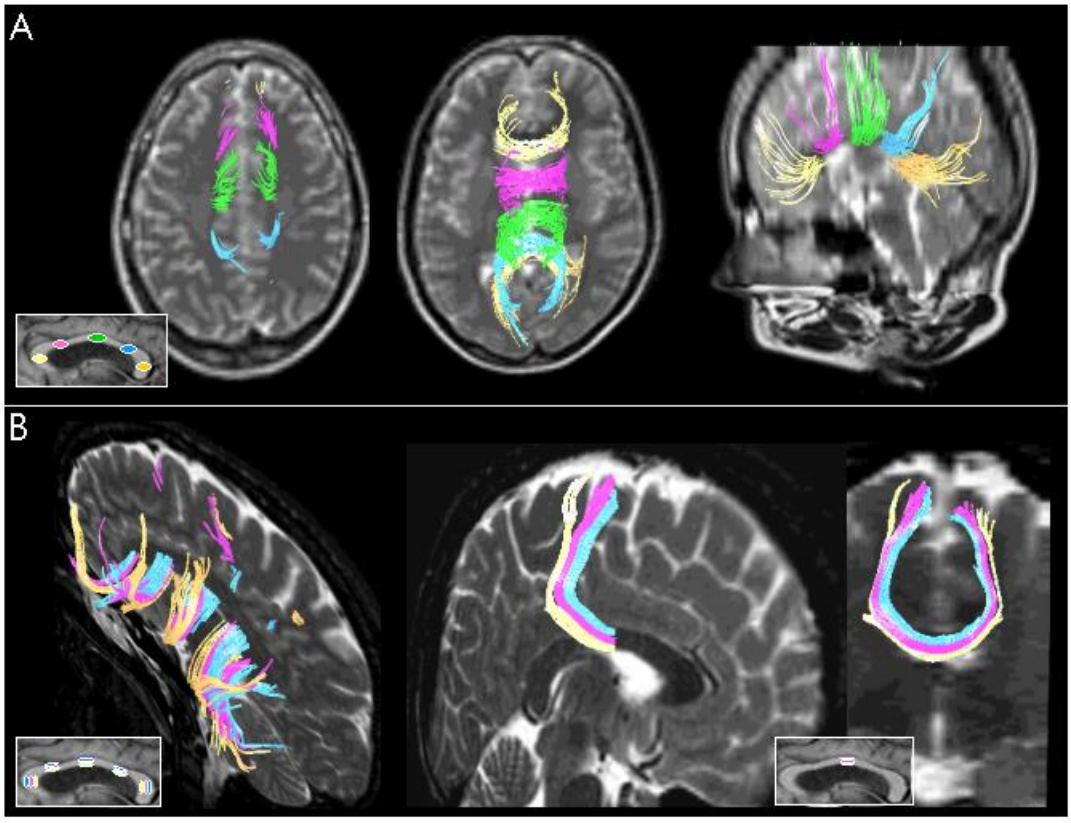

Figura 15: A. Em detalhe, o posicionamento rostro-caudal dos ROIs coloridos ao longo do eixo longitudinal do CC para a reconstrução de fibras (identificadas com cores de acordo com o ROI correspondente). **B**. Em detalhe, o posicionamento dorso-ventral dos ROIs coloridos ao longo do eixo transverso do CC para a reconstrução de fibras (identificadas com cores de acordo com o ROI correspondente). Fibras reconstruídas projetadas em imagens de RM ponderadas em T2 nos planos axial, sagital e coronal.

Outra observação importante em nossos resultados sugere que, a exemplo do CC normal, estruturas anômalas presentes nos pacientes com DCC parecem manter uma certa ordenação topográfica de suas fibras. Isto é o que parece ocorrer nos remanescentes calosos (**Figura 16**) e nos FP (**Figura 17**).

A manutenção de uma ordem topográfica do nos FP (**Figura 17**) semelhante à de CC (**Figura 15**), sugere que as fibras do FP podem estar obedecendo a sinais intrínsecos do feixe, suficientes para tal organização e independentes do trajeto ou do meio externo.

Figura 16: Segmentação topográfica do remanescente caloso na DCC

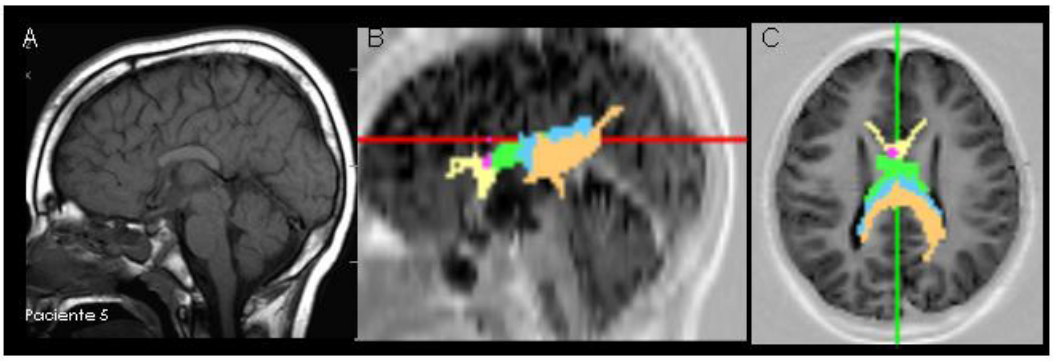

Figura 16: Disposição topográfica de fibras calosas em um caso de hipoplasia do CC (**A**). **B-C**. observa-se o padrão topográfico de fibras mantido na hipoplasia do CC. As linhas coloridas representam o plano transversal (em vermelho, em **B**) e o plano sagital (em verde, em **C**).

Figura 17*:* Segmentação do Feixe de Probst

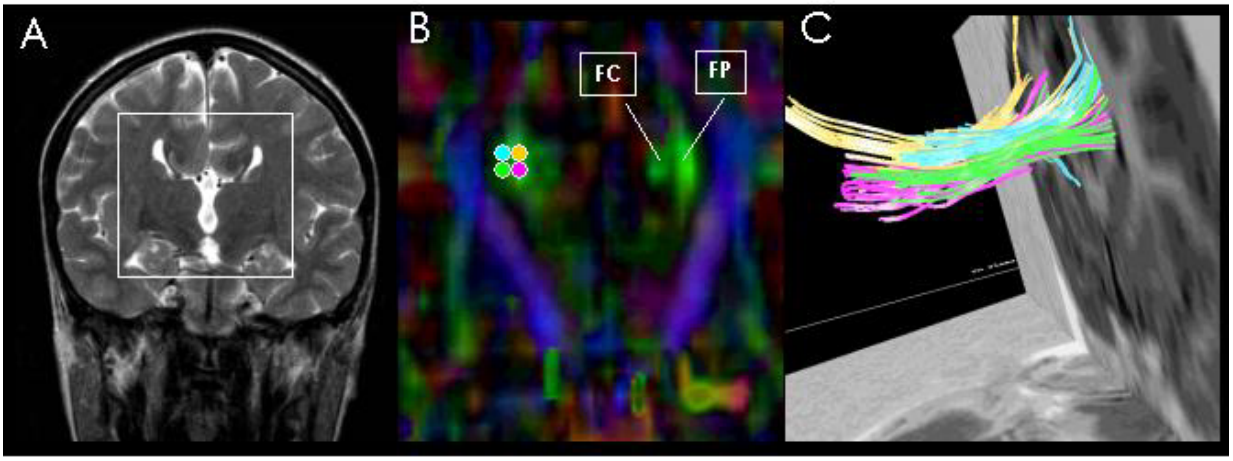

Figura 17: A. Imagem de RM ponderada em T2 no plano coronal. Detalhe (quadrado) indica região ampliada em **B**. **B**. Mapa de FA codificado em cores segundo orientação dos feixes no plano coronal, com o feixe do cíngulo (**FC**) e o feixe de Probst (**FP**) codificados em verde. Quatro ROIs coloridos foram posicionados no FP esquerdo. **C**. Fibras dos FP exibindo uma organização topográfica dorso-ventral e médio-lateral. Fibras em plano sagital projetadas sobre imagem de RM ponderada em T2 no plano coronal e angulada para melhor visualização.

Um exemplo de reestruturação plástica de conexões calosas deriva dos feixes robustos e aberrantes que se formam em muitos casos de DCC: os FP (PROBST, 1901), extensamente estudados em modelos animais (LENT, 1982; 1983; OZAKI et al., 1987; 1989; OZAKI e SHIMADA, 1988; OZAKI e WAHLSTEN, 1993). Em humanos, os FP são consistentemente observados em casos de DCC (LASSONDE et al., 2003). Em roedores, os FP usualmente mostram trajetórias tortuosas, saindo e retornando ao feixe, e eventualmente atravessando a linha média através do septo (LENT, 1982; 1983), sendo descritas conexões em forma de U nos setores mediais do córtex ipsilateral. A maioria dos autores assume que os FP são formados por fibras calosas cuja passagem pela linha média foi impedida durante o desenvolvimento. As semelhanças topográficas entre os alvos corticais do CC normal e das conexões

ipsilaterais estabelecidas pelos FP em animais e, de acordo com os nossos achados, em humanos, fortemente apoiam esta possibilidade (**Figura 18**).

Figura 18: Comparação dos alvos corticais de fibras calosas normais com os alvos corticais do Feixe de Probst

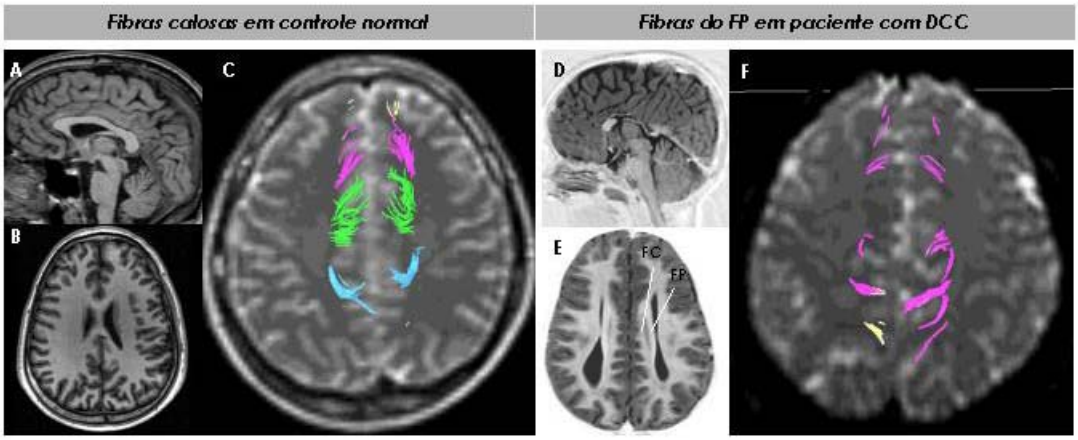

Figura 18: A-C. Conformação do CC normal. Imagens de RM ponderadas em T1 no plano sagital (**A**) e axial (**B**) de indivíduo controle. **C**. Fibras calosas reconstruídas por fascigrafia projetadas em imagem de RM ponderada em T2 no plano axial. **D-F**. Conformação do CC e dos FP em um caso de disgenesia parcial do CC. Remanescente caloso evidenciado em imagem de RM ponderada em T1 no plano sagital (**D**). **E**. imagem de RM ponderada em T1 no plano axial, demonstra relação entre o FP e o feixe do cíngulo (FC). **F**. Fibras do FP (rosa) reconstruídas por fascigrafia projetadas em imagem de RM ponderada em T2 no plano axial. Note a semelhança dos alvos corticais entre as fibras calosas normais (**C**) e as do FP (**F**).

Ainda que a maior parte das fibras do remanescente caloso possua a organização esperada (ao se basear em conexões do joelho em indivíduos normais), algumas parecem assumir uma conformação não usual (ou plástica), ao formar o Feixe Sigmóide aqui descrito e identificado em 4 pacientes com disgenesia parcial ou hipoplasia do CC (**Figura 19**). Este feixe, ainda não identificado histologicamente em animais ou humanos, foi entretanto, recentemente descrito em outro estudo por imagem (RM) (PAUL et al., 2007). Em nosso estudo, a trajetória do feixe sigmóide é descrita,

bem como medidas de controle para eventuais artefatos da técnica. A descrição detalhada da metodologia utilizada, resultados e discussão encontra-se no Anexo 4.

Figura 19*:* Feixe Sigmóide

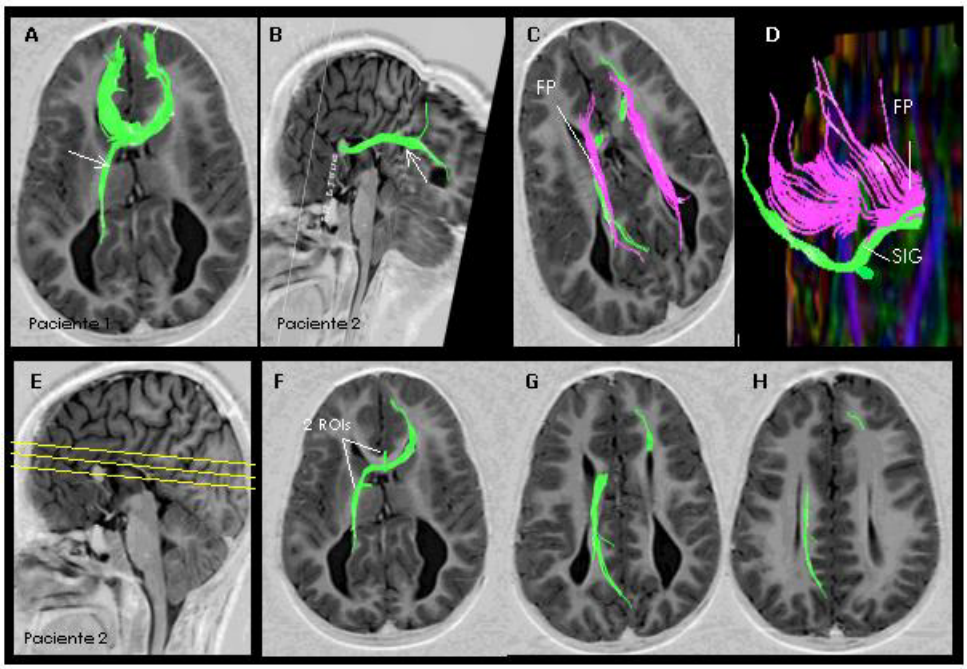

Figura 19: A-H. Reconstrução do Feixe Sigmóide (SIG) por fascigrafia em pacientes com disgenesia parcial do CC. **A-B.** Feixes Sigmóides (seta) projetados em imagens de RM ponderadas em T1 no plano axial (**A**), coronal e sagital (**B**). **C-D**. Relação entre SIG e FP. Feixes projetados em RM ponderadas em T1 no plano axial (**C**) e em mapa de FA codificada em cores no plano coronal (**D**). **E-H**. Detalhe da trajetória do SIG. Projetados em imagens ponderadas em T1 no plano axial. **E**. Imagem ponderada em T1 no plano sagital, indicando a localização das imagens axiais (**F-H**). Em **F**, regiões de interesse utilizadas para a reconstrução do SIG identificado em **F**,**G** e **H**.

Os mecanismos que regulam a trajetória dos feixes nos pacientes com DCC parecem gerar graus variados de plasticidade. Deste modo, em algumas circunstâncias conformações usuais são mantidas, porém em outras, o poder adaptativo do cérebro em desenvolvimento parece permitir a reorganização cerebral e o desenvolvimento de feixes anômalos. A descrição anatômica detalhada destes feixes, aliada à determinação

do papel funcional dos mesmos (e conseqüentes sintomas ou adaptações compensatórias determinadas em cada caso), pode ser uma das chaves para o melhor entendimento do vasto panorama clínico nas DCC.

6 CONCLUSÕES

Neste trabalho, relatamos quatro achados básicos em pacientes com DCC:

(1) *Conectividade do remanescente caloso*: quando havia um remanescente caloso rostral, suas fibras não expandiram seu território de conexão neocortical para outras áreas, como seria de esperar considerando a ampliação do território sináptico disponível pela ausência da maioria das fibras calosas; ao contrário, obedeceram, em sua maioria, o esperado padrão topográfico de conectividade. Assim como nos controles normais, fibras do joelho (no caso, remanescente) restringiram-se a conectar as regiões pré-frontais;

(2) *Manutenção de organização topográfica interna das fibras calosas remanescentes:* os segmentos remanescentes calosos e CC hipoplásicos apresentaram topografia de fibras compatível com um CC normal, conectando as áreas neocorticais esperadas;

(3) *Neuroplasticidade — feixes anômalos:* pelo menos dois feixes longos anormais foram formados nos pacientes com anomalias do CC: i) os feixes de Probst, há muito conhecidos, e ii) o feixe sigmóide, aberrante e assimétrico, que conecta o lobo frontal direito ao córtex occípito-parietal contralateral;

(4) *Organização topográfica do Feixe de Probst:* o FP mantém organização topográfica, embora ipsilateral, como as fibras do CC o fazem inter-hemisfericamente.

Nesta tese foi empregada a técnica de DTI na investigação de plasticidade em pacientes com DCC. A metodologia aplicada foi sensível a alterações de reorganização cerebral de grandes feixes de SB, como a caracterização do remanescente caloso (no caso das disgenesias parciais do CC), da conectividade dos FP e mapeamento de um

circuito aberrante não antes descrito. A investigação de plasticidade cerebral com metodologia semelhante foi mais recentemente aplicada para caracterizar feixes anômalos em modelos animais de DCC (REN et al., 2007) e em humanos portadores de outras patologias do desenvolvimento (MARENCO et al., 2007).

A diversidade de apresentação clínica e anatômica dos pacientes com DCC dificulta a elaboração de uma classificação ao mesmo tempo abrangente e lógica. Entretanto, estes pacientes apresentam características clínicas e anatômicas em comum, o que permite agrupá-los. Neste contexto, a reorganização anatômica comprovada em alguns casos de DCC pode ser incluída como sinal característico desta patologia. Revisão recente sobre mecanismos e critérios diagnósticos das DCC enfatizou as alterações neuroplásticas nos pacientes com distúrbio do desenvolvimento do CC, ressaltando a importância dos FP e do feixe sigmóide (PAUL et al., 2007). Nossos resultados e os de estudos relacionados (LEE et al., 2004; REN et al., 2007; PAUL et al., 2007) sugerem que a caracterização destes feixes anômalos requer técnicas avançadas de neuroimagem, como DTI e RM volumétrica. Entretanto, com a disponibilidade crescente de magnetos de RM de alto campo e a disseminação de novas seqüências de pulso e *softwares* de pós-processamento, atualmente estes protocolos de imagem podem ser incorporados à rotina clínica, facilitando a identificação destas alterações anatômicas e o diagnóstico minucioso das DCC.

Os protocolos clínicos e de imagem aplicados na presente tese possuem limitações. Não foi possível a realização de testagem cognitiva específica ou a aquisição de dados eletrofisiológicos. Recursos atuais permitem a execução de protocolos de imagem mais sensíveis às alterações anatômicas sutis que podem estar

presentes nos pacientes com DCC. A seguir, descrevemos alguns pontos relevantes para exploração futura.

7 PERSPECTIVAS FUTURAS: LINHAS DE PROJETOS EM DESENVOLVIMENTO OU A SEREM DESENVOLVIDAS

7.1 INVESTIGAÇÃO DA FUNCIONALIDADE DOS FEIXES ANÔMALOS PRESENTES EM PACIENTES COM DCC

O FP é estrutura relativamente comum e peculiar em pacientes com DCC, que parece derivar de axônios calosos presumivelmente funcionantes. Embora a maior parte das alterações funcionais em pacientes com DCC tenda a ser atribuída à ausência do CC, o papel de estruturas como os FP nos sintomas ou em mecanismos compensatórios destes pacientes ainda é obscuro. O fato de estes feixes serem relativamente prevalentes e mantidos em pacientes com DCC, sugere uma função compensatória ou adaptativa do FP (LASSONDE et. al., 1988; 1991; SAUERWEIN e LASSONDE, 1994; LESSARD et al., 2002). Entretanto, estudos funcionais eletrofisiológicos não foram abordados na presente Tese.

Além do FP, o feixe anômalo sigmóide, que parece conectar o lobo frontal e o córtex occipital contralateral cruzando pelo remanescente caloso, foi mapeado em 4 dos 7 pacientes com disgenesia parcial do CC. No entanto, como os FP, as implicações fisiopatológicas e clínicas deste feixe ainda são desconhecidas.

Estudos eletrofisiológicos, como EEG de alta resolução e múltiplos canais, aliados a dados anatômicos detalhados dos pacientes com DCC, podem contribuir para o estabelecimento da função e importância destes feixes na fisiopatologia das DCC.

Ainda, o estudo específico das funções destes feixes anômalos pode permitir a diferenciação entre alterações plásticas benéficas ou compensatórias, de alterações

disfuncionantes e sintomatogênicas nos pacientes com DCC. Tal conhecimento pode contribuir para o melhor entendimento da ampla gama de manifestações clínicas observadas em pacientes com DCC. Desta forma, caso um determinado feixe anômalo possua um efeito deletério sobre a função cerebral, este pode vir a ser alvo de potencial intervenção terapêutica (por exemplo, transecção cirúrgica).

7.2 APLICAÇÃO DE PROTOCOLOS OTIMIZADOS DE AQUISIÇÃO E/OU PÓS-PROCESSAMENTO DE IMAGEM PARA UM MAIOR DETALHAMENTO DAS ALTERAÇÕES ANATÔMICAS EM PACIENTES COM DCC

Técnicas recentemente desenvolvidas de DTI podem trazer benefícios na investigação dos pacientes com DCC. O exame de DTI pode ser otimizado com aquisições de alta resolução, voxel isotrópico e gradientes de difusão aplicados a um maior número de direções, o que acarreta diretamente aumento na confiabilidade da reconstrução dos feixes por fascigrafia (JONES et al., 1999; MORI et al., 2002). A otimização do protocolo de aquisição pode contribuir para a confirmação e detalhamento da trajetória dos feixes já estudados (FP e sigmóide), bem como para a investigação de outros feixes menos robustos. O desenvolvimento e a aplicação de protocolos de pós-processamento, como a análise baseada em voxel (TBSS–FSL) (SMITH et al., 2006), facilitarão a investigação de alterações comuns aos pacientes com DCC (quando comparados a controles) de maneira randômica.

Além disso, etapas de pós-processamento como correção de movimento, correção de artefato de Eddy-corrente e aquisição de múltiplas seqüências para aumentar a relação sinal-ruído das imagens não foram utilizadas na presente Tese. Estas são estratégias atualmente disponíveis e de eficácia bem estabelecida, podendo

trazer benefícios a futuras análises dos pacientes com DCC. Estes métodos são detalhados no capítulo 4 e nos Anexos 1 e 2.

A aquisição de novos protocolos otimizados de imagem e o investimento em novos métodos de pós-processamento de dados fazem parte de nossas diretrizes futuras.

Na **Figura 20** são demonstrados alguns resultados preliminares de protocolos realizados recentemente e não incluídos entre os resultados da presente Tese. Foram adquiridas imagens ponderadas em difusão (DWI) com seqüência eco-planar single-shot adquiridas em plano axial com cortes contínuos de 2,5 mm de espessura, com voxel isotrópico. Gradientes de difusão foram aplicados em 33 direções não-colineares e foi utilizado *b-factor* elevado – b=1000 sec/mm². A seqüência foi repetida três vezes com o objetivo de aumentar a relação sinal-ruído da imagem.

Figura 20: Resultados preliminares recentes

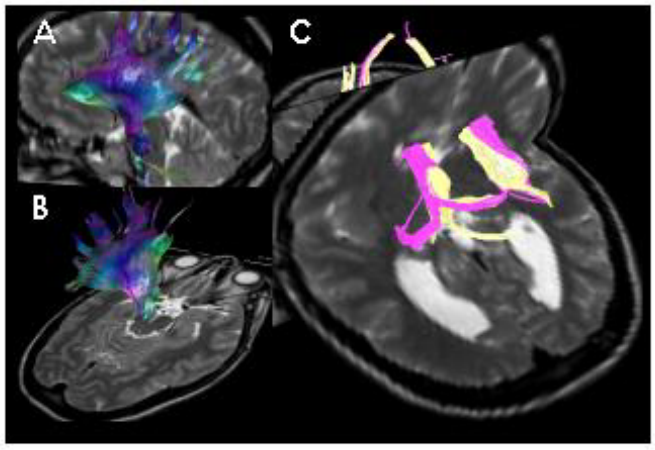

Figura 20: A-C. Exemplo da qualidade da reconstrução de feixes de substância branca em paciente com disgenesia parcial do CC. Resultados obtidos com protocolo recente de aquisição. Feixes projetados em imagens de RM ponderadas em T2 nos planos axial, coronal e sagital. **A-B**. Feixe córtico-espinhal; **C**. Feixe do cíngulo (amarelo) e feixe de Probst (rosa).

7.3 A INVESTIGAÇÃO DE ALTERAÇÕES DA COMISSURA ANTERIOR NA DCC

A comissura anterior (CA) é a primeira comissura telencefálica a ser formada, ao redor da oitava semana de gestação. Devido a limitações do protocolo de imagem, a CA não foi alvo de análise na presente Tese. Entretanto, análise preliminar em nossos pacientes não sugere aumento da CA na maior parte deles. A **Figura 22** apresenta imagens sagitais e axiais de três pacientes com disgenesia parcial do CC.

Figura 21: Presença da comissura anterior nos pacientes com DCC

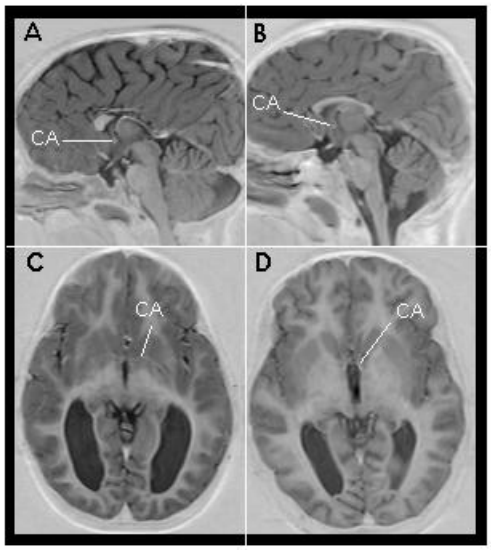

Figura 21: A-D. Imagens de RM ponderadas em T1 de dois casos de pacientes com disgenesia parcial do CC nos planos sagital (**A e B**) e axial (**C-D**). CA, comissura anterior.

Acredita-se que CA poderia ser uma via alternativa, suprindo parte da deficiência de transferência inter-hemisférica em pacientes com DCC. Ainda que a CA possa estar aumentada em alguns pacientes com DCC, os dados são controversos na literatura e estudos de imagem mais recentes reportam aumento de CA em somente 10% dos

pacientes com DCC e, ainda ausência completa ou diminuição em 10% dos casos (BARR et al., 2002). Entretanto, estudos em modelos animais reportam o aumento do número de fibras amielínicas (sem aumento concomitante da área transversa) na CA de camundongos com DCC (LIVY et al., 1997).

Protocolos de técnicas volumétricas de alta resolução e de DTI otimizados podem permitir o estudo acurado do volume (ou da área transversa) e da conectividade da comissura anterior nos pacientes com DCC.

A **Figura 22** demonstra resultados recentes de aquisições de DTI em que o objetivo foi a realização de seqüência com cortes finos e resolução e sinal suficientes para a posterior reconstrução de feixes menos robustos, como a CA. As imagens ponderadas em difusão foram adquiridas com seqüência eco-planar *single-shot* em plano axial, cortes contínuos de 1,5 mm de espessura, com voxel isotrópico. Gradientes de difusão aplicados em 33 direções não-colineares e *b-factor* b=1000 sec/mm².

Figura 22. Protocolo de alta resolução

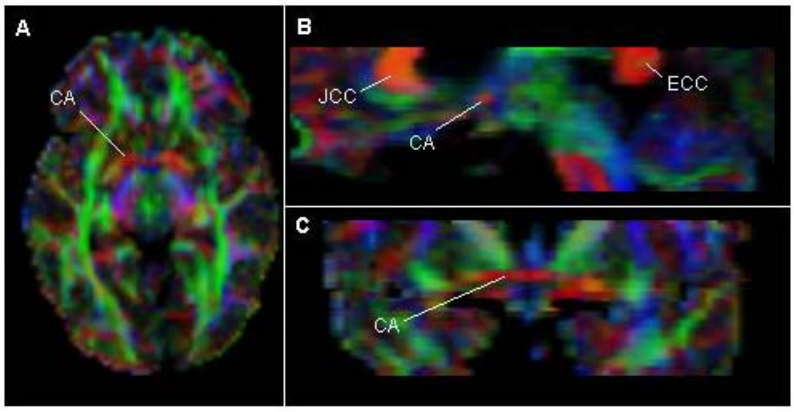

Figura 22: A-C. Mapas de FA codificada em cores segundo orientação dos feixes de voluntário normal nos planos axial (**A**), sagital (**B**) e coronal (**C**). CA, comissura anterior; JCC, joelho do CC; ECC, esplênio do CC.

7.4 ESTUDO DA CORRELAÇÃO ENTRE ALTERAÇÕES ANATÔMICAS DOS PACIENTES COM DCC E FUNÇÕES COGNITIVAS ESPECÍFICAS

Ausência de síndrome de desconexão em casos de DCC (SPERRY et al., 1970) - A despeito da imensa quantidade de estudos voltados à determinação dos caminhos neurais que promovem a integração inter-hemisférica nos casos de DCC (minimizando, ou mesmo anulando, a ocorrência de síndrome de desconexão), esta questão permanece em aberto. A nosso ver, a resposta para esta pergunta-chave se encontra, hoje, ao alcance das tecnologias disponíveis. A possibilidade de quantificação de vias e estruturas subcorticais em pacientes submetidos a tarefas especificamente desenvolvidas para testar a integração inter-hemisférica (ex., práxis intermanual, estimulação visual e visuo-afetiva mono-hemisférica, mensuração de respostas vegetativas periféricas como a resposta galvânica cutânea a estímulos padronizados) deverá, em breve, apontar alguns candidatos prováveis para mediar a integração inter-hemisférica na ausência total ou parcial do CC. O exame do olfato, um dos sentidos mais negligenciados em estudos de integração inter-hemisférica, deverá fornecer resultados únicos, uma vez que um pequeno contingente das projeções centrípetas do bulbo olfativo, majoritariamente ipsilaterais, atravessa a CA e se dirige para as áreas olfativas secundárias contralaterais. Esta característica única do olfato permite determinar o estado funcional da CA e das divisões mais anteriores e basais dos lobos frontal e temporal. A determinação última das vias que compensam a desconexão inter-hemisférica nos casos de DCC poderá ser esclarecida por estudos anatômicos combinados a RMf, que permitiriam estabelecer os respectivos graus de assimetria e dominância hemisférica em tarefas lateralizadas, como, por exemplo, a identificação e a

denominação de objetos apresentados à mão esquerda sem auxílio da visão. Estes estudos deverão ser controlados não apenas pelos resultados obtidos em pessoas normais submetidas aos mesmos protocolos de investigação, mas, sobretudo, em indivíduos submetidos à calosotomia cirúrgica na vida adulta.

Alterações e normalidade cognitiva, afetiva e sócio-ocupacional em indivíduos com DCC - Um dos aspectos mais desafiadores observados em casos de DCC é a fraca, ou inexistente, associação entre as alterações anatômicas individuais e o grau de comprometimento cognitivo, afetivo e sócio-ocupacional (BOSSY, 1970). Diante da freqüência com que a DCC se acompanha de outras malformações, é imprescindível aprofundarmos o conhecimento de casos assintomáticos de agenesia do CC para determinar seu estado neuropsicológico e sócio-ocupacional. A demonstração de que esses indivíduos são, de fato, “assintomáticos” mesmo quando submetidos a provas comportamentais e anatômicas de alta sensibilidade é fundamental para a compreensão dos mecanismos em jogo nos casos sintomáticos.

7.5 ESTUDO DE ALTERAÇÕES GENÉTICAS DOS PACIENTES COM DCC PERTENCENTES À MESMA FAMÍLIA

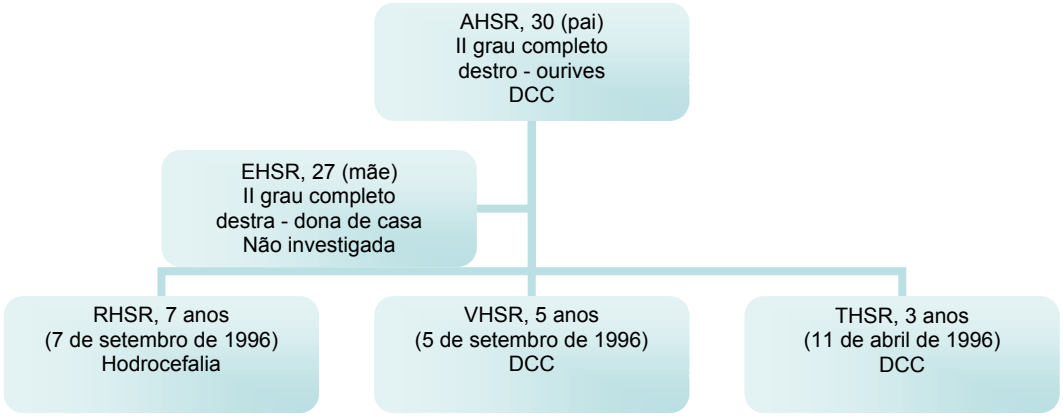

Figura 23: Esquema de representação dos membros da família HSR

Relato breve de VHSR e THSR:

VHSR - (idade da investigação clinica-5 anos)
O mais "agitado" dos três irmãos. Parto a termo, sem intercorrências (Fernandes Figueira). A mãe tomou medicamento no sexto mês para reter o feto. Andou com 9 meses. Falou com 1½; fala muito, mas "embolado". Controle dos esfíncteres aos 3 anos apenas parcial, com enurese noturna quase diariamente. Nunca teve crises convulsivas. Emocionalmente instável, baixo limiar de frustração ("se chateia com tudo"). Quando insatisfeito ou contrariado, se atira no chão e grita. Belisca e bate no irmão mais novo. A agitação se acentuou a partir dos 3 anos de idade. Desatento, distraído e estabanado. Sono agitado, fala dormindo.

THSR – (idade da investigação clínica-3 anos)
Gestação de 9 meses, sem intercorrências. Parto normal (Fernandes Figueira). Submetido a TC de crânio logo que nasceu porque o irmão mais velho RHSR) teve hidrocefalia. Detectada "disgenesia do corpo caloso". Engatinhou com 6 meses. Falou com 1 ano ("papai", "mamãe"). Mamou até 8 meses. Andou com um ano e meio. Bom controle esfincteriano. A mãe tomou medicamento no sexto mês de gravidez para reter o feto. Pede para ir ao banheiro. Entrou na escola no início de 2003. A mãe notou dificuldade e "imaturidade" em trabalhos manuais passados pela escola (incoordenação para cobrir figuras e desenhar). Convulsão febril, isolada, aos 9 meses, após vacina tríplice. Tomou 35 gotas / dia de Gardenal® durante 2 anos. Sem antecedentes familiares de doença neurológica.
Ao exame, destro para manipular objetos (caneta, lanterna). Muito ativo, mexe em tudo ao alcance (ex. interruptor do negatoscópio), vocalizando e gesticulando para a mãe, para dividir suas percepções com ela, ou para pedir ajuda (ex. acender / desligar a lanterna). Quando se

demonstra como proceder, aprende com facilidade e passa a fazê-lo sozinho. Na sala de espera, foi ao filtro e serviu-se de água corretamente e sem ajuda.
Nervos cranianos, marcha, coordenação e equilíbrio normais. Boa expressão facial emocional.

Itens do Denver Development Screening Test:
Capaz de copiar linha vertical (figura). Coloca sandálias, lava e enxuga as mãos, veste-se sozinho mas precisa de ajuda para abotoar; come com colher sem sujar, não larga a mãe, brinca com jogos interativos. Despe-se em parte sozinho. Vê e denomina cores, denomina figuras (cachorro), não usa plural, com dificuldade diz seu primeiro nome. Não pedala velocípede, pula no lugar e para adiante, não fica em um pé só, arremessa bola de cima para baixo, não segue comandos em 3 tempos.

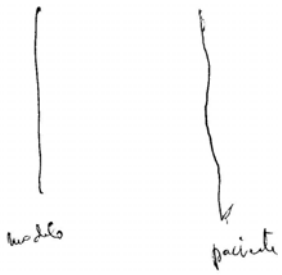

Nesta família foram identificados três portadores de DCC (**Figuras 23 e 24**). A incidência familiar é rara, com a maior parte dos casos com identificação de causa genética relacionada a mutações autossômicas esporádicas. Como relatado no capitulo 3, vários genes foram associados a DCC e poderiam estar envolvidos no caso desta família. Estudo específico de possibilidades genéticas seria interessante com o mapeamento de possíveis genes envolvidos. Para tal, um estudo familiar seria necessário com rastreamento das alterações anatômicas e genéticas no maior número possível de parentes (a mãe, por exemplo, não foi investigada).

Os três pacientes possuem parte do CC: em todos, o joelho está presente, o que sugere que os fatores que determinam o cruzamento inicial dos neurônios calosos rostrais, possivelmente envolvendo, entre outros, neurônios pioneiros do cíngulo, estejam preservados. Dois pacientes possuem FP, o que sugere que fatores iniciais de

emissão de neurônios calosos a partir do córtex estão presentes. Fatores fundamentais para o cruzamento da linha média em porções medianas ou caudais do CC parecem estar comprometidos. Tal comprometimento parece ter graus variados, de modo que um dos descendentes não desenvolveu nem o corpo nem o esplênio do CC, outro descendente não desenvolveu parte do corpo e parte do esplênio, enquanto o progenitor não desenvolveu o esplênio. Isto sugere que, se uma ou mais alterações genéticas estão presentes, sua penetrância é variável.

O estudo do perfil genético desta família pode contribuir para o entendimento do papel de um ou mais dos vários genes e fatores por eles determinados (como moléculas sinalizadoras atrativas ou repulsivas ao crescimento neurítico) envolvidos na formação do CC.

Figura 24: Características anatômicas dos pacientes THSR (paciente 2), VHSR (paciente 3) e AHSR (paciente 4)

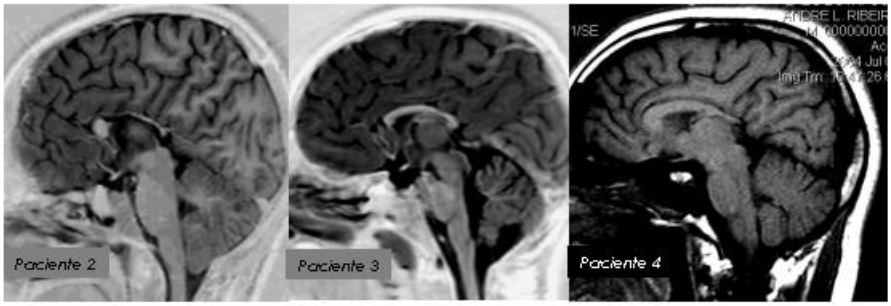

Figura 24: Imagens de RM ponderada em T1 no plano sagital (linha média) evidenciando alteração do CC nos três pacientes com DCC.

8 REFERÊNCIAS

ABE, O.; MASUTANI, Y.; AOKI, S.; YAMASUE, H.; YAMADA, H.; KASAI, K.; MORI, H.; HAYASHI, N.; MASUMOTO, T.; OHTOMO, K. **Topography of the human corpus callosum using diffusion tensor tractography**. J Comput Assist Tomogr, 2004; 28:533-539.

ABOITIZ, F.; LOPEZ, J.; MONTIEL, J. **Long distance communication in the human brain: timing constraints for inter-hemispheric synchrony and the origin of brain lateralization.** Biol Res, 2003; 36: 89-99.

ABOITIZ, F.; SCHEIBEL, A. B.; FISHER, R. S.; ZAIDEL, E. **Fiber composition of the human corpus callosum.** Brain Res. 1992; 598(1-2):143-53.

ABOITIZ, F.; SCHEIBEL, A. B.; FISHER, R. S.; ZAIDEL, E. **Individual differences in brain asymmetries and fiber composition in the human corpus callosum**. Brain Res. 1992; 598(1-2):154-61.

ABOITIZ, F.; IDE, A.; OLIVARES, R. **Corpus callosum morphology in relation to cerebral assymetries in the postmortem human.** The parallel brain: the cognitive neuroscience of the corpus callosum. Zaidel E e Iacoboni M. The Mit Press. 2003. Massachusetts. pp. 33-46.

ALEXANDER, G. E.; DELONG, M. R,; STRICK, P. L. **Parallel organization of functionally segregated circuits linking basal ganglia and cortex.** Annu Rev Neurosci 1986; 9:357-381.

BAGNARD, D.; LOHRUM, M.; UZIEL, D.; PUSCHEL, A. W.; BOLZ, J. **Semaphorins act as attractive and repulsive guidance signals during the development of cortical projections**. Development, 1998; 125: 5043-5053.

BAGNATO, F.; FRANK, J. A. **The role of non-conventional magnetic resonance imaging techniques in demyelinating disorders.** Curr Neurol Neurosci Rep 2003; 3: 238-245.

BARBAS, H.; PANDYA, D. N. **Topography of commissural fibers of the prefrontal cortex in the rhesus monkey.** Exp Brain Res, 1984; 55:187-191.

BARKHOF, F. **MRI in multiple sclerosis: correlation with expanded disability status scale (EDSS).** Mult Scler 1999, 5: 283-286.

BARR, M. S.; CORBALLIS, M. C. **The Role of the Anterior Commissure in Callosal Agenesis.** Neuropsychology, 2002; 16: 459–471.

BASSER, P. J.; MATTIELLO, J.; LEBIHAN, D. **Estimation of the effective self-diffusion tensor from the NMR spin echo.** J Magn Reson B, 1994; 103: 247-254.

BASSER, P. J.; PAJEVIC, S.; PIERPAOLI, C.; DUDA, J.; ALDROUBI, A**. In vivo fiber tractography using DT-MRI data**. Magn Reson Med, 2000; 44:625-632.

BEAULIEU, C.; FENRICH, F. R.; ALLEN, P. S. **Multicomponent water proton transverse relaxation and T2-discriminated water diffusion in myelinated and nonmyelinated nerve**. Magn Reson Imaging. 1998; 16:1201-10.

BEDESCHI, M. F.; BONAGLIA, M. C.; GRASSO, R.; PELLEGRI, A.; GARGHENTINO, R. R.; BATTAGLIA, M. A.; PANARISI, A. M.; ROCCO, M. D.; BALOTTIN, U.; BRESOLIN, N.; BASSI, M. T.; BORGATTI, R. **Agenesis of the Corpus Callosum: Clinical and Genetic Study in 63 Young Patients.** Pediatr Neurol 2006; 34:186-193.

BEHRENS, T. **MR diffusion tractography: methods and applications.** Oxford, 2004. (Dissertação - Tese de doutorado). Oxford Center for Functional Magnetic Resonance Imaging of the Brain and Department of Engineering Science, University of Oxford,

2004.

BERLUCCHI, G.; AGLIOTI, S.; MARZI, C. A.; TASSINARI, G. **Corpus callosum and simple visuomotor integration.** Neuropsychologia. 1995; 33:923-36.

BERNASCONI, A.; BERNASCONI, N.; LASSONDE, M.; TOUSSAINT, P. J.; MEYER, E.; REUTENS, D. C.; GOTMAN, J.; ANDERMANN, F.; VILLEMURE, J. G. **Sensorimotor organization in patients who have undergone hemispherectomy: a study with (15)O-water PET and somatosensory evoked potentials.** NeuroReport. 2000; 28:3085-3090.

BLITZ, D. M.; FOSTER, K. A.; REGEHR, W. G. **Short-term synaptic plasticity: a comparison of two synapses.** Nat Rev Neurosci, 2004; 5:630-640.

BLOOM, J. S.; HYND, G. W. **The Role of the Corpus Callosum in Interhemispheric Transfer of Information: Excitation or Inhibition?** Neuropsychology Review, 2005, 15: 59-71.

BLUM, A.; ANDRÉ, M.; DROULLÉ, P.; HUSSON, S.; LEHEUP, B. **Prenatal echographic diagnosis of corpus callosum agenesis.** The Nancy experience 1982-1989. Genet Couns. 1990; 1:115-26

BOSSY, J. G. **Morphological study of a case of complete, isolated, and asymptomatic agenesis of the corpus callosum.** Arch Anat Histol Embryol. 1970; 53:289-340.

BRIELLMANN, R. S.; MITCHELL, L. A.; WAITES, A. B.; ABBOTT, D. F.; PELL, G. S.; SALING, M. M.; JACKSON, G. D. **Correlation between language organization and diffusion tensor abnormalities in refractory partial epilepsy.** Epilepsia. 2003; 44:1541-5.

BROWN, R. **A brief account of microscopical observations made in the months of June, July, and August 1827 on the particles contained in the pollen of plants; and on the general existence of active molecules in organic and inorganic bodies.** Philosoph Mag, 1828; 4: 161.

BROWN, W. S.; JEEVES, M. A.; DIETRICH, R.; BURNISON, D. S. **Bilateral field advantage and evoked potential interhemispheric transmission in commissurotomy and callosal agenesis**. Neuropsychologia , 1999; 37, 1165–1180.

CATANI, M.; HOWARD, R. J.; PAJEVIC, S.; JONES, D. K. **Virtual in Vivo Interactive Dissection of White Matter Fasciculi in the Human Brain**. Neuroimage. 2002; 17:77-94.

CICCARELI, O.; WERRING, D. J.; WHEELER-KINGSHOTT, C. A. et al. **Investigation of MS normal-appearing brain using diffusion tensor MRI with clinical correlations.** Neurology, 2001; 56: 926-933.

CIFELLI, A.; ARRIDGE, M.; JEZZARD, P.; ESIRI, M. M.; PALACE, J.; MATTHEWS, P. M. **Thalamic neurodegeneration in multiple sclerosis**. Ann Neurol 2002; 52:650-653.

CIPOLLONI, P. B.; PANDYA, D. N. **Topography and trajectories of commissural fibers of the superior temporal region in the rhesus monkey.** Exp Brain Res, 1985; 57:381-389.

CLARKE, S.; KRAFTSIK, R.; VAN DER LOOS, H.; INNOCENTI, G. M. **Forms and measures of adult and developing human corpus callosum: is there sexual dimorphism?** J Comp Neurol, 1989; 280:213-230.

CORBALLIS, P. M.; INATI, S.; FUNNELL, M. G.; GRAFTON, S. T.; GAZZANIGA, M. S. **MRI assessment of spared fibers following callosotomy: A second look**. Neurology, 2001; 57 1345-1346.

DEAZEVEDO, L. C.; HEDIN-PEREIRA, C.; LENT, R. **Callosal neurons in the cingulate cortical plate and subplate of human fetuses.** J Comp Neurol, 1997; 386:60-70.

DELACOSTE, M. C.; KIRKPATRICK, J. B.; ROSS, E. D. **Topography of the human corpus callosum.** J Neuropathol Exp Neurol, 1985; 44:578-591.

DEQUARDO, J. R.; BOOKSTEIN, F. L.; GREEN, W. D.; BRUNBERG, J. A.; TANDON, R. **Spatial relationships of neuroanatomic landmarks in schizophrenia**. Psychiatry Res. 1996; 67:81-95.

DOBYNS, W. B. **Absence Makes the Search Grow Longer**. Am. J. Genet., 1996; 58:7-16.

DOUAUD, G.; SMITH, S.; JENKINSON, M.; BEHRENS, T.; JOHANSEN-BERG, H.; VICKERS, J.; JAMES, S.; VOETS, N.; WATKINS, K.; MATTHEWS, P. M.; JAMES, A. **Anatomically related grey and white matter abnormalities in adolescent-onset schizophrenia**. Brain. 2007; 130:2375-86.

DUPRÉ, N.; HOWARD, H. C.; MATHIEU, J.; KARPATI, G.; VANASSE, M.; BOUCHARD, J. P.; CARPENTER, S.; ROULEAU, G. A. **Hereditary Motor and Sensory Neuropathy with Agenesis of the Corpus Callosum.** Ann Neural, 2003; 54: 9-18.

ECKSTEIN, K.; FRIEDERICI, A. D. **It's Early: Event-related Potential Evidence for Initial Interaction of Syntax and Prosody in Speech Comprehension**. Journal of Cognitive Neuroscience, 2006; 18: 1696–1711.

EINSTEIN, A. **Investigations on the theory of Brownian motion.** In R. Furthe and A. D. Cowper, editors. Dover, New York, 1956.

ELBERT, T; STERR, A.; ROCKSTROH, B.; PANTEV, C.; MULLER, M. M.; TAUB, E. **Expansion of the tonotopic area in the auditory cortex of the blind.** J Neurosci, 2002; 22:9941-9944.

FIELD, A. S.; ALEXANDER, A. L. **Diffusion tensor imaging in cerebral tumor diagnosis and therapy.** Top Magn Reson Imaging. 2004; 15:315-24.

FINGER, S.; WOLF, C. **The 'Kennard effect' before Kennard. The early history of age and brain lesions.**Arch Neurol. 1988; 45:1136-42.

GARCEZ, P. P.; HENRIQUE, N. P.; FURTADO, D. A.; BOLZ, J.; LENT, R.; UZIEL, D. **Axons of callosal neurons bifurcate transiently at the white matter before consolidating an interhemispheric projection.** Eur J Neurosci. 2007; 25:1384-94.

GARCIA-ABREU, J.; SILVA, L. C.; TOVAR, F. F.; ONOFR, G. R.; CAVALCANTE, L. A.; MOURA NETO, V. **Compartmental distribution of sulfated glycosaminoglycans in lateral and medial midbrain astroglial cultures.** Glia. 1996; 17:339-44.

GAZZANIGA, M. S. **Forty-five years of split-brain research and still going strong.** Neuroscience, 2005; 6:653-659.

GAZZANIGA, M. S. **Perceptual and attentional processes following callosal section in humans.** Neuropsychologia. 1987; 25:119-33.

GAZZANIGA, M. S. **Principles of Human Brain Organization Derived from Split-Brain Studies.** Neuron, 1995, 14: 217-228.

GE, Y.; LAW, M.; GROSSMAN, R. I. **Applications of diffusion tensor MR imaging in multiple sclerosis.** Ann N Y Acad Sci. 2005; 1064:202-19.

GEURTS, J. J.; REULING, I. E.; VRENKEN, H. et al. **MR spectroscopic evidence for thalamic and hippocampal, but not cortical, damage in multiple sclerosis.** Magn Reson Med, 2006; 55:478-483.

GRIFFIN, C. M.; CHARD, D. T.; CICCARELLI, O. et al. **Diffusion tensor imaging in early relapsing-remitting multiple sclerosis**. Multi Scler, 2001; 7:290-297.

HAGMANN, P.; JONASSON, L.; MAEDER, P.; THIRAN, J. P.; WEDEEN, V. J.; MEULI, R. **Understanding diffusion MR Imaging Techniques: From Scalar Diffusion-weighted to Diffusion Tensor Imaging and Beyond.** Radiographics, 2006; 26:S205-223.

HEDIN-PEREIRA, C.; LENT, R.; JHAVERI, S. **Morphogenesis of callosal axons in hamsters.** Cerebral Cortex, 1999; 9: 50-64.

HEIMER, L. **The Human Brain and Spinal Cord**. Springer-Verlag New York inc.1983; p. 31,75-76.

HERCULANO-HOUZEL, S.; COLLINS, C. E.; WONG, P.; KAAS, J.H. **Cellular scaling rules for primate brains.** Proc Natl Acad Sci U S A. 2007; 104:3562-7.

HERCULANO-HOUZEL, S.; MOTA, B.; LENT, R. **Cellular scaling rules for rodent brains**. Proc Natl Acad Sci U S A. 2006; 103:12138-43.

HOFER, S.; FRAHM, J. **Topography of the human corpus callosum revisited—Comprehensive fiber tractography using diffusion tensor magnetic resonance imaging.** NeuroImage 2006; 32: 989-94.

HOUZEL, J. C.; CARVALHO, M. L.; LENT, R**. Interhemispheric connections between primary visual areas: beyond the midline rule**. Braz J Med Biol Res. 2002; 35:1441-53.

HU, Z.; YUE, X.; SHI, G.; YUE, Y.; CROCKETT, D. P.; BLAIR-FLYNN, J.; REUHL, K.; TESSAROLO, L.; ZHOU R. **Corpus callosum deficiency in transgenic mice expressing a truncated Ephrin-A receptor**. J Neurosci, 2003; 23:10963-10970.

INGLESE, M.; GE, Y.; FILIPPI, M.; FALINI, A.; GROSSMAN, R. I.; GONEN, O. **Indirect evidence for early widespread gray matter involvement in relapsing-remitting multiple sclerosis**. Neuroimage, 2004; 21: 1825-1829.

INGLESE, M.; LIU, S.; BABB, J. S.; MANNON, L. J.; GROSSMAN, R. I.; GONEN, O. **Three dimensional proton spectroscopy of deep gray matter nuclei in relapsing-remitting MS**. Neurology, 2004; 63:170-172.

INNOCENTI, G. M.; CLARKE, S. **The organization of immature callosal connections**. J Comp Neurol, 1984; 230:287-309.

INNOCENTI, G. M.; ANSERMET, F.; PARNAS, J. **Schizophrenia, neurodevelopment and corpus callosum.**Mol Psychiatry. 2003; 8:261-74.

INNOCENTI, G. M.; PRICE, D. J. **Exuberance in the development of cortical networks**. Nat Rev Neurosci, 2005; 6:955-965.

IVANCO, T. L.; PELLIS, S. M.; WHISHAW, I. Q. **Skilled forelimb movements in prey catching and in reaching by rats (Rattus norvegicus) and opossums (Monodelphis domestica): relations to anatomical differences in motor systems.** Behav Brain Res. 1996; 79:163-81.

JELLISON, B. J.; FIELD, A. S.; MEDOW, J.; LAZAR, M.; SALAMAT, M. S.; ALEXANDER, A. L. **Diffusion tensor imaging of cerebral white matter: a pictorial review of physics, fiber tract anatomy, and tumor imaging patterns**. AJNR Am J Neuroradiol. 2004; 25:356-69

JIANG, H.; VAN ZIJL, P. C.; KIM, J.; PEARLSON, G. D.; MORI, S. **DtiStudio: resource program for diffusion tensor computation and fiber bundle tracking**. Comput Methods Programs Biomed, 2006; 81: 106-116.

JINKINS, J. R.; WHITTEMORE, A. R.; BRADLEY, W. G**. MR imaging of callosal and corticocallosal dysgenesis.** AJNR 1989; 10:339–44

JONES, D. K.; SIMMONS, A.; WILLIAMS, S. C.; HORSFIELD, M. A. **Non-invasive assessment of axonal fiber connectivity in the human brain via diffusion tensor MRI.** Magn Reson Med. 1999; 42:37-41.

KAMNASARAN, D. **Agenesis of the Corpus Callosum: Lessons from Humans and Mice**. Clin Invest Med, 2005; 28: 267-282.

KARLSGODT, K. H.; VAN ERP, T. G. M.; POLDRACK, R. A.; BEARDEN, C. E.; NUECHTERLEIN, K. H.; CANNON, T. D. **Diffusion Tensor Imaging of the Superior Longitudinal Fasciculus and Working Memory in Recent-Onset Schizophrenia.** Biol Psychiatry, 2007; 1-7.

KEEBLE, T. R.; COOPER, H. M. **Ryk: a novel Wnt receptor regulating axon pathfinding**. Int J Biochem Cell Biol. 2006; 38:2011-7.

KENDALL, D. A. **Direct and indirect responses to metabotropic glutamate receptor activation in the brain.** Biochem Soc Trans. 1993; 21:1120-3.

KENNARD, M. A. **Cortical reorganization of motor function: studies on a series of monkeys of various ages from infancy to maturity**. Arch Neur Psychiat, 1942; 48:227-240.

KESHAVAN, M. S.; DIWADKAR, D. A.; DEBELLIS, M.; DICK, E.; KOTWAL, R.; ROSENBERG, D. R.; SWEENEY, J. A.; MINSHEW, N.; PETTEGREW, J. W.

Development of the corpus callosum in childhood, adolescence and early adulthood. Life Sci, 2002; 70:1909-1922.

KIDWELL, C. S.; ALGER, J. R.; SAVER, J.L. **Beyond mismatch: evolving paradigms in imaging the ischemic penumbra with multimodal magnetic resonance imaging**. Stroke. 2003; 34:2729-35.

KIER, E. L.; TRUWIT, C. L. **The lamina rostralis: modification of concepts concerning the anatomy, embryology, and MR appearance of the rostrum of the corpus callosum.** AJNR Am J Neuroradiol, 1997; 18:715-722.

KIER, E. L.; TRUWIT, C. L. **The normal and abnormal genu of the corpus callosum: an evolutionary, embryologic, anatomic, and MR analysis**. AJNR Am J Neuroradiol, 1996; 17:1631-1641.

KOESTER, S. E.; O'LEARY, D.D**. Axons of early generated neurons in cingulate cortex pioneer the corpus callosum.** J Neurosci, 1994; 14:6608-6620.

KOLODKIN, A.L. **Semaphorins: mediators of repulsive growth cone guidance**. Trends in Cell Biology, 1996; 6: 15-22.

KUKER, W.; MAYRHOFER, H.; MADER, I.; NAGELE, T.; KRAGELOH-MANN, I. **Malformations of the midline commissures: MRI findings in different forms of callosal dysgenesis.** Eur Radiol, 2003; 13:598-604.

KUTZELNIGG, A.; LASSMANN, H. **Cortical lesions and brain atrophy in MS.** J Neurol Sci, 2005; 233:55-59.

LAMANTIA, A. S.; RAKIC, P. **Axon overproduction and elimination in the corpus callosum of the developing rhesus monkey**. J Neurosci. 1990; 10:2156-75.

LASSONDE, M.; SAUERWEIN, H.; CHICOINE. A. J.; GEOFFROY, G. **Absence of disconnexion syndrome in callosal agenesis and early callosotomy: brain reorganization or lack of structural specificity during ontogeny?** Neuropsychologia, 1991; 29:481-495.

LASSONDE, M.; SAUERWEIN, H.; MCCABE, N.; LAURENCELLE, L.; GEOFFROY, G. **Extent and limits of cerebral adjustment to early section or congenital absence of the corpus callosum**. Behav Brain Res, 1988; 30:165-181.

LASSONDE, M.; SAUERWEIN, H. C.; LEPORE, F. **Extent and limits of collosal plasticity: presence of disconnection symptoms in callosal agenesis**. Neuropsychology, 1995; 33: 989-1007.

LASSONDE, M. C.; SAUERWEIN, H. C.; LEPORE, F. **Agenesis of the corpus callosum**. In: Zaidel E, Iacoboni M, eds. The Parallel Brain. Cambridge: MIT Press, 2003; pp. 357-369.

LEE, S. K.; MORI, S.; KIM, D. J.; KIM, S. Y.; KIM, D. I. **Diffusion Tensor MR Imaging Visualizes the Altered Hemispheric Fiber Connection in Callosal Dysgenesis**. AJNR Am J Neuroradiol, 2004; 25:25–28.

LEE, S. K.; KI, D. I.; KIM, D. I.; KIM, D. J.; KIM, H. D.; KIM, D. S.; MORI, S. **Diffusion-tensorMR imaging and fiber tractography: A new method of describing aberrant fiber connections in developmental CNS anomalies**. Radiographics, 2005; 25:53-65.

LENT, R. **Neuroanatomical effects of neonatal transection of the corpus callosum in hamsters.** J Comp Neurol, 1982; 223: 548-555.

LENT, R. **Cortico-cortical connections reorganize in hamsters after neonatal transection of the callosal bridge.** Dev Brain Res, 1983; 11: 137-142.

LENT, R. **Cem bilhões de neurônios: conceitos fundamentais de neurociências.** São Paulo, ed. Atheneu, 2001; p. 643.

LENT, R.; UZIEL, D.; BAUDRIMONT, M.; FALLET, C. **Cellular and molecular tunnels surrounding the forebrain commissures of human fetuses.** J CompNeurol, 2005; 483: 375-382.

LESSARD, N.; LEPORE, F.; VILLEMAGNE, J.; LASSONDE, M. **Sound localization in callosal agenesis and early callosotomy subjects: brain reorganization and/or compensatory strategies.** Brain, 2002; 125:1039-1053.

LI, M.; SHIBATA, A.; LI, C.; BRAUN, P.E.; MCKERRACHER, L.; RODER, J.; KATER, S.B.; DAVID, S. **Myelin-associated glycoprotein inhibits neurite/axon growth and causes growth cone collapse.** Journal of Neuroscience Research, 1996; 46: 404-414.

LINDWALL C, FOTHERGILL T, RICHARDS LJ. **Commissure formation in the mammalian forebrain.** Curr Opin Neurobiol, 2007; 17: 3-14.

LIVY, D. J.; SCHALOMON, P. M.; ROY, M.; ZACHARIAS, M. C.; PIMENTA, J.; LENT, R.; WAHLSTEN, D. **Increased axon number in the anterior commissure of mice lacking a corpus callosum.** Exp Neurol, 1997; 146:491–501.

MARENCO, S.; SIUTA, M. A.; KIPPENHAN, J. S.; GRODOFSKY, S.; CHANG, W. L.; KOHN, P.; MERVIS, C. B.; MORRIS, C. A.; WEINBERGER, D. R.; MEYER-LINDENBERG, A.; PIERPAOLI, C.; BERMAN, K. F. **Genetic contributions to white matter architecture revealed by diffusion tensor imaging in Williams syndrome**. Proc Natl Acad Sci U S A. 2007; 104:15117-22.

MATSUNAMI, K.; KAWASHIMA, T.; UEKI, S.; FUJITA, M.; KONISHI, T. **Topography of commissural fibers in the corpus callosum of the cat: a study using WGA-HRP method.** Neurosci Res, 1994; 20:137-148.

MCFARLAND, H. F.; BARKHOF, F.; ANTEL, J.; MILLER, D. H. **The role of MRI as a surrogate outcome measure in multiple sclerosis.** Mult Scler, 2002; 8:40-51.

MCKINSTRY, R. C.; MATHUR, A.; MILLER, J. H.; OZCAN, A.; SNYDER, A. Z.; SCHEFFT, G. L.; ALMLI, C. R.; SHIRAN, S. I.; CONTURO, T. E.; NEIL, J. J. **Radial organization of developing preterm human cerebral cortex revealed by non-invasive water diffusion anisotropy MRI.** Cereb Cortex. 2002; 12:1237-43.

MEYER, B. U.; RÖRICHT, S.; WOICIECHOWSKY, C. **Topography of fibers in the human corpus callosum mediating interhemispheric inhibition between the motor cortices.** Ann Neurol, 1998a, 43:360-369.

MEYER, B. U.; RÖRICHT, S.; NIEHAUS, L**. Morphology of acallosal brains as assessed by MRI in six patients leading a normal life.** J Neurol, 1998b, 245: 106-110.

MIHRSHAHI, R. **The Corpus Callosum as an Evolutionary Innovation**. Journal of Experimental Zoology (Mol Dev Evol), 2006; 306B:8–17.

MONTANDON, C.; RIBEIRO, F. A. S.; LOBO, L. V. B.; JR, M. E. M.; TEIXEIRA, K. I. S. S**. Disgenesia do Copo Caloso e más-formações associadas: Achados de tomografia computadorizada e ressonância magnética.** Radiol Bras 2003; 36: 311-316.

MORI, S.; CRAIN, B. J.; CHACKO, V. P.; VAN ZIJL, P. C. M. **Three-dimensional tracking of axonal projections in the brain by magnetic resonance imaging.** Ann Neurol, 1999; 45:265–269.

MORI, S.; VAN ZIJL, P. C. **Fiber tracking: principles and strategies - a technical review.** NMR Biomed, 2002; 15:468-480.

NAKAMURA, H.; KANASEKI, T. **Topography of the corpus callosum in the cat.** Brain Res, 1989; 485:171-175.

NORDEEN, K. W.; NORDEEN, E. J. **Synaptic and molecular mechanisms regulating plasticity during early learning.** Ann N Y Acad Sci, 2004; 1016:416-437.

O'SULLIVAN, M.; SINGHAL, S.; CHARLTON, R.; MARKUS, H. S. **Diffusion tensor imaging of thalamus correlates with cognition in CADASIL without dementia**. Neurology, 2004; 62: 702-707.

OLAVARRIA, J.; SERRA-OLLER, M. M.; YEE, K. T.; VAN SLUYTERS, R. C. **Topography of interhemispheric connections in neocortex of mice with congenital deficiencies of the callosal commissure.** J Comp Neurol, 1988; 270:575-590.

OLIVARES, R.; MONTIEL, J.; ABOITIZ, F**. Species differences and similarities in the fine structure of the mammalian corpus callosum**.Brain Behav Evol. 2001; 57:98-105.

OZAKI, H. S.; WAHLSTEN, D. **Timing and Origin of the First Cortical Axons to Project Through the Corpus Callosum and the Subsequent Emergence of Callosal Projection Cells in Mouse.** The Journal of Comparative Neurology, 1998; 400:197–206.

OZAKI, H. S.; IWAHASHI, K.; SHIMADA, M. **Ipsilateral corticocortical projections of fibers which course within Probst's longitudinal bundle seen in the brains of mice with congenital absence of the corpus callosum: a study with the horseradish peroxidase technique.** Brain Res, 1989; 493:66-73.

OZAKI, H. S.; MURAKAMI, T. H.; TOYOSHIMA, T.; SHIMADA, M. **The Fibers which Leave the Probst's Longitudinal Bundle seen in the Brain of an Acallosal Mouse: a Study with the Horseradish Peroxidase Technique.** Brain Research, 1987; 400:239-

246.

OZAKI, H. S.; MURAKAMI, T. H.; TOYOSHIMA, T.; SHIMADA, M. **The fibers which leave the Probst longitudinal bundle seen in the brain of an acallosal mouse: A study with the horseradish peroxidase technique.** Brain Res, 1987; 400:239-246.

OZAKI, H. S.; SHIMADA, M. **The fibers which course within the Probst's longitudinal bundle seen in the brain of a congenitally acallosal mouse: a study with the horseradish peroxidase technique.** Brain Res, 1988; 441:5-14.

OZAKI, H. S.; WAHLSTEN, D. **Cortical axon trajectories and growth cone morphologies in fetuses of acallosal mouse strains**. J Comp Neurol, 1993; 336:595-604.

OZAKI, H. S.; WAHLSTEN, D. **Prenatal formation of the normal mouse corpus callosum: a quantitative study with carbocyanine dyes.** J Comp Neurol, 1992; 323:81-90.

OZAKI, H. S.; WAHLSTEN, D. **Timing and origin of the first cortical axons to project through the corpus** callosum and the subsequent emergence of callosal projection cells in mouse. J Comp Neurol, 1998; 400: 197-206.

PAJEVIC, S.; PIERPAOLI, C.**Color schemes to represent the orientation of anisotropic tissues from diffusion tensor data: application to white matter fiber tract mapping in the human brain.** Magn Reson Med, 1999; 42: 526-40.

PARKER, G. J. M.; STEPHAN, K. E.; BARKER, G. J.; ROWE, J. B.; MACMANUS, D. G.; WHEELER-KINGSHOTT, C. A. M.; CICCARELLI, O.; PASSINGHAM, R. E.; SPINKS, R. L.; LEMON, R. N.; TURNER, R**. Initial demonstration of in vivo tracing of axonal projections in the macaque brain and comparison with the human brain**

using diffusion tensor imaging and fast marching tractography. NeuroImage, 2002; 15:787-809.

PAUL, L. K.; BROWN, W. S.; ADOLPHS, R.; TYSZKA, J. M.; RICHARDS, L. J.; MUKHERJEE, P.; SHERR, E. H. **Agenesis of the corpus callosum: genetic, developmental and functional aspects of connectivity.** Nat Rev Neurosci, 2007; 8: 287-299.

PAUL, L. K.; SIDTIS, D. V. L.; SCHIEFFER, B.; ROSALIND, D.; BROWN, W. S. **Communicative deficits in agenesis of the corpus callosum: Nonliteral language and affective prosody.** Brain and Language, 2003; 85: 313–324.

PIERPAOLI, C.; BARNETT, A.; PAJEVIC, S.; CHEN, R.; PENIX, L. R.; VIRTA, A.; BASSER, P. **Water diffusion changes in Wallerian degeneration and their dependence on white matter architecture.** NeuroImage, 2001; 13:1174-1185.

PIERPAOLI, C.; BARNETT, A.; PAJEVIC, S. et al. **Water diffusion changes in Wallerian degeneration and their dependence on white matter architecture**. Neuroimage, 2001; 13:1174-1185.

POLLEUX, F.; GIGER, R. J.; GINTY, D. D.; KOLODKIN, A. L.; GHOSH, A**. Patterning of cortical efferent projections by semaphorin-neuropilin interactions.** Science, 1998; 282:1904-1906.

PROBST, M. **Ueber den Bau des balkenlosen Grosshirns, sowie uber Mikrogirie und Heterotopie der grauen Substanz.** Arch Psychiatr Nervenkr, 1901; 34:709-786.

RAKIC, P.; YAKOVLEV, P. I. **Development of the corpus callosum and the cavum septi in man.** J Comp Neurol, 1968; 132:45-72.

RASH, B. G.; RICHARDS, L.J. **A role for cingulate pioneering axons in the development of the corpus callosum.** J Comp Neurol, 2001; 434:147–157.

REN, T.; ANDERSON, A.; SHEN, W. B.; HUANG, H.; PLACHEZ, C.; ZHANG, J.; MORI, S.; KINSMAN, S. L.; RICHARDS, L. J. **Imaging, Anatomical and Molecular Analysis of Callosal Formation in the Developing Human Fetal Brain**. The Anatomical Record Part A, 2006; 288A:191–204.

REN, T.; ZHANG, J.; PLACHEZ, C.; MORI, S.; RICHARDS, L. J. **Diffusion Tensor Magnetic Resonance Imaging and Tract-Tracing Analysis of Probst Bundle Structure in Netrin1- and DCC-Deficient Mice.** The Journal of Neuroscience, 2007; 27:10345–10349.

RICHARDS, L. J.; PLACHEZ, C.; REN, T. **Mechanisms regulating the development of the corpus callosum and its agenesis in mouse and human**. Clin Genet, 2004; 66:276-289.

RICHARDS, L. J. **Axonal pathfinding mechanisms at the cortical midline and in the development of the corpus callosum.** Braz J Med Biol Res, 2002; 35:1431-1439.

RICHERT, N. D.; OSTUNI, J. L.; BASH, C. N.; DUYN, J. H.; MCFARLAND, H. F.; FRANK, J. A. **Serial whole-brain magnetization transfer imaging in patients with relapsing-remitting multiple sclerosis at baseline and during treatment with interferon beta-1b**. AJNR Am j Neuroradiol, 1998; 19:1705-1713.

RISSE, G. L.; GATES, J.; LUND, G.; MAXWELL, R.; RUBENS, A. **Interhemispheric transfer in patients with incomplete section of the corpus callosum. Anatomic verification with magnetic resonance imaging.** Arch Neurol. 1989; 46:437-43.

ROCKLAND, K. S.; PANDYA, D. N. **Topography of occipital lobe commissural connections in the rhesus monkey**. Brain Res, 1986; 365:174-178.

SAUERWEIN, H. C.; LASSONDE, M. **Cognitive and sensory-motor functioning in the absence of the corpus callosum: neuropsychological studies in callosal agenesis and callosotomized patients.** Behav Brain Res, 1994; 64:229-240.

SAVAZZI, S.; FABRI, M.; RUBBOLI, G.; PAGGI, A.; TASSINARI, C. A.; MARZI, C. A. **Interhemispheric transfer following callosotomy in humans: Role of the superior colliculus**. Neuropsychologia, 2007; 45 2417–2427.

SCHAEFER, P. W.; COPEN, W. A.; LEV, M. H.; GONZALEZ, R. G. **Diffusion-weighted imaging in acute stroke.Neuroimaging** Clin N Am. 2005; 15:503-30.

SCHALOMON, P. M.; WAHLSTEN, D. **Wheel running behavior is impaired by both surgical section and genetic absence of the mouse corpus callosum.** Brain Research Bulletin, 2002; 57: 27–33.

SERAFINI, T.; COLAMARINO, S. A.; LEONARDO, E. D.; WANG, H.; BEDDINGTON, R.;, SKARNES, W. C.; TESSIER-LAVIGNE, M. **Netrin-1 is required for commissural axon guidance in the developing vertebrate nervous system**. Cell, 1996; 87: 1001-1004.

SHANG, F.; ASHWELL, K. W. S.; MAROTTE, L. R.; WAITE, P. M. E**. Development of commissural neurons in the wallaby (Macropus eugenii)** J Comp Neurol. 1997; 387:507-23.

SHARMA, J.; ZIVADINOV, R.; JAISANI, Z. et al. **A magnetization transfer MRI study of deep gray matter involvement in multiple sclerosis**. J Neuroimaging, 2006; 16: 302-310.

SHEN, Y.; MANI, S.; DONOVAN, S. L.; SCHWOB, J. E.; MEIRI, K. F. **Growth-ssociated protein-43 is required for commissural axon guidance in the developing vertebrate nervous system**. J. Neurosci. 2002; 22: 239–247.

SHRAGER, R. I.; BASSER, P. J. **Anisotropically weighted MRI**. Magn Reson Med, 1998; 40:160-165.

SHU, T.; RICHARDS, L. J. **Cortical axon guidance by the glial wedge during the development of the corpus callosum.** J Neurosci, 2001; 21: 2749-2758.

SHU, T.; BUTZ, K. G.; PLACHEZ, C.; GRONOSTAJSKI, R. M.; RICHARDS, L. J. **Abnormal development of forebrain midline glia and commissural projections in Nfia knock-out mice**. J. Neurosci. 2003; 23: 203–212.

SMITH, K. M.; OHKUBO, Y.; MARAGNOLI, M. E.; RASIN, M. R.; SCHWARTZ, M. L.; SESTANT, N.; VACCARINO, F. M. **Midline radial glia translocation and corpus callosum formation require FGF signaling**. Nature Neurosci. 2006; 9: 787–797.

SMITH, S. M.; JENKINSON, M.; JOHANSEN-BERG, H.; RUECKERT, D.; NICHOLS, T. E.; MACKAY, C. E.; WATKINS, K. E.; CICCARELLI, O.; CADER, M. Z.; MATTHEWS, P. M.; BEHRENS, T. E. **Tract-based spatial statistics: voxelwise analysis of multi-subject diffusion data.** Neuroimage. 2006; 31:1487-505.

SPERRY, R. W. **Perception in the absence of the neocortical commissures. In: Perception and its Disorders (Research Publication of the Association for Research in Nervous and Mental Diseases, vol. 48).** Baltimore: Williams & Wilkins, 1970; 123-138.

STEELE-PERKINS, G.; PLACHEZ, C.; BUTZ, K. G.; YANG, G.; BACHURSKI, C. J.; KINSMAN, S. L.; LITWACK, E. D.; RICHARDS, L. J.; GRONOSTAJSKI, R. M. **The**

transcription factor gene Nfib is essential for both lung maturation and brain development. Mol. Cell Biol. 2005; 25: 685–698.

TAILBY, C.; WRIGHT, L. L.; METHA, A. B.; CALFORD, M. B. **Activity-dependent maintenance and growth of dendrites in adult cortex.** Proc Natl Acad Sci USA, 2005; 102:4631-4636.

THOMPSON, P. M.; GIEDD, J. N.; WOODS, R. P.; MACDONALD, D.; EVANS, A. C.; TOGA, A. W. **Growth patterns in the developing brain detected by using continuum mechanical tensor maps**. Nature, 2000; 404:190-193.

TOVAR-MOLL, F.; MOLL, J.; BRAMATI, I. E.; OLIVEIRA-SOUZA, R. **The Pyramidal Syndrome Redux: Clinical and Neuroimaging Findings in a Patient with a Discrete Pyramid Lesion.** Neuroreport, 2007; 18:1417-1421.

UTSUNOMIYA, H.; OGASAWARA, T.; HAYASHI, T.; HASHIMOTO, T.; OKAZAKI, M. **Dysgenesis of the corpus callosum and associated telencephalic anomalies: MRI**. Neuroradiology. 1997; 39:302-10.

UZIEL, D.; GARCEZ, P.; LENT, R.; PEUCKERT, C.; WETH, F.; BOLZ, J. **Connecting Thalamus and Cortex:The Role of Ephrins.** Anat Rec A Discov Mol Cell Evol Biol. 2006; 288: 135-42.

Villablanca, J. R.; HOVDA, D. A. **Developmental neuroplasticity in a model of cerebral hemispherectomy and stroke.** Neuroscience, 2000; 95:625-637.

WAHLSTEN, D.; BULMAN-FLEMING, B. **retarded growth of the mesial septum: a major gene effect in acallosal mice.** Developmental Brain Research. 1994; 77: 203-214.

WESTERHAUSEN, R.; WALTER, C.; KREUDER, F.; WITTLING, R. A.; SCHWEIGER, E.; WITTLING, W. **The influence of handedness and gender on the microstructure of the human corpus callosum: a diffusion-tensor magnetic resonance imaging study.** Neurosci Lett. 2003; 351:99-102.

WITELSON, S. F. **Neuroanatomical bases of the hemispheric functional specialization in the human brain: Possible developmental factors**. Em hemispheric Communications: Mechanisms and Models. F.L. Ketterle, ed. Hillsdale, NJ: Lawrence Erlbaum Associates, 1995; pp. 61.

XU, D.; MORI, S.; SOLAIYAPPAN, M.; VAN ZIJL, P. C.; DAYATZIKOS, C. **A framework for callosal fiber distribution analysis**. NeuroImage, 2002, 17:1131-1143.

XUE, R. ;VAN ZIJL, P. C. M.; CRAIN, B. J.; SOLAIYAPPAN, M.; MORI, S. **In vivo three dimensional reconstruction of rat brain axonal projections by diffusion tensor imaging**. Magn Res Med, 1999, 42:1123–1127.

ANEXOS

Thalamic involvement and its impact on clinical disability in patients with Multiple Sclerosis: a Diffusion Tensor Imaging study at 3.0 T

Fernanda Tovar-Moll, MD[1], Iordanis Evangelou, DPhil[1], Annie W Chiu, BA[1], Nancy Richert, MD, PhD[1], John Ostuni, PhD[1], Joan Ohayon, CRNP[1] , Sungyoung Auh, PhD[2], Mary Ehrmantraut, CRNP[1], Lalith Talagala, PhD[3], Henry McFarland, MD[1], Francesca Bagnato, MD, PhD[1]

[1]Neuroimmunology Branch, National Institute of Neurological Disorders and Stroke, NIH, Bethesda, MD, USA; [2]Office of the Clinical Director, National Institute of Neurological Disorders and Stroke, NIH, Bethesda, MD, USA; [3]NIH-MRI Research Facility, NINDS, NIH, Bethesda, MD, USA

Running title: Thalamic involvement in Multiple Sclerosis

Keywords: Thalamus, Grey matter, Multiple Sclerosis, DTI, 3-Tesla magnetic resonance imaging

Corresponding Author:

Francesca Bagnato, MD-PhD

NIB-NINDS-NIH

Building 10, Room 5B16

10 Center Drive

Bethesda, MD, 20892-1400 MSC

Phone number: (301) 594-1415

Fax number: (301) 402-0373

e-mail: bagnatof@ninds.nih.gov

Abbreviated Title Page

Title: Thalamic involvement and its impact on clinical disability in patients with Multiple Sclerosis: a Diffusion Tensor Imaging study at 3.0 T

Article type: Original Research

Presented at the 92nd annual meeting of the Radiological Society of North America, Chicago, IL, 2006

Advances in knowledge:

1. Diffusion tensor imaging at 3 Tesla is sensitive in detecting damage in the normal-appearing thalamus.
2. Subtle thalamic damage strongly explains functional scores in multiple sclerosis.
3. Thalamic damage is moderately correlated with extra-thalamic white matter disease, suggesting that grey and white matter damage may play partially independent roles.

Implication for patient care:

1. Disease in normal appearing tissue, like thalamic nuclei, plays an important role in determining physical and cognitive impairment of patients with multiple sclerosis.
2. Quantitative MRI methods, such as diffusion tensor imaging, provide metrics for disclosing and quantifying subtle disease-mediated changes not visible with conventional imaging and should be included when monitoring multiple sclerosis patients in clinical practice.

ABSTRACT

PURPOSE: Several studies have suggested that gray matter involvement may play an important role in multiple sclerosis (MS) pathology. High field magnetic resonance imaging (MRI) can potentially improve the assessment of subtle abnormalities in patients with MS. We have investigated the sensitivity of Diffusion Tensor Imaging (DTI) at 3.0T in detecting thalamic damage in MS patients, and the relationship of these changes with clinical disability and white matter (WM) damage.

MATERIALS AND METHODS: Twenty-four patients with relapsing remitting (RR) or secondary progressive (SP) MS and twenty-four age- and gender matched healthy volunteers (HVs) underwent DTI at 3.0T. Thalamic fractional anisotropy (FA) and mean diffusivity (MD) were measured in regions of interest (ROIs) outlined within the thalamus. Differences in MD and FA were examined by using either two sample *t*-test (between patients and HVs) or analysis of variance (among RR MS, SP MS, and HVs). Relationship between DTI-derived metrics and clinical scores or other MRI metrics within the patient group was investigated using Pearson correlation.

RESULTS: MS patients had higher FA ($p < 0.0001$) and MD ($p = 0.035$) values compared to HVs. MD values correlated with the cognitive ($r = -0.43$, $p = 0.034$) and motor ($r = 0.47$, $p = 0.021$) scores. In RR patients, MD values were correlated with global expanded disability status scale (EDSS) ($r = 0.75$, $p = 0.003$) and motor scores ($r = 0.68$, $p = 0.010$). Weaker but significant correlations were found between MD values and WM lesions or brain volume ($p < 0.05$).

CONCLUSION: DTI at 3.0T is sensitive in detecting thalamic changes in MS patients. Increased thalamic MD correlates with physical and cognitive decline in MS patients. The

moderate correlation between grey matter (GM) and WM involvement indicates that WM pathology partially explains GM disease in MS, which may also occur independently as a primary process.

INTRODUCTION

Magnetic resonance imaging (MRI) has revolutionized the diagnosis and follow-up of patients with multiple sclerosis (MS) by providing reliable detection and quantitative estimation of focal white matter (WM) lesions *in vivo*. WM lesion load, however, is only moderately correlated with MS patients' disability (1, 2). Recognizing the limited sensitivity of conventional MRI combined with new advances in the neuroimmunology and pathology of MS, researchers have extended their focus on subtle pathological changes in the so-called normal appearing WM (NAWM) and normal appearing grey matter (NAGM) damage hoping to better explain the neurological symptoms of MS patients (3, 4).

Post-mortem and *in vivo* studies have demonstrated that the deep GM can also be affected in MS. Diffuse microscopic damage in the absence of typical acute inflammatory or macroscopic lesions can be present in the NAGM of the thalamus and basal ganglia (5, 6). The thalamus, in particular, is a critical structure for a wide range of neurological functions, including motor, sensory, and cognitive abilities (7). Because thalamic axons convey information between multiple, discrete sub-cortical and specific cortical regions, both direct microstructural damage to thalamic nuclei and indirect changes induced by axonal degeneration secondary to WM MS lesions could be intimately related to functional disability in MS.

Although previous studies have used high-resolution volumetric MRI metrics, MR spectroscopy, diffusion weighted and magnetization transfer imaging to investigate the normal appearing tissue in the thalamus of patients with MS, there are a number of issues still unresolved. Some studies found no differences between MS patients and healthy controls (8-10), while others suggested that thalamic involvement is detectable in patients with MS (5, 11-17).The time course of thalamic involvement in MS is still an unanswered

question. While some studies have suggested that thalamic involvement starts early (14, 18, 19), others have only identified damage in later stages of the disease (17).

Diffusion Tensor imaging (DTI) allows for the estimation of vector fields describing the anisotropic properties of water diffusion on a voxel basis *in vivo*, thus reflecting important details of fiber tract orientation and providing information regarding microstructural tissue integrity in both WM and GM structures (20-23). A limited number of studies have employed DTI (9, 10, 24) to investigate whether abnormal changes occur in the thalamus of patients with MS. Although some of these studies have demonstrated changes in DTI-derived metrics, the specific findings have been conflicting, and so far, the sensitivity of DTI to detect thalamic involvement and functional disability remains unclear. It is however of importance that high field MRI is increasing in research and clinical settings. A recent volumetric and DTI study reports the feasibility and the contribution of improved MRI techniques at 3.0T in detecting atrophy and diffusivity abnormalities in normal appearing tissue (WM and overall GM) in patients with RR MS (25). This study reproduced previous findings obtained at lower field MRI, but also suggested the validity of the biological changes detected by these techniques. In addition, methodological studies have suggested that the increased signal-to-noise ratio (SNR) provided by high-field MRI and multi-array coils can lead to significant improvement in DTI-derived metrics. It has been shown that such improvements have an impact on the quantitative measurements obtained by DTI (26-27).

In this study, we used 3.0 Tesla (3.0T) MRI to investigate microstructural damage in normal-appearing thalami of both relapsing remitting (RR) and secondary progressive (SP) MS patients. Possible relationships between thalamic DTI-derived metrics and clinical disability or other MRI metrics were also investigated.

MATERIALS AND METHODS

Subjects and study design

This is a cross-sectional study performed at the Neuroimmunology Branch of the National Institute of Neurological Diseases and Stroke (NINDS). The study was approved by Institutional Review Board and all participants signed an informed written consent.

Twenty-four patients with MS in accordance with Poser criteria (28) and classified as RR or SP MS according to standard criteria (32) were studied. No exclusion criteria were employed to select subjects rather than: (i) inability to provide a written consent form; (ii) contraindication to undergo a 3.0T MRI; (iii) presence of clinical relapse or steroids treatment within one month of the study.

Each patient had a neurological exam performed by an examiner blinded to the MRI characteristics of the patient. The Expanded Disability Status Scale (EDSS) (29) and the 3-second version of the Paced Auditory Serial Addition Task (PASAT) (30, 31) scores were used to assess the physical and cognitive ability of patients. Inability to perform the PASAT test due to MS related disability was taken as the maximum score. Twenty-four healthy volunteers (HVs) age- and gender-matched to the patient group were consecutively recruited and imaged using the same protocol. In order to evaluate inter-scan variability DTI parameters, four HVs were rescanned using the same DTI protocol two weeks apart.

HVs, RR and SP patients' clinical, demographic and MRI characteristics at the time of enrollment are summarized in Table 1. Fifteen patients were undergoing a chronic therapy at the time of the study. Six patients were on immunomodulatory therapy while nine patients were on immunosuppressive therapy.

MRI Acquisition

MRI was performed on a 3.0T GE Excite scanner (General Electric Medical Systems, Milwaukee, WI, USA) using an 8-channel head receive–coil array (MRI Devices, Pewaukee, WI, USA). The following sequences were acquired in the axial plane in each patient: i) Spin-Echo (SE) T1-weighted (W) with 54 contiguous slices of 2.4 mm thickness, TR/TE = 700 ms / 11 ms, Matrix = 256 x 256, Field of view (FOV) = 240 x 240 mm^2, before and within 10 minutes of the injection of a single dose of gadopentate dimeglumine (GD) (Magnevist, Berlex Labs, Cedar Knolls, NJ, USA); ii) Fast Spin Echo (FSE) T2-W with 54 contiguous slices of 2.4 mm thickness, TR/TE = 5100 ms / 120 ms, Matrix = 256x256, and FOV = 240 x 240 mm^2; iii) T1-W 3D Inversion Recovery Fast Spoiled Gradient Echo (T1-W-IR-FSPGR) with TR/TE = 7.5 ms / 3 ms, Matrix = 256 x 256, FOV = 240 x 240 mm^2, TI = 750ms, flip angle = 16°, bandwidth = 31.25kHz with 1.0 mm thickness; and iv) two DTI acquisitions using a single-shot, spin-echo echoplanar imaging (SS-SE-EPI) sequence with 54 contiguous slices of 2.4mm thickness, TR/TE = 13000 ms / 76 ms, Matrix = 96 x 96 (reconstructed to 256 x 256), FOV = 240 x 240 mm^2, with ASSET acceleration factor of 2. The DTI acquisition consisted of 3 volumes with no diffusion gradients applied ($b = 0$) and 33 volumes in which diffusion gradients were applied in non-collinear directions, with $b = 1000$ s/mm^2. T1, T2, and DTI acquisitions were matched for slice location, thickness and spacing.

The HVs underwent the same MRI protcol with the exclusion of the post-contrast T1W sequence.

Post-processing and image analysis

T1 and T2 lesion load computation. T2 hyperintense and T1 hypointense lesion number and volume were marked by two independent observers using a semi-automated local threshold method in MEDx (33). A chronic T1-hypointense lesion was defined as any hypointense region visible on T1-W image with a corresponding region of high signal intensity on the T2-W image in the absence of corresponding contrast enhancement (34). Contrast enhancing lesions (CELs) were counted from hard-copies.

Brain Parenchymal Fraction (BPF) computation. The 3D-IR-FSPGR images were used to automatically calculate BPF, GM fraction (GMF), and WM fraction (WMF) using the SIENA (structural image evaluation, using normalization, of atrophy) software (35).

Mean diffusivity (MD) and fractional anisotropy (FA) measurements (DTI-Analysis). After correction for movement and EPI induced distortion artifacts (36), image data were inspected for any apparent artifacts. Then, the diffusion tensor (DT) was calculated on a voxel to voxel basis and then decomposed into eigenvalues and eigenvectors using multivariate fitting in the DTI-Studio software version 6_9 (37). MD and FA maps were then produced according to the procedures described in (38).

Region of Interest (ROI) placement. For each subject, the T2-W and T1-W images were registered to the first ($b = 0$) image using a 12-parameter affine registration algorithm (39, 40). The thalamus was inspected for the presence of lesions on both the registered and un-registered T1-W and T2-W images. No lesions were found in any of the subjects included in the study. In each hemisphere, two symmetrical circular ROIs (area = 68 pixels) (21, 24) were placed in the thalamus on three consecutive slices (above the plane of the anterior comissure) on the ($b = 0$) image by one investigator. Care was taken to ensure that the thalamus could be identified bilaterally on at least one slice dorsally and one slice caudally

from the target slices so that no adjacent structures were included (Figure 1). The ROIs were overlaid on the FA and MD maps and mean thalamic FA and MD values were obtained from the average across the 3 ROIs between the right and left hemisphere values.

In order to evaluate potential intra-observer variability, all post-processing steps were repeated with FA and MD values re-calculated in five patients and five HVs, chosen randomly, two weeks from the first measurements and intra-observer coefficient of variation (COV) was obtained. Inter-observer variability was also evaluated by a second investigator by placing ROIs within the thalamus on both the calculated FA and MD maps, on the same 3 consecutive slices in five patients and five HVs

Statistical analysis

First, a two sample *t*-test was used to test differences in mean thalamic FA values between MS patients and HVs. A Welch's variance-weighted two sample *t*-test, accounting for the heterogeneous variances of thalamic MD values, was performed to investigate differences between MS patients and HVs.

Second, a regression analysis was used to investigate the effect of age on FA and MD values of each of the three groups (HVs, RR and SP) before comparing the three groups. Either analysis of variance (ANOVA) or Welch's variance-weighted ANOVA was used to test differences in mean thalamic FA and MD values among the three groups followed by a *post hoc* multiple pairwise comparison with Bonferroni correction. *P*-values only less than 0.0167 were considered significant for multiple comparisons after Bonferroni correction. Correlation analyses were conducted using the Pearson's correlation coefficient to investigate relationships of DTI measurements with clinical and MRI metrics. Significance was established at an alpha level of 0.05. The coefficient of variation (COV), given by

standard deviation (SD) divided by the mean, was used to evaluate the inter-scan, intra- and inter-observer variability. All statistical analysis was performed using the SAS software version 9.1 (SAS Institute Inc., Cary, NC, USA).

RESULTS

Conventional MRI exams were found to be normal in HVs based on radiological evaluation. The inter-scan variability results showed good reproducibility for both FA (COV of 4.0 %) and MD (COV of 2.1 %) in the thalamus. The intra-observer variability results also showed good reproducibility for both FA (COV of 1.3 %) and MD (COV of 0.2 %). In addition, the inter-observer variability showed good reproducibility for both FA (COV of 0.83%) and MD (COV of 0.39%).

Differences in FA and MD values between MS patients and HVs

As shown in table 2, both FA (t_{46}=-5.92, $p < 0.0001$) and MD ($t_{33.3}$=-2.19, $p = 0.035$) values in the thalamus were higher in patients than in HVs.

When RR and SP patients were examined as a single cohort or as separate cohorts, age effect was not significant on either FA ($p = 0.81$) or MD (p=0.66) values. Thus we examined differences in mean FA and MD values among the three groups without correcting for the effect of age.

Among the three groups, significant mean differences were found in mean FA ($F_{2,45}$ = 17.15, $p < 0.0001$) and MD ($F_{2,18.37}$ = 4.16, $p = 0.0324$) values. As shown in Figure 2a, specifically for FA values, there was a significant difference between HV and RRMS patients (t_{35}=-4.76, $p < 0.0001$), between HVs and SPMS patients (t_{33}=-5.08, $p < 0.0001$),

but not between patients with RRMS and SPMS (t_{22}=-0.07, p = 0.94). In figure 2b one can see that a significant difference was found in MD values between HVs and SPMS patients groups (t_{33}=-3.32, p = 0.002), but not between either HVs and RRMS patients ($t_{14.2}$=-0.98, p = 0.34) or RRMS and SPMS patients (t_{22}=-0.85, p = 0.40).

Correlation between FA and MD and other MRI metrics

Details on the output of the correlations analyses between FA and MD values and T1 and T2 lesion volumes (LV) and BPF are described in Table 3. A significant correlation was found between thalamic FA and the T2LV in the entire group of patients (r = 0.48, p = 0.020). Such a correlation was lost when RR and SP patients were considered separately.

Thalamic MD was correlated with T2LV (r = 0.58, p = 0.004), T1LV (r = 0.58, p = 0.003) and BPF (r = -0.46, p = 0.024) in the entire group of patients (Figure 3). When considering RR and SP MS patients separately, MD values were significantly correlated to T2LV in both RR (r = 0.56, p = 0.046) and SP (r = 0.78, p = 0.007) patients and to T1LV only in SP group (r = 0.80, p = 0.005).

Correlation between thalamic FA and MD and clinical scores

Disease duration did not significantly affect DTI-derived metrics in the entire group of patients, as reported on table 3. In the same cohort of individuals, significant correlations were observed between the motor EDSS (r = 0.47, p = 0.021) and PASAT (r = -0.43, p = 0.034) scores and MD (Figure 4) but not FA values.

When RR and SP patients were considered separately, correlations were seen between thalamic MD and functional scores of RR patients only. While disease duration was significantly related to thalamic FA changes only in the SP group, in the RR patients, MD

values were strongly correlated with EDSS (r = 0.75, p = 0.003) and motor-specific EDSS scores (r = 0.68, p = 0.010) (Figure 5).

DISCUSSION

The role of GM disease, alone or together with WM damage, in explaining patients' disability and in predicting disease progression in MS is now becoming more evident (41-43).

Primary or secondary damage of thalamic tissue and/or radiations may play an important role in motor, sensory and cognitive symptoms of these patients. This can be attributed to the existence of massive reciprocal connections between thalamic nuclei and cortical areas (7, 44).

To provide further insight into the role of thalamus in MS patients, in this study we used 3.0T DTI acquisition to probe for structural thalamic changes in patients with MS. Our three major findings were as follows: (1) FA and MD from DTI at 3.0T are both sensitive to detect thalamic damage in patients with MS; (2) increase in thalamic MD correlates with cognitive and motor scores when all MS patients were considered; (3) in RR-MS patients, thalamic involvement strongly explained patients' disability. These main findings are discussed in detail below.

Sensitivity of DTI in detecting thalamic involvement in patients with MS

MS patients exhibited higher FA values compared with HVs, when we considered either the overall MS population or each MS subgroup separately. These results confirmed previous findings of increased FA values in the thalamus and basal ganglia of MS patients

compared to HVs (24). In this study, FA values also differed between RR patients' subgroup and HVs, indicating that subtle thalamic damage can be present in patients with mild disease. Supporting this finding, thalamic atrophy was recently demonstrated in patients with early disease (14, 18), and decreased thalamic metabolism was observed in RR patients with low disability scores compared to matched HVs (19).

The biological basis of this effect is still poorly understood. Interpreting small anisotropy changes in thalamic tissue, in which several fiber pathways typically intersect, is a difficult task (23, 24, 47) that requires validation by combined MRI and post-mortem studies. Nevertheless, a possible explanation is that greater or isolated axonal degeneration of a specific group of crossing fibers may be occurring, leading to a paradoxically increased FA of the specific region measured by the ROI approach (47). Future studies with histopathological correlation will be critical for clarifying this effect.

A significant increase in thalamic MD was detected, when all MS patients were considered and also in the SP subgroup, but not in RR subgroup. In contrast to our findings, three previous studies (9, 10, 24) did not show differences in MD between patients and HVs. Specifically, Griffin and colleagues did not find thalamic changes in DTI-derived metrics values in patients with early RR-MS compared to controls (9). The lower disability score of MS patients in this study (median EDSS of 1.0) compared to ours, could have contributed to the differences between their and our results. In fact, we also did not find differences when comparing the thalamic MD values of RR-MS and HVs. Ciccarelli and colleagues (24) did not report MD changes in the thalamus of MS patients with a mean disability score (median EDSS of 3.9) similar to ours. In contrast to our study, their cohort included approximately 20 % of patients with primary progressive (PP) MS and 28 % with benign MS. Indeed, while absence of detectable MD changes in early MS patients supports the

findings of Griffin and colleagues, lack of disease pathology in the thalamus of PP-MS is explained by the fact that little disease is known to occur in the brain of PP-MS patients who likely experience mostly spinal cord abnormalities. Interestingly, Filippi and colleagues (10) also did not report an increase in thalamic diffusivity of MS patients with disability score and MS subtypes comparable to ours. Although the differences between patients and HVs were based mainly on SP-MS patients, we believe that the higher sensitivity in detecting MD changes may be due to the increased SNR from the use of a high field MRI (3.0T) and multi-channel receive-only coil (26). In addition, a higher resolution DTI technique (both in-plane and out of plane) employed in the present study may also explain the discrepancies between our findings and those of previous studies. Also, the improved pre-processing steps followed prior to tensor calculation, such as correction for movement artifacts and EPI-induced distortions (26, 27), may be accountable for these differences.

Other MRI methods have also demonstrated thalamic abnormalities in MS. A decreased magnetization transfer rate was reported in MS patients (17), as well as decreases in N-acetyl aspartate, a neuronal marker (16, 48). These findings point to loss of tissue integrity, and concur with the demonstration of axonal tract damage in histopathological studies (5, 49). The increased MD values in the thalamus in our study most likely correspond to increased water component in the normal appearing tissue, which agrees with the possibility of demyelination and/or axonal damage

Correlation between DTI–derived and other MRI metrics

In the present study, correlations were found between DTI-derived metrics in the thalamus and remote WM damage reflected in T2LV (MD and FA), T1LV (MD) or BPF (MD).

Those results are in agreement with previous ones obtained by applying other MRI techniques. Increase in thalamic myo-inositol was also shown to be correlated to WM T2 lesion load in a spectroscopy study of patients with MS (16). Because several WM tracts linking the thalamus with different cortical regions cross the deep WM, one plausible hypothesis would be that structural damage to WM networks could induce trans-synaptic axonal degeneration within thalamic nuclei. Yet, whether the relationship between these two processes is causal or indirect remains uncertain. The relative importance of direct microscopic damage to the thalamus in MS is also an interesting issue that will require further investigation.

Relationship between DTI-derived metrics and clinical scores

The thalamus is densely interconnected with many cortical regions, especially with the frontal and parietal areas (7, 44, 46). Thus, thalamic damage can potentially trigger a range of motor and cognitive dysfunctions in patients with MS. Our results support this hypothesis, as motor EDSS and PASAT were significantly correlated to MD changes in the thalamus in the patient cohort of our study. In the RR subgroup, MD was strongly correlated to total EDSS and motor EDSS, and a trend was observed with sensory EDSS and PASAT. Remarkably, the increase in thalamic MD explained the 55% of variance in EDSS in RR-MS patients. Future studies using thalamic nuclei segmentation and correlation to regional WM disease will be crucial for understanding whether changes in thalamic MD are topographically related to damage or dysfunction of specific thalamo-cortical networks.

In patients with SP-MS, there were no significant correlations between clinical scores and DTI-derived metrics. This result is not necessarily a contradictory finding and may reflect

the fact that the functional disability scores were high but restricted within a narrow range (i.e. 5.0 to 7.5) in most patients belonging to the SP subgroup, thus reducing the variability due to a ceiling effect. Furthermore, it is well known that spinal cord pathology also accounts for disability in SP-MS patients. A larger study of patients with RR and SP, with wider ranges of functional scores will confirm and extend our results.

In general, disease duration was not correlated to changes in FA or MD in MS patients, except for a moderate correlation between disease duration and FA changes in the SP group. This result supports the view that structural damage is better explained by the severity of functional impairment than by the duration of the disease.

In conclusion, DTI-derived metrics at 3.0T were sensitive in detecting microstructural damage in the normal appearing thalamus of patients with MS, with both FA and MD being higher in MS patients as compared to HVs. MD was correlated with motor and cognitive symptoms in the MS patients and strongly correlated with disability in the RR group. MD was also moderately correlated with WM lesion load. It is therefore possible that both direct and indirect damage to the thalamus occurs in MS. These findings further strengthen the importance of GM damage in the symptomatology of MS patients. Future studies addressing the relationships between non-invasive imaging and histopathology will be necessary to explain the nature of thalamic involvement in MS patients.

Acknowledgments:

We thank Drs. Susumu Mori, Xin Li and Talin A. Tasciyan for software support. We are grateful to Jeanette Black, Renée Hill, Dr. Kristina Symonian and Dr. Vasiliki Ikonomidou for their help with image acquisition. We thank Mr. Roger Stone, Ms. Helen Griffin and Dr. Valentina Durastanti for helping with the clinical data collection and organization.

We are most grateful to all the patients and their families as well as all the healthy volunteers for their time, patience and cooperation.

This work was supported by the Intramural Program of the National Institute of Neurological Disorders and Stroke, National Institutes of Health. Dr. Fernanda Tovar-Moll was partially supported by LABS – D'Or Hospital Network, Rio de Janeiro, Brazil.

REFERENCES:

1. Barkhof F. MRI in multiple sclerosis: correlation with expanded disability status scale (EDSS). Mult Scler 1999; 5:283-286.
2. McFarland HF, Barkhof F, Antel J, Miller DH. The role of MRI as a surrogate outcome measure in multiple sclerosis. Mult Scler 2002; 8:40-51.
3. Bagnato F, Frank JA. The role of nonconventional magnetic resonance imaging techniques in demyelinating disorders. Curr Neurol Neurosci Rep 2003; 3:238-245.
4. Filippi M. Non-conventional MR techniques to monitor the evolution of multiple sclerosis. Neurol Sci 2001; 22:195-200.
5. Cifelli A, Arridge M, Jezzard P, Esiri MM, Palace J, Matthews PM. Thalamic neurodegeneration in multiple sclerosis. Ann Neurol 2002; 52:650-653.
6. Kutzelnigg A, Lassmann H. Cortical lesions and brain atrophy in MS. J Neurol Sci 2005; 233:55-59.
7. Alexander GE, DeLong MR, Strick PL. Parallel organization of functionally segregated circuits linking basal ganglia and cortex. Annu Rev Neurosci 1986; 9:357-381.
8. Richert ND, Ostuni JL, Bash CN, Duyn JH, McFarland HF, Frank JA. Serial whole-brain magnetization transfer imaging in patients with relapsing-remitting multiple sclerosis at baseline and during treatment with interferon beta-1b. AJNR Am J Neuroradiol 1998; 19:1705-1713.
9. Griffin CM, Chard DT, Ciccarelli O, et al. Diffusion tensor imaging in early relapsing-remitting multiple sclerosis. Mult Scler 2001; 7:290-297.

10. Filippi M, Bozzali M, Comi G. Magnetization transfer and diffusion tensor MR imaging of basal ganglia from patients with multiple sclerosis. J Neurol Sci 2001; 183:69-72.

11. Sharma J, Zivadinov R, Jaisani Z, et al. A magnetization transfer MRI study of deep gray matter involvement in multiple sclerosis. J Neuroimaging 2006; 16:302-310.

12. Inglese M, Ge Y, Filippi M, Falini A, Grossman RI, Gonen O. Indirect evidence for early widespread gray matter involvement in relapsing-remitting multiple sclerosis. Neuroimage 2004; 21:1825-1829.

13. Fabiano AJ, Sharma J, Weinstock-Guttman B, et al. Thalamic involvement in multiple sclerosis: a diffusion-weighted magnetic resonance imaging study. J Neuroimaging 2003; 13:307-314.

14. Audoin B, Ranjeva JP, Au Duong MV, et al. Voxel-based analysis of MTR images: a method to locate gray matter abnormalities in patients at the earliest stage of multiple sclerosis. J Magn Reson Imaging 2004; 20:765-771.

15. Bermel RA, Innus MD, Tjoa CW, Bakshi R. Selective caudate atrophy in multiple sclerosis: a 3D MRI parcellation study. Neuroreport 2003; 14:335-339.

16. Geurts JJ, Reuling IE, Vrenken H, et al. MR spectroscopic evidence for thalamic and hippocampal, but not cortical, damage in multiple sclerosis. Magn Reson Med 2006; 55:478-483.

17. Cao M, Calabrese M, Gupta S, et al. Deep grey matter disease in multiple sclerosis: a primary or secondary pathogenetic process? Mult Scler 2005; 11:232.

18. Davies GR, Altmann DR, Hadjiprocopis A, et al. Increasing normal-appearing grey and white matter magnetisation transfer ratio abnormality in early relapsing-remitting multiple sclerosis. J Neurol 2005; 252:1037-1044.

19. Derache N, Marie RM, Constans JM, Defer GL. Reduced thalamic and cerebellar rest metabolism in relapsing-remitting multiple sclerosis, a positron emission tomography study: correlations to lesion load. J Neurol Sci 2006; 245:103-109.

20. Basser PJ, Pierpaoli C. Microstructural and physiological features of tissues elucidated by quantitative-diffusion-tensor MRI. J Magn Reson B 1996; 111:209-219.

21. O'Sullivan M, Singhal S, Charlton R, Markus HS. Diffusion tensor imaging of thalamus correlates with cognition in CADASIL without dementia. Neurology 2004; 62:702-707.

22. Hagmann P, Thiran JP, Jonasson L, et al. DTI mapping of human brain connectivity: statistical fibre tracking and virtual dissection. Neuroimage 2003; 19:545-554.

23. Hagmann P, Jonasson L, Maeder P, Thiran JP, Wedeen VJ, Meuli R. Understanding Diffusion MR Imaging Techniques: From Scalar Diffusion-weighted Imaging to Diffusion Tensor Imaging and Beyond. Radiographics 2006; 26 Suppl 1:S205-223.

24. Ciccarelli O, Werring DJ, Wheeler-Kingshott CA, et al. Investigation of MS normal-appearing brain using diffusion tensor MRI with clinical correlations. Neurology 2001; 56:926-933.

25. Ceccarelli A, Rocca MA, Falini A, et al. Normal-appearing white and grey matter damage in MS: A volumetric and diffusion tensor MRI study at 3.0 Tesla. J Neurol 2007; 254(4):513-8.

26. Alexander AL, Lee JE, Wu YC, Field AS. Comparison of diffusion tensor imaging measurements at 3.0 T versus 1.5 T with and without parallel imaging. Neuroimaging Clin N Am 2006; 16:299-309, xi.

27. Fushimi Y, Miki Y, Okada T, et al. Fractional anisotropy and mean diffusivity: comparison between 3.0-T and 1.5-T diffusion tensor imaging with parallel imaging using histogram and region of interest analysis. NMR Biomed 2007; (Epub ahead of print).

28. Poser CM, Paty DW, Scheinberg L, et al. New diagnostic criteria for multiple sclerosis: guidelines for research protocols. Ann Neurol 1983; 13:227-231.

29. Kurtzke JF. Rating neurologic impairment in multiple sclerosis: an expanded disability status scale (EDSS). Neurology 1983; 33:1444-1452.

30. Gronwall D, Wrightson P. Delayed recovery of intellectual function after minor head injury. Lancet 1974; 2:605-609.

31. Gronwall D, Wrightson P. Memory and information processing capacity after closed head injury. J Neurol Neurosurg Psychiatry 1981; 44:889-895.

32. Lublin FD, Reingold SC. Defining the clinical course of multiple sclerosis: results of an international survey. National Multiple Sclerosis Society (USA) Advisory Committee on Clinical Trials of New Agents in Multiple Sclerosis. Neurology 1996; 46:907-911.

33. Gupta S, Solomon JM, Tasciyan TA, et al. Interferon-beta-1b effects on re-enhancing lesions in patients with multiple sclerosis. Mult Scler 2005; 11:658-668

34. Bagnato F, Jeffries N, Richert ND, et al. Evolution of T1 black holes in patients with multiple sclerosis imaged monthly for 4 years. Brain 2003; 126:1782-1789.

35. Smith SM, Zhang Y, Jenkinson M, et al. Accurate, robust, and automated longitudinal and cross-sectional brain change analysis. Neuroimage 2002; 17:479-489.

36. Basser PJ, Mattiello J, LeBihan D. Estimation of the effective self-diffusion tensor from the NMR spin echo. J Magn Reson B 1994; 103:247-254.

37. Jiang H, van Zijl PC, Kim J, Pearlson GD, Mori S. DtiStudio: resource program for diffusion tensor computation and fiber bundle tracking. Comput Methods Programs Biomed 2006; 81:106-116.

38. Pajevic S, Pierpaoli C. Color schemes to represent the orientation of anisotropic tissues from diffusion tensor data: application to white matter fiber tract mapping in the human brain. Magn Reson Med 1999; 42:526-540.

39. Crum WR, Hartkens T, Hill DL. Non-rigid image registration: theory and practice. Br J Radiol 2004; 77 Spec No 2:S140-153.

40. Catani M, Jones DK, Donato R, Ffytche DH. Occipito-temporal connections in the human brain. Brain 2003; 126:2093-2107.

41. Codella M, Rocca MA, Colombo B, Martinelli-Boneschi F, Comi G, Filippi M. Cerebral grey matter pathology and fatigue in patients with multiple sclerosis: a preliminary study. J Neurol Sci 2002; 194:71-74.

42. Rovaris M, Judica E, Gallo A, et al. Grey matter damage predicts the evolution of primary progressive multiple sclerosis at 5 years. Brain 2006; 129:2628-2634.

43. Rovaris M, Bozzali M, Iannucci G, et al. Assessment of normal-appearing white and gray matter in patients with primary progressive multiple sclerosis: a diffusion-tensor magnetic resonance imaging study. Arch Neurol 2002; 59:1406-1412.

44. Behrens TE, Johansen-Berg H, Woolrich MW, et al. Non-invasive mapping of connections between human thalamus and cortex using diffusion imaging. Nat Neurosci 2003; 6:750-757.

45. Hasan KM, Gupta RK, Santos RM, Wolinsky JS, Narayana PA. Diffusion tensor fractional anisotropy of the normal-appearing seven segments of the corpus callosum in healthy adults and relapsing-remitting multiple sclerosis patients. J Magn Reson Imaging 2005; 21:735-743.

46. Johansen-Berg H, Behrens TE, Sillery E, et al. Functional-anatomical validation and individual variation of diffusion tractography-based segmentation of the human thalamus. Cereb Cortex 2005; 15:31-39.

47. Pierpaoli C, Barnett A, Pajevic S, et al. Water diffusion changes in Wallerian degeneration and their dependence on white matter architecture. Neuroimage 2001; 13:1174-1185.

48. Inglese M, Liu S, Babb JS, Mannon LJ, Grossman RI, Gonen O. Three-dimensional proton spectroscopy of deep gray matter nuclei in relapsing-remitting MS. Neurology 2004; 63:170-172.

49. Kidd D, Barkhof F, McConnell R, Algra PR, Allen IV, Revesz T. Cortical lesions in multiple sclerosis. Brain 1999; 122 (Pt 1):17-26.

Table 1: Demographic, clinical, and MRI characteristics of healthy volunteers and patients.

	HV (n=24)	RR (n=13)	SP (n=11)
Age	41.9 ± 8.3 years	41.7± 6.1 years	46.9± 9.6 years
EDSS	–	2.2 ± 1.2**	5.9 ± 1.0 **
EDSS-motor	–	1.7 ± 1.1 **	3.5 ± 0.8 **
EDSS-sens	–	1.2 ± 1.0*	2.2 ± 0.9*
DD	–	11.1 ± 6.5 *	17.6 ± 4.7 *
PASAT	–	47.5 ± 15.9	37.1± 11.1
T1LV	–	3.82 ± 3.43cm^3	6.08 ± 3.70cm^3
T2LV	–	14.41 ± 10.79cm^3	17.89 ± 14.95cm^3
BPF	0.84 ± 0.02 #	0.80 ± 0.04 * #	0.75± 0.04 * #
CELs	–	1	0

Note: Data are mean ± standard deviation. HV: healthy volunteers; RR: relapsing-remitting multiple sclerosis patients; SP: secondary-progressive multiple sclerosis patients; EDSS: Expanded Disability Status Scale; EDSS-motor: partial motor score of the EDSS; EDSS-sens: partial sensory score of the EDSS; DD: disease duration; PASAT: Paced Auditory Serial Addition task; T1LV: T1 lesion volume; T2LV: T2 lesion volume; BPF: brain parenchymal fraction. CELs: number of patients with contrast-enhancing lesions.

* $p < 0.05$, comparison between RR and SP

** $p < 0.001$, comparison between RR and SP

# $p < 0.001$, comparison to HV

Table 2: Thalamic DTI derived measures of healthy volunteers and patients.

	HV (n=24)	All MS (n=24)	RR (n=13)	SP (n=11)
FA	0.276 ± 0.017	0.308 ± 0.020[#]	0.307 ± 0.022[#]	0.308 ± 0.017[#]
MD	0.737 ± 0.019	0.757 ± 0.039*	0.751 ± 0.046	0.764 ± 0.028**

Note: Data are mean ± standard deviation. HV: healthy volunteers; All MS: overall multiple sclerosis patients; RR: relapsing-remitting multiple sclerosis patients; SP: secondary-progressive multiple sclerosis patients; FA: fractional anisotropy; MD: mean diffusivity. MD in $mm^2/s \times 10^{-3}$

* $p < 0.05$, comparison to HV

** $p < 0.01$, comparison to HV

[#] $p < 0.0001$, comparison to HV

Table 3: Pearson's correlation coefficient between DTI measurements (FA and MD) and clinical and MRI metrics.

	All MS patients (n=24)		RRMS patients (n=13)		SPMS patients (n=11)	
	FA	MD	FA	MD	FA	MD
DD	0.291	0.132	0.187	0.06	0.638*	0.018
EDSS	0.174	0.351	0.193	0.748*	0.545	-0.475
EDSS-motor	0.287	0.468*	0.396	0.683*	0.340	-0.049
EDSS-sens	0.087	0.317	-0.019	0.535	0.286	-0.328
PASAT	-0.042	-0.434*	-0.235	-0.502	0.400	-0.122
T1LV	0.321	0.584*	0.318	0.534	0.325	0.804*
T2LV	0.481*	0.582*	0.544	0.562*	0.439	0.784*
BPF	-0.093	-0.458*	-0.293	-0.521	0.208	-0.292

Note: All MS: overall multiple sclerosis patients; RR: relapsing-remitting multiple sclerosis patients; SP: secondary-progressive multiple sclerosis patients; FA: fractional anisotropy; MD: mean diffusivity; DD: disease duration; EDSS: Expanded Disability Status Scale; EDSS-motor: partial motor score of the EDSS; EDSS-sens: partial sensory score of the EDSS; PASAT: Paced Auditory Serial Addition Task; T1LV: T1 lesion volume; T2LV: T2 lesion volume; BPF: brain parenchymal fraction; * indicates correlations at a significant level of 0.05.

Figure 1: Bilateral thalamic region-of interest (ROIs) placed in three consecutive levels (slices) in the axial plane of a representative healthy volunteer: (A) b0-image, (B) fractional anisotropy (FA), (C) color-coded FA and (D) mean diffusivity maps.

Figure 2: (A) Fractional anisotropy values and (B) mean diffusivity values of the thalamus in healthy volunteers (HV) compared to patients with relapsing-remitting multiple sclerosis (RR) and patients with secondary progressive multiple sclerosis (SP).

Note: Box plots indicate median and upper and lower quartiles. Error bars indicate the range between the 90th and 10th percentiles. Circles indicate individual cases above the 90th percentile or below 10th percentile.

* $p < 0.05$, compared to HV

****** $p < 0.001$, compared to HV

Figure 3: Correlation plots between mean diffusivity (MD) values and (a) T1 lesion volume (T1LV), (b) T2 lesion volume (T2LV) and (c) brain parenchimal fraction (BPF) in the entire cohort of multiple sclerosis patients.

Note: Mean diffusivity in $mm^2/s \times 10^{-3}$

Figure 4: Correlation plots between mean diffusivity (MD) values and (a) Paced Auditory Serial Addition Task (PASAT) and (b) partial motor score of the Expanded Disability Status Scale (EDSS-motor) in the entire cohort of multiple sclerosis patients.

Note: Mean diffusivity in $mm^2/s \times 10^{-3}$

Figure 5: Correlation plots between mean diffusivity (MD) values and (a) Expanded Disability Status Scale (EDSS) and (b) partial motor score of the Expanded Disability Status Scale (EDSS-motor) in relapsing-remitting multiple sclerosis patients.

Note: Mean diffusivity in $mm^2/s \times 10^{-3}$

Figure 1:

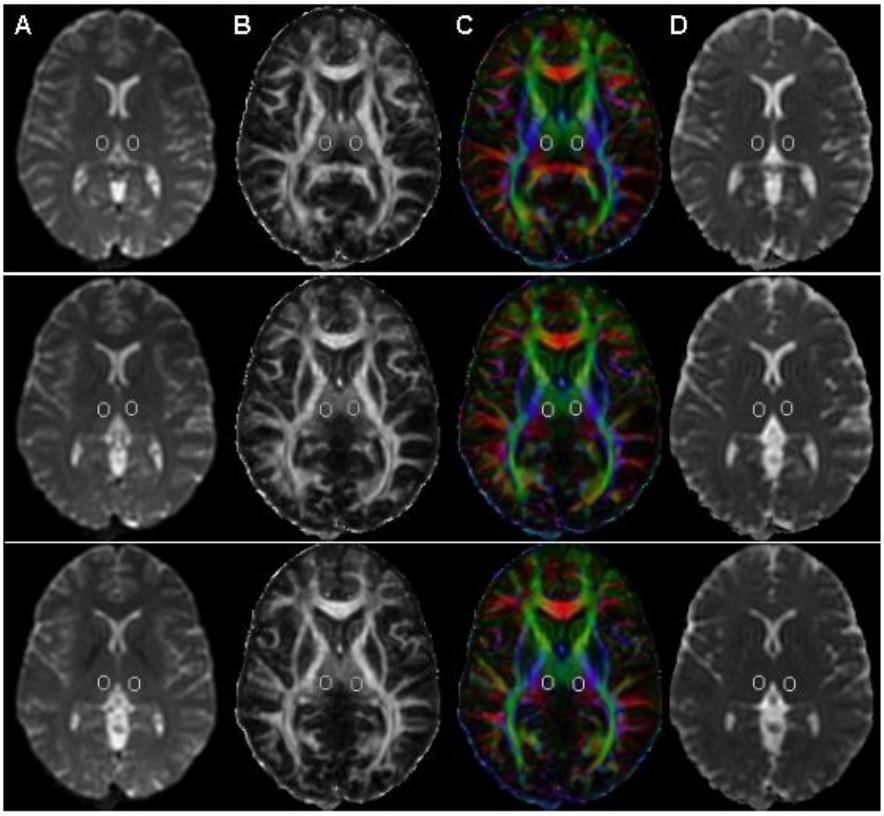

Figure 2:

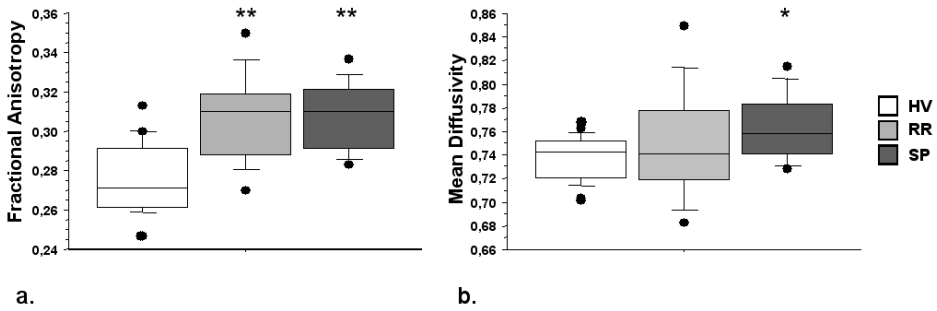

Figure 3:

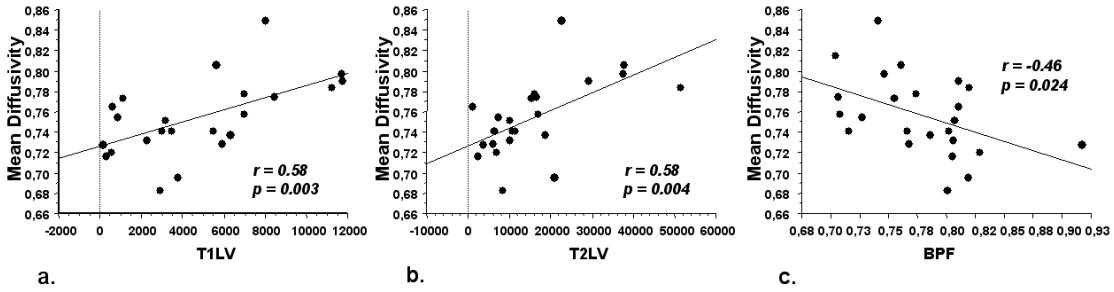

Figure 4:

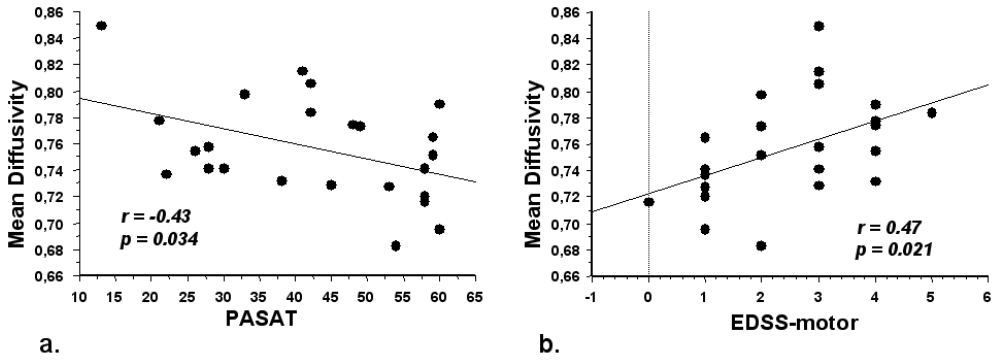

Figure 5:

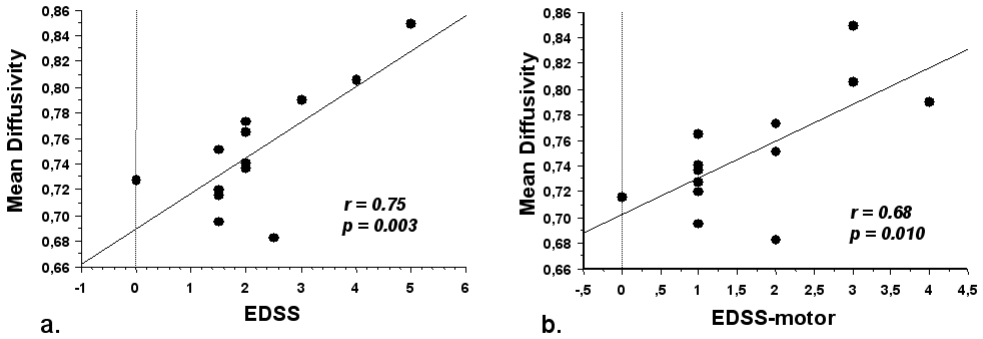

Brain Advance Access published December 14, 2007

doi:10.1093/brain/awm303 *Brain* (2007) Page 1 of 13

Focal white matter changes in spasmodic dysphonia: a combined diffusion tensor imaging and neuropathological study

Kristina Simonyan,[1] Fernanda Tovar-Moll,[2] John Ostuni,[3] Mark Hallett,[4] Victor F. Kalasinsky,[5] Michael R. Lewin-Smith,[5] Elisabeth J. Rushing,[6] Alexander O. Vortmeyer[7] and Christy L. Ludlow[1]

[1]Laryngeal and Speech Section, Medical Neurology Branch, [2]Neuroimmunology Branch, [3]Clinicial Neurosciences Program, [4]Human Motor Control Section, Medical Neurology Branch, [5]Department of Environmental and Infectious Disease Sciences, [6]Department of Neuropathology and Ophthalmic Pathology, Armed Forces Institute of Pathology and [7]Surgical Neurology Branch, National Institute of Neurological Disorders and Stroke, National Institutes of Health

Correspondence to: Kristina Simonyan, MD, PhD, Laryngeal and Speech Section, Medical Neurology Branch, National Institute of Neurological Disorders and Stroke, National Institutes of Health, 10 Center Drive, Building 10, Room 5D38, Bethesda, MD 20892-1416, USA
E-mail: simonyak@ninds.nih.gov

Spasmodic dysphonia is a neurological disorder characterized by involuntary spasms in the laryngeal muscles during speech production. Although the clinical symptoms are well characterized, the pathophysiology of this voice disorder is unknown. We describe here, for the first time to our knowledge, disorder-specific brain abnormalities in these patients as determined by a combined approach of diffusion tensor imaging (DTI) and *postmortem* histopathology. We used DTI to identify brain changes and to target those brain regions for neuropathological examination. DTI showed right-sided decrease of fractional anisotropy in the genu of the internal capsule and bilateral increase of overall water diffusivity in the white matter along the corticobulbar/corticospinal tract in 20 spasmodic dysphonia patients compared to 20 healthy subjects. In addition, water diffusivity was bilaterally increased in the lentiform nucleus, ventral thalamus and cerebellar white and grey matter in the patients. These brain changes were substantiated with focal histopathological abnormalities presented as a loss of axonal density and myelin content in the right genu of the internal capsule and clusters of mineral depositions, containing calcium, phosphorus and iron, in the parenchyma and vessel walls of the posterior limb of the internal capsule, putamen, globus pallidus and cerebellum in the *postmortem* brain tissue from one patient compared to three controls. The specificity of these brain abnormalities is confirmed by their localization, limited only to the corticobulbar/corticospinal tract and its main input/output structures. We also found positive correlation between the diffusivity changes and clinical symptoms of spasmodic dysphonia ($r = 0.509$, $P = 0.037$). These brain abnormalities may alter the central control of voluntary voice production and, therefore, may underlie the pathophysiology of this disorder.

Keywords: laryngeal dystonia; corticobulbar tract; basal ganglia; neuroimaging; neuropathology

Abbreviations: ABSD = abductor spasmodic dysphonia; ADSD = adductor spasmodic dysphonia; CBT/CST = corticobulbar/corticospinal tract; CV = coefficient of variance; DTI = diffusion tensor imaging; FA = fractional anisotropy; HV = healthy volunteer; ROI = region of interest; SD = spasmodic dysphonia; SEM-EDXA = scanning electron microscopy with energy dispersive X-ray analysis; TBSS = tract-based spatial statistics

Received May 10, 2007. Revised November 20, 2007. Accepted November 22, 2007

Introduction

Spasmodic dysphonia (SD) is a primary focal dystonia characterized by loss of voluntary control of vocal fold movements during speech production due to involuntary spasms in the laryngeal muscles. After onset in mid-life, symptoms progress gradually and remain chronic for life (Ludlow *et al.*, 1995). This disorder presents most often as the adductor type (ADSD) characterized by spasmodic bursts in the closing muscles of the vocal folds during vowel production, which result in voice breaks (Nash and

Ludlow, 1996). The less common abductor type (ABSD) exhibits slow vocal fold closure following voiceless consonants with intermittent breathy voice breaks (Edgar *et al.*, 2001). SD is a task-specific disorder, affecting voice only during speech, while emotional vocal expressions, such as laughter and cry, remain intact (Bloch *et al.*, 1985).

The pathophysiology of SD is poorly understood. Generally, the focal dystonias are assumed to involve basal ganglia dysfunction and disturbances in the sensory system that play an important role in development of motor control abnormalities (Berardelli *et al.*, 1998). Recent functional neuroimaging studies during voice and narrative speech production in ADSD found activation changes in the laryngeal/orofacial sensorimotor cortex and basal ganglia (Haslinger *et al.*, 2005; Ali *et al.*, 2006), which may contribute to the pathophysiology of SD. However, a fundamental question about the neurobiology of primary dystonia is whether an underlying pathology can be identified. Recently, *postmortem* abnormalities have been found in patients with Meige's syndrome (Kulisevsky *et al.*, 1988) and DYT1 dystonia (Zweig and Hedreen, 1988; McNaught *et al.*, 2004), but these were limited only to the brainstem. Surprisingly, no significant abnormalities have been found in the basal ganglia of these patients. Furthermore, neuropathology has never been reported in isolated focal dystonias, and, in particular, structural brain abnormalities in patients with spasmodic dysphonia have never been investigated.

Despite the paucity of neuropathological studies, an increasing number of neuroimaging studies have reported the presence of structural changes in patients with other forms of dystonia. Using DTI, reduced white matter integrity has been found in the subgyral region of the sensorimotor cortex in both manifesting and unaffected DYT1 carriers (Carbon *et al.*, 2004). In cervical dystonia, white matter changes have been identified in the genu and body of the corpus callosum as well as in the basal ganglia (Colosimo *et al.*, 2005). Another study in a group of patients with cervical dystonia, generalized dystonia and one patient with SD has found abnormalities in the white matter underlying the middle frontal and postcentral gyri and in the basal ganglia and thalamus with adjacent white matter (Bonilha *et al.*, 2007).

In this study, we aimed to examine the organization of white matter in SD using combined DTI and histopathological approaches. We hypothesized that these patients would have abnormalities in white matter tracts connecting the brain regions involved in voluntary voice production for speech. Task-specificity (Bloch *et al.*, 1985) suggests a separation of the affected voluntary voice production system, controlled by the laryngeal motor cortex, from the unaffected emotional voice production system, controlled by the anterior cingulate cortex (Jurgens, 2002). We hypothesized, therefore, that microstructural white matter changes in SD would be found only in the voluntary voice production system for speech, involving the corticobulbar pathway.

Material and Methods

DTI quantifies the random displacement of water molecules and provides an *in vivo* estimation of axonal organization in brain tissue (Basser *et al.*, 1994). DTI measures include anisotropy indices (e.g. fractional anisotropy, FA) to quantify the directionality of water diffusion and, therefore, reflect axonal integrity and tissue coherence. Diffusivity indices [e.g. Trace of diffusion tensor, Trace (*D*) and mean diffusivity, MD] quantify the magnitude of water movement independent of direction (Pierpaoli *et al.*, 1996). These measures are sensitive to *microstructural* brain tissue abnormalities not evident on conventional MRI (Pierpaoli *et al.*, 2001; Pfefferbaum and Sullivan, 2003).

Participants

Twenty patients with SD (14 ADSD, 6 ABSD; age 55.0 ± 10.0 years, mean $\pm$ standard deviation; 8 males/12 females) and 20 healthy volunteers (HV) (age 52.7 ± 9.5 years, mean $\pm$ standard deviation; 8 males/12 females) participated in the study. Physical examination was normal in all participants; none had a history of neurological disorders (other than SD in the patient group), psychiatric or otolaryngological problems. No other forms of primary or secondary dystonia were present in the patients or their immediate family members based on patients' medical histories.

The median duration of SD was 11.0 years (range from 1.5 to 27 years). All patients had failed to respond to voice and speech therapy; it was, however, unknown whether these patients' voice symptoms had worsened since onset. Sixteen patients had been on a regimen of botulinum toxin injections into their laryngeal muscles for several years to maintain their voice symptoms reduction. The median interval between the last botulinum toxin treatment and scanning session was 9 months (range from 3 to 42 months). Two ADSD and two ABSD patients had not previously been treated with botulinum toxin.

Video fiberoptic nasolaryngoscopy and speech testing confirmed diagnosis of SD as well as normal laryngeal function in HV. To assure that the patients had SD and not a functional or psychogenic voice disorder, all patients were required to have disorder-specific spasmodic voice breaks during conversational speech (Sapienza *et al.*, 2000; Barkmeier *et al.*, 2001; Edgar *et al.*, 2001). Diagnostic criteria included hyperadduction of the vocal folds during intermittent voice breaks on vowels for ADSD and prolonged vocal fold opening during breathy breaks on voiceless consonants for ABSD. None of the patients reported symptom-free periods after onset of SD or following voice therapy without regular botulinum toxin treatment. For the purposes of this study, patients agreed to forgo their usually scheduled botulinum toxin treatment in order to be symptomatic at the time of voice and speech testing and scanning. All participants provided written informed consent before taking part in the study, which was approved by the Institutional Review Board of the National Institute of Neurological Disorders and Stroke, National Institutes of Health.

Speech symptom recording and measurement

We quantified symptoms specific to SD that is voice breaks on vowels in ADSD patients and on prolonged voiceless consonants in ABSD patients (Barkmeier *et al.*, 2001; Edgar *et al.*, 2001). Before the scanning, voice and speech of 17 patients were recorded

digitally, while they repeated two sets of sentences: 10 sentences containing a high number of glottal stops before vowels to elicit symptoms of ADSD, and 10 sentences containing a high number of voiceless consonants (f/s/h/p/t/k) to elicit symptoms of ABSD. In all patients, digital speech recordings were made with a microphone positioned at a constant 2 inch mouth to microphone distance. The recorded samples were randomly ordered and anonymized before voice break counts were made by a speech-language pathologist with more than seven years of specialized experience with SD. The frequency of voice breaks in 20 sentences either on vowels or on voiceless consonants was counted (Bielamowicz and Ludlow, 2000; Barkmeier *et al.*, 2001); voice harshness in ADSD and breathiness in ABSD were rated using the Consensus Auditory-Perceptual Evaluation of Voice (CAPE-V) (Karnell *et al.*, 2007). Pearson correlation coefficients were computed to examine relationships between the speech symptoms and diffusion parameters ($P \leqslant 0.05$).

Data acquisition

Participants were scanned on a 3.0 Tesla GE Excite scanner using an eight-channel receive-only coil (General Electric Medical System, Milwaukee, WI, USA). A DTI sequence for whole brain coverage used a single-shot spin-echo echo-planar imaging sequence with paired gradient pulses positioned 180° around the refocusing pulse for diffusion weighting and sensitivity-encoding (ASSET) for rate 2 acceleration. Imaging parameters for the diffusion-weighted sequence were TE/TR = 73.4/13 000 ms, FOV = 2.4 × 2.4 cm^2; matrix = 96 × 96 mm^2 zero-filled to 256 × 256 mm^2; 54 contiguous axial slices with slice thickness of 2.4 mm. Diffusion was measured along 33 non-collinear directions with a b factor of 1000 s/mm^2. Three reference images were acquired with no diffusion gradients applied (b_0 scans). The same acquisition sequence was repeated two times.

For clinical evaluation, the T_2-weighted images were acquired (FSE-T2: TE/TR = 120/5100 ms; FOV = 2.4 × 2.4 cm^2; matrix = 256 × 256 mm; 54 axial slices with slice thickness of 2.4 mm; FLAIR: TE/TR = 12 000/102 ms; FOV = 2.4 × 2.4 cm^2; matrix = 160 × 160 mm; 28 slices with slice thickness of 5.0 mm).

Image post-processing

For each subject, DTI images were co-registered to correct for movement artifacts and eddy current distortion effects on EPI readout (Woods *et al.*, 1998; Jiang *et al.*, 2006). Raw diffusion-weighted images were visually inspected slice-by-slice for each subject, and distorted slices were excluded from analysis before tensor calculation. The diffusion tensor for each voxel was calculated based on the eigenvectors (v_1, v_2, v_3) and eigenvalues ($\lambda_1, \lambda_2, \lambda_3$) using multivariate fitting and diagonalization. After the FA and Trace (D) maps were calculated from the eigenvalues, colour-coded maps were generated from the FA values and the three vector elements of v_1 to visualize the white matter tract orientation (DtiStudio software) (Pajevic and Pierpaoli, 1999; Jiang *et al.*, 2006). The derived FA and Trace data were further analysed using two approaches: the unbiased whole-brain tract-based spatial statistics (TBSS) (Smith *et al.*, 2006) and *a priori* regions of interest (ROI) analyses.

To assess scanner inter-session variability, four HVs were re-scanned at least 2 weeks apart with the post-processing and calculation of the DTI-derived parameters repeated. Inter-session variability for FA and Trace was represented as percent coefficient of variance [CV = (standard deviation/mean) × 100].

Unbiased whole-brain analysis

To assess the global differences in the white matter fibre tracts between the SD and HV groups, whole-brain voxelwise statistical analyses of FA and Trace data were conducted using TBSS *without an a priori* assumption (FSL, FMRIB Software Library) (Smith *et al.*, 2006). Because two comparisons were being conducted, a criterion alpha of 0.025 ($P = 0.05/2$) was applied for analyses of both the FA and Trace datasets. FA and Trace images were first brain-extracted (Smith, 2002) and registered to a common space (MNI152) using constrained nonlinear registration (Image Registration Toolkit) (Rueckert *et al.*, 1999). The mean of all registered FA maps was generated and used to create a mean FA skeleton, which represented the centers of all tracts common to all subjects. Each subject's aligned FA and Trace data were registered to the common FA skeleton via a perpendicular search from each tract in the mean FA skeleton to each image's local tract center forming a sparse (skeletonized) 4D image. Statistical analyses for each point of the mean skeleton were conducted for both FA and Trace maps using univariate general linear modelling design (FEAT, FSL, FMRIB Software Library) to test for significant differences between the two groups. Correction for multiple comparisons was performed using permutation-based inference (5000 permutations) (Nichols and Holmes, 2002) with a cluster-forming threshold of $t > 3$ and a corrected cluster size significance level of $P \leqslant 0.025$ (randomize, FSL, FMRIB Software Library) (Smith *et al.*, 2006). This approach controlled for familywise errors (FWE) due to the chance of one or more false positives occurring anywhere on the skeleton while searching over the entire skeleton for regions of significant effect (Smith *et al.*, 2006).

ROI analysis

Because we hypothesized that regions involved in the control of voluntary voice production for speech, but not for emotional vocal expressions, would be affected in SD, we identified the two sets of ROIs for analysis. *A priori* ROIs were defined along the corticobulbar/corticospinal tract (CBT/CST) in the genu and the posterior third quarter of the posterior limb of the internal capsule, the mid-third of the cerebral peduncle and the pyramid. Furthermore, the ROIs were defined in the main input/output structures contributing to the CBT/CST: in the lentiform nucleus, the ventral thalamus and the middle third of the middle cerebellar peduncle. On the other hand, the ROIs in the cingulum underlying the anterior cingulate cortex were chosen to test the hypothesis that changes would not be present in the white matter tracts connecting the brain regions involved in the control of voice initiation and voice expression of emotional states (Jurgens, 2002), which remain unaffected in SD patients.

Prior to ROI analysis, the FA and Trace datasets were anonymized and randomized across the subjects and groups (J.O.). All ROIs were placed by the same rater (K.S.) blind to participants identity and diagnosis using a DTI-MRI atlas of human white matter (Mori, 2005) for determining fibre tract orientation. For each subject, the ROIs were outlined on the colour-coded FA maps in the axial plane as fixed-size squares to avoid arbitrary size of ROIs across participants (25 pixels/ROI along the CBT/CST; 36 pixel/ROI in the lentiform nucleus; 64 pixel/ROI in the thalamus) and then automatically loaded onto the FA and Trace

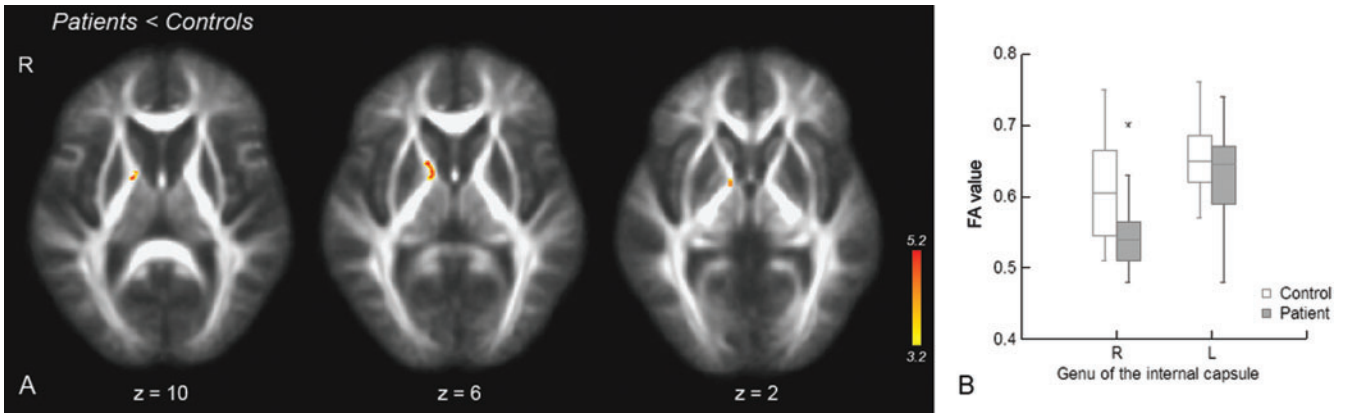

Fig. 1 Group differences in fractional anisotropy. (**A**) TBSS whole-brain and (**B**) a priori ROI analyses found significant FA decrease in the right genu of the internal capsule in SD patients. Group differences (patients < controls) are overlaid onto the average FA map across all subjects; plane coordinates of axial brain images are in Talairach-Tournoux standard space, respectively; colour bar indicates the significance range at $Z > 3.2$. Box plots indicate median and upper and lower quartiles. Error bars indicate the range between the 90th and 10th percentiles. Asterisk indicates significant difference between two groups. R = right; L = left.

maps (see supplementary Fig. 1 online). All ROIs were visually checked to confirm their location, to ensure that partial volume effects were minimized and that each ROI contained homogeneous fibre populations through examination of slices one dorsal and one caudal from the target. The mean values and standard deviations of FA and Trace measures within each ROI were automatically recorded.

To control for intra-observer variability, FA and Trace ROI values were re-calculated in six subjects at least 2 weeks apart to assess the percent coefficient of variance as a measure of repeatability.

Regression analyses examined age and gender effects on the FA and Trace values within each group to determine whether these factors needed to be used as covariates in group comparisons (Furutani *et al.*, 2005). Two-way repeated analyses of variance (ANOVA) were used for group (independent) comparisons, including all ROIs (repeated) on the right and left hemispheres (repeated) for both the FA and Trace values. The overall significance level was set at 0.025 ($P = 0.05/2$) for each of FA and Trace ANOVAs. If the group effects or their interactions on overall ANOVAs were statistically significant at $P \leqslant 0.025$, *post hoc* univariate *F*-tests determined which brain regions differed significantly between the groups. Because the Bonferroni correction for multiple comparisons for each of FA and Trace values resulted in an overly conservative correction ($P = 0.0016$) reducing power on the individual tests and increasing the possibility of a type II error, the statistical significance for post hoc tests was set at $P < 0.01$. The relationship between the FA and Trace values was assessed using Pearson's correlation coefficients at an alpha level of 0.05.

DTI-guided *postmortem* brain tissue sampling

To evaluate possible bases for DTI changes in SD, we targeted and sampled *postmortem* brain tissue in one SD patient and three controls from regions corresponding to FA and Trace changes between SD and HV groups. These matched *postmortem* tissue samples included regions of the right internal capsule, lentiform nucleus and cerebellum. *Postmortem* brain tissue from patient's left hemisphere as well as brain tissue from the regions of the sensorimotor cortex, corona radiata, thalamus and cerebral peduncle in the right hemisphere was not available to us for neuropathological examination. *Antemortem*, the patient (male, 65 years old) diagnosed with ADSD presented with strained voice quality and moderate adductor voice breaks during vowel production. The onset of the disorder was at age 36 years. The patient was diagnosed and treated at the National Institutes of Health with botulinum toxin injections into the thyroarytenoid muscles at regular intervals over 10 years. The brain tissue from this patient was obtained following death, which occurred during cardiac bypass surgery. The control brain tissue was obtained from three subjects (females; age range 58–86 years) without any history of neurological or psychiatric disorders, who died due to cardiovascular disease, disseminated intervascular coagulation, and dehydration with hypernatraemia, respectively.

The brain tissue from all subjects was fixed in 10% formalin solution and sectioned into 2-cm thick coronal slices for gross examination. Guided by the hardcopy of the T_1-weighted images in coronal plane with overlaid FA and Trace group differences, tissue samples were dissected from the right genu and posterior limb of the internal capsule, the lentiform nucleus and the cerebellum for paraffin embedding. For histopathological examination, paraffin sections (thickness 5 μm) were stained with hematoxylin and eosin (H&E) and luxol-fast blue/periodic acid Schiff (LFB/PAS) to assess cell morphology and myelin changes. The immunohistochemical markers, KP1 (anti-CD68) and anti-neurofilament triplet protein (anti-NFTP), were used for visualization of microglia/macrophage activation and the intermediate filament proteins of neuronal differentiation, respectively. In brief, sections were pre-treated with DAKO Target Retrieval Solution (DakoCytomation, Carpinteria, CA) at 95°C for 20 min, cooled at room temperature and incubated with primary antibody at dilution of 1 : 100 for 30 min (monoclonal mouse anti-human CD68, Clone KP1; monoclonal mouse anti-human neurofilament protein, Clone 2F11; DakoCytomation, Denmark). Primary antibodies were omitted for negative controls. The sections were then incubated with a refined avidin-biotin visualization kit (LSAB+ System-HRP, DakoCytomation, Carpinteria, CA) for 1 h.

For evaluation of Trace differences between SD and HV groups, subsequent sections from the internal capsule, lentiform nucleus and cerebellum were additionally processed with alizarin red S stain for visualization of calcium deposition, with von Kossa stain

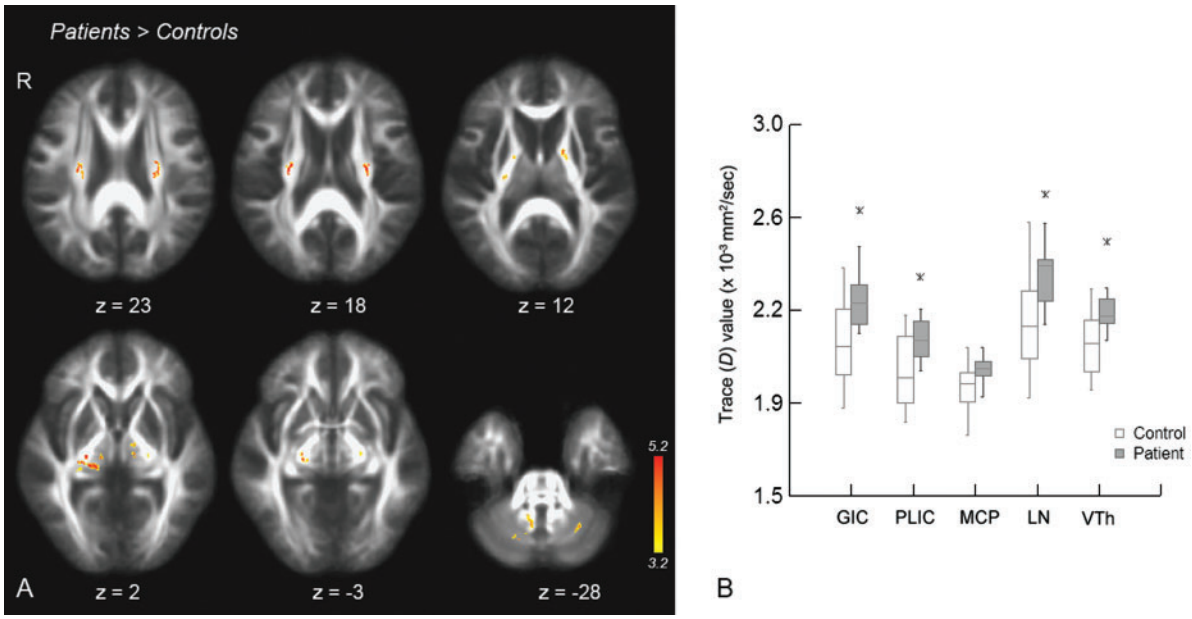

Fig. 2 Group differences in Trace (*D*). (**A**) TBSS whole-brain analysis found significant increase of overall diffusivity in the corona radiata, genu and posterior limb of the internal capsule, cerebral peduncle, ventral thalamus, and cerebellum. Group differences (patients > control) are overlaid onto the average FA map across all subjects; plane coordinates of axial brain images are in Talairach-Tournoux standard space, respectively; colour bar indicates the significance range at $Z > 3.2$. (**B**) *A priori* ROI analysis found significant increase of Trace values ($\times 10^{-3}$ mm^2/s) in the genu (GIC) and posterior limb (PLIC) of the internal capsule, lentiform nucleus (LN), and ventral thalamus (VTh) with a trend in the middle cerebellar peduncle (MCP) in SD patients. Box plots indicate median and upper and lower quartiles. Error bars indicate the range between the 90th and 10th percentiles. Asterisks indicate significant difference between two groups. R = right; L = left.

for phosphates and other anions, and with Prussian blue stain for iron accumulations, respectively. Furthermore, infrared spectroscopy was performed for routine molecular characterization of tissue depositions. Infrared spectra were obtained by focusing the infrared light onto tissue sections mounted on aluminium-coated glass slides (ThermoNicolet, Madison, WI). Spectra were recorded at 4 cm^{-1} spectral resolution. The measured infrared spectra were compared with those of the authentic samples and to spectra stored in a digital spectral library. To obtain the broader spectrum of elemental compositions of depositions found on H&E sections, a scanning electron microscope (Hitachi Instruments, Inc., San Jose, CA) with energy dispersive X-ray analysis (ThermoNoran, Madison, WI) (SEM-EDXA) was used to determine the particles with atomic numbers as low as that of beryllium. However, because of the difficulties in co-localization of the clusters on unstained section using SEM-EDXA, the analysis was limited to the parenchymal clusters located closely to the identifiable vessels in an unstained tissue sample. The EDXA detected the X-rays produced by the elements in the tissue samples when exposed to a 20 kV electron beam. X-rays were directed to the liquid-nitrogen-cooled silicon detector fitted with a Norvar® window.

Results

Conventional MRI was normal without any structural differences between patients and controls based on radiological evaluation. The inter-session variability results showed good reproducibility for both FA (CV of 4%) and Trace (CV of 2.1%). The intra-observer variability results also showed good reproducibility for both FA (CV of 2.30%) and Trace (CV of 0.53%). No significant relationships were found in either group between the diffusion parameters and age (FA: $r_{SD} = 0.088$, $P_{SD} = 0.713$; $r_{control} = 0.300$, $P_{control} = 0.199$; Trace: $r_{SD} = 0.141$, $P_{SD} = 0.552$; $r_{control} = 0.282$, $P_{control} = 0.228$) or gender (FA: $r_{SD} = 0.133$, $P_{SD} = 0.577$; $r_{control} = 0.084$, $P_{control} = 0.725$; Trace: $r_{SD} = 0.208$, $P_{SD} = 0.379$; $r_{control} = 0.137$, $P_{control} = 0.564$). Therefore, group comparisons were conducted without covariates.

Fractional anisotropy

The TBSS whole-brain analysis showed decreased FA only in the right genu of the internal capsule in SD patients compared with HV (Fig. 1A). The ANOVA comparison of ROI FA values did not demonstrate significant overall group differences ($F_{1,38} = 0.057$, $P = 0.812$), but determined significant ROI effect ($F_{7,266} = 584.525$, $P = 0.0005$) and group by ROI interaction ($F_{7,32} = 2.727$, $P = 0.024$) as well as a trend for a group by hemispheric laterality interaction ($F_{1,38} = 4.201$, $P = 0.047$). Significant regional differences between the two groups were again found in the right genu of the internal capsule ($F_{1,38} = 9.494$, $P = 0.004$) (Fig. 1B).

Trace (*D*) diffusivity

The TBSS whole-brain group comparison found increased Trace values in the corona radiata, the genu and posterior third quarter of the internal capsule, the middle third of cerebral peduncle, the cerebellar white and grey matter, and the ventral thalamus bilaterally in SD patients (Fig. 2A).

Table 1 DTI-derived measures in healthy controls and SD patients based on ROI analysis

Anatomical region		Fractional anisotropy		Trace (*D*) ($\times 10^{-3}$ mm^2/s)	
		Controls	Patients	Controls	Patients
Genu of internal capsule	R	0.61 ± 0.07	0.55 ± 0.05[a]	2.10 ± 0.20	2.22 ± 0.14[a]
	L	0.65 ± 0.05	0.63 ± 0.07	2.14 ± 0.17	2.34 ± 0.18[a]
Posterior limb of internal capsule	R	0.69 ± 0.05	0.70 ± 0.03	1.99 ± 0.15	2.11 ± 0.11[a]
	L	0.69 ± 0.04	0.70 ± 0.04	2.03 ± 0.15	2.12 ± 0.11[a]
Cerebral peduncle	R	0.74 ± 0.04	0.74 ± 0.05	2.14 ± 0.15	2.17 ± 0.14
	L	0.76 ± 0.05	0.76 ± 0.05	2.09 ± 0.17	2.17 ± 0.21
Pyramid	R	0.51 ± 0.08	0.52 ± 0.05	2.06 ± 0.18	2.15 ± 0.21
	L	0.51 ± 0.08	0.54 ± 0.07	2.09 ± 0.19	2.13 ± 0.14
Middle cerebellar peduncle	R	0.66 ± 0.05	0.66 ± 0.11	1.94 ± 0.11	2.04 ± 0.10
	L	0.62 ± 0.06	0.62 ± 0.08	1.94 ± 0.11	1.97 ± 0.08
Lentiform nucleus	R	0.19 ± 0.03	0.19 ± 0.07	2.11 ± 0.18	2.41 ± 0.21[a]
	L	0.15 ± 0.03	0.15 ± 0.04	2.17 ± 0.17	2.32 ± 0.11[a]
Ventral thalamus	R	0.28 ± 0.05	0.26 ± 0.03	2.04 ± 0.31	2.19 ± 0.19[a]
	L	0.31 ± 0.04	0.29 ± 0.05	2.10 ± 0.15	2.20 ± 0.27[a]
Cingulum	R	0.46 ± 0.09	0.49 ± 0.07	2.20 ± 0.30	2.26 ± 0.21
	L	0.52 ± 0.11	0.53 ± 0.08	2.30 ± 0.25	2.41 ± 0.21

Values report mean ± standard deviation. (a) indicates brain regions significantly different between patients and controls ($P \leqslant 0.01$). R = right, L = left.

The ANOVA overall group effect for the ROI analysis of Trace measures was significant ($F_{1,38} = 10.161$, $P = 0.003$) with non-significant group by ROI ($F_{7,32} = 1.433$, $P = 0.227$) or group by hemispheric laterality ($F_{1,38} = 1.812$, $P = 0.186$) interactions. Because of the lack of hemispheric differences, the right and left ROIs for Trace values were combined for univariate comparisons. Regional differences in Trace were found in the genu ($F_{1,38} = 10.601$, $P = 0.002$) and the posterior limb of the internal capsule ($F_{1,38} = 7.743$, $P = 0.008$), the lentiform nucleus ($F_{1,38} = 9.360$, $P = 0.004$) and the ventral thalamus ($F_{1,38} = 8.959$, $P = 0.005$). A group trend was found in the middle cerebellar peduncle ($F_{1,38} = 6.156$, $P = 0.018$) (Fig. 2B). Mean and standard deviation of FA and Trace values in SD patients and healthy controls are reported in Table 1.

Correlations between diffusion parameters and clinical scores

In all ROIs taken together, the mean FA and Trace values had significant inverse correlation, which was greater in SD patients ($r = -0.737$, $P = 0.0005$) than in HVs ($r = -0.465$, $P = 0.039$) (Fig. 3A). When the relationship between FA and Trace was examined in the regions that differed between the two groups, a significant inverse correlation was observed in the genu of the internal capsule in the patients ($r = -0.639$, $P = 0.002$), which was greater than the correlation in the HVs ($r = -0.454$, $P = 0.044$) (Fig. 3B).

The FA and Trace measures in the regions that differed between the two groups (FA in the right genu and Trace in the genu and posterior limb of the internal capsule, the lentiform nucleus and the ventral thalamus) were also examined for their relationships with numbers of voice breaks in sentences and duration of disorder in SD patients. We found positive correlation between the Trace values in the ventral thalamus and number of breaks during speech production ($r = 0.509$, $P = 0.037$) in SD patients (Fig. 3C).

Neuropathological evaluation

No gross abnormalities were found in either the patient or the control brains. Histopathological analysis of the genu of the right internal capsule revealed reduced white matter density due to moderate reduction of myelin content surrounded by scattered microglial/macrophage activation in the SD patient. Moderate focal reduction of axonal density was observed in the same locus in the SD patient (Fig. 4). No such changes were found in the tissue sampled from the anterior and posterior limbs of the internal capsule in either a patient or controls.

Neuropathological examination of the H&E sections, where Trace differences were found, identified clusters of dark-blue/black basophilic precipitates in the parenchyma and small-caliber vessels in the putamen, globus pallidus and the posterior limb of the internal capsule in the SD patient compared to controls (Fig. 5A–C). In the patient's cerebellum, small areas of basophilic deposits were distributed in the cortex and white matter. No axonal loss or demyelination was found in either of these brain regions. Histochemical stains of the brain sections from the putamen, globus pallidus and cerebellum with adjacent white matter demonstrated that the parenchymal clusters were selectively positive for calcium and phosphate with single scattered iron deposits. Depositions in the vessel wall were stronger positive for iron in addition to calcium and phosphorus (Fig. 5D and F). None of these changes was found in controls.

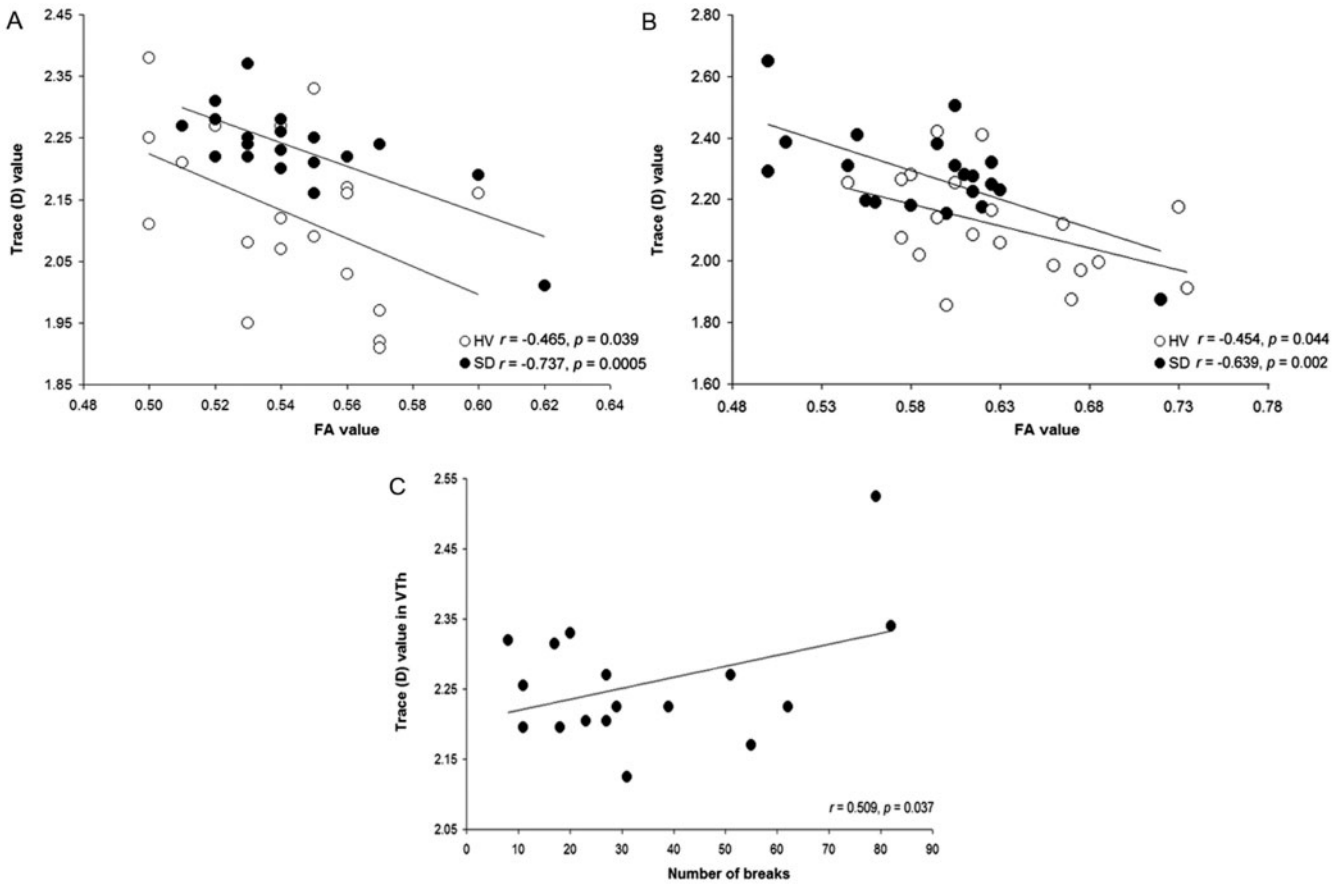

Fig. 3 Correlation between diffusion parameters. (**A**) Significant inverse correlation between overall mean values of fractional anisotropy (FA) and Trace (*D*) was stronger in SD patients than in HV. (**B**) Significant inverse correlation between the FA and Trace values were found in the genu of the internal capsule. (**C**) Positive significant correlation was determined between the Trace values in the ventral thalamus (VTh) and number of breaks in SD patients.

By infrared spectroscopy, spectra characteristic of phosphate were obtained from both the parenchymal and vessel wall deposits in the putamen, globus pallidus, internal capsule and cerebellum of the patient's tissue. The phosphate spectra most closely resembled the authentic infrared spectrum of apatite. SEM-EDXA of the representative deposition in the parenchyma demonstrated focal collocation of phosphorus and calcium in SD brain (Fig. 6A). This calcium phosphate was present admixed with protein, probably representing degenerated tissue protein. In the vessel wall, the SEM-EDXA map showed presence of iron in addition to calcium and phosphorus (Fig. 6B).

Discussion

In this study, we combined, for the first time to our knowledge, the neuroimaging and neuropathological approaches to examine the structural brain organization in patients with SD. Using DTI, we identified white matter changes along the CBT/CST and in the brain regions directly or indirectly contributing to this tract in SD patients. Consequently, we substantiated these findings with *postmortem* histopathological abnormalities presented as a focal reduction of axonal density and myelin content in the genu of the internal capsule and clusters of mineral accumulations in the parenchyma and vessel walls in the internal capsule, putamen, globus pallidus and cerebellum in SD. We also identified a significant statistical relationship between disorder symptom severity and the brain water diffusivity changes in SD. The brain abnormalities in SD found here could, therefore, be considered as primary brain changes contributing to the pathophysiology of this disorder.

Corticobulbar/corticospinal tract

Significant microstructural abnormalities were found in the CBT/CST in SD patients compared with controls. We suggest that SD may be associated with alterations in anatomical connectivity of the corticobulbar tract (CBT) descending from the laryngeal/orofacial motor cortex to the brainstem phonatory nuclei (Kuypers, 1958; Iwatsubo *et al.*, 1990). The CBT descends together with the CST via the corona radiata, internal capsule, cerebral peduncle and

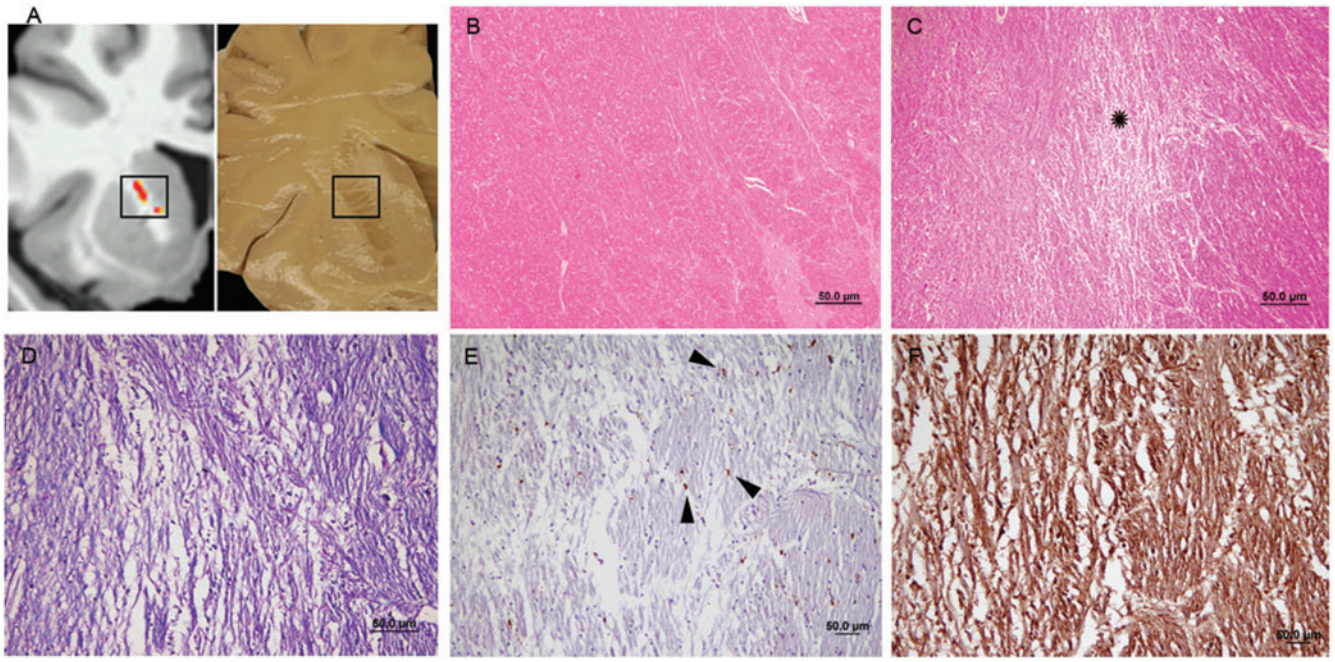

Fig. 4 DTI-guided postmortem neuropathological examination of FA changes in the genu of the internal capsule. (**A**) An example of T_1-weighted image in coronal plane with overlaid FA group differences (*left*) and visually matched *postmortem* coronal brain slice (*right*). The black box indicates the region of tissue extraction from the *postmortem* specimen. (**B**) Photomicrograph of the control sample shows well-organized white matter in the genu of the internal capsule (GIC) and (**C**) reduced white matter density (*) in the GIC in an SD patient (H&E stain). Area of reduced white matter density in the GIC reveals (**D**) reduction of myelin content (LFB/PAS stain), (**E**) diffusely scattered reactive microglial/macrophage cells (KPI stain) and (**F**) moderate reduction of axonal density (anti-NFTP stain).

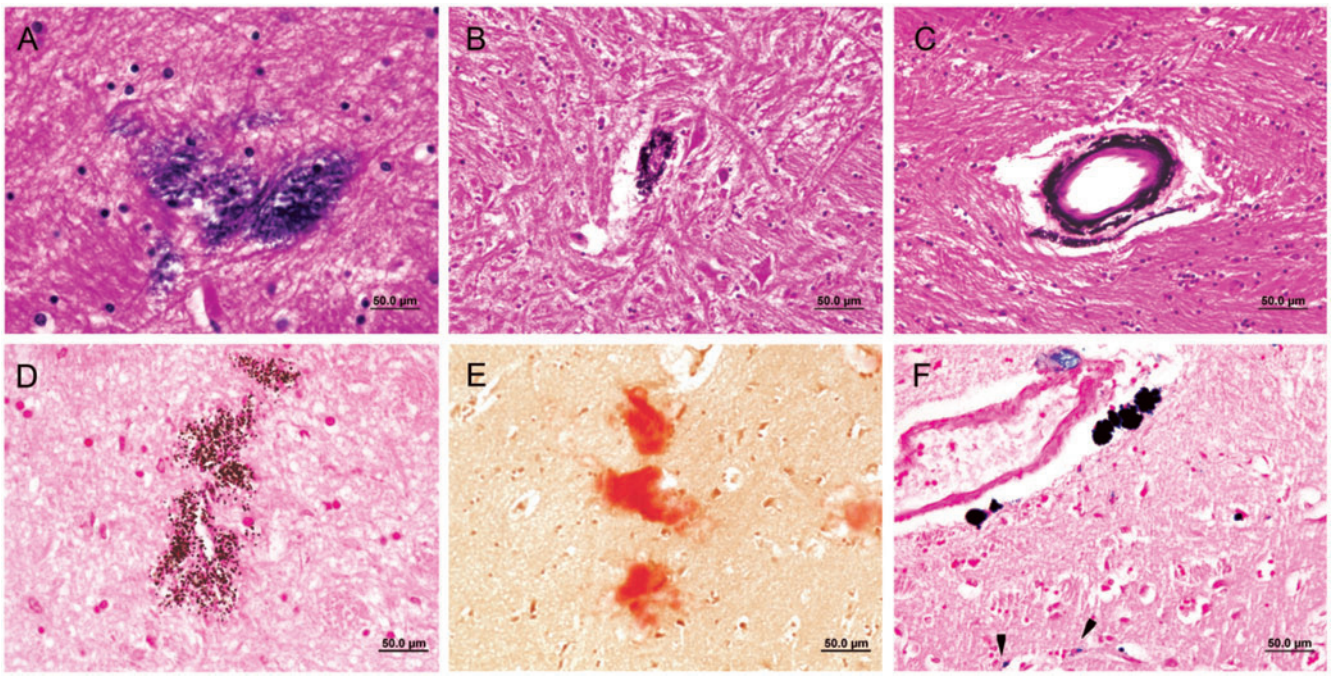

Fig. 5 DTI-guided postmortem neuropathological examination of Trace (*D*) changes in an SD patient. Photomicrographs of the mineral depositions (dark-blue/black visualization product) in the parenchyma of the putamen (**A**) and globus pallidus (**B**) and in the vessel wall in the posterior limb of the internal capsule (**C**) (H&E stain). An example from putaminal tissue shows accumulations of phosphorus (von Kossa stain) (**D**) and calcium (alizarin red S stain) (**E**) in the parenchyma and deposition of iron in the vessel wall (Prussian blue stain) (**F**) with scattered single iron-positive cells in the parenchyma (arrowheads).

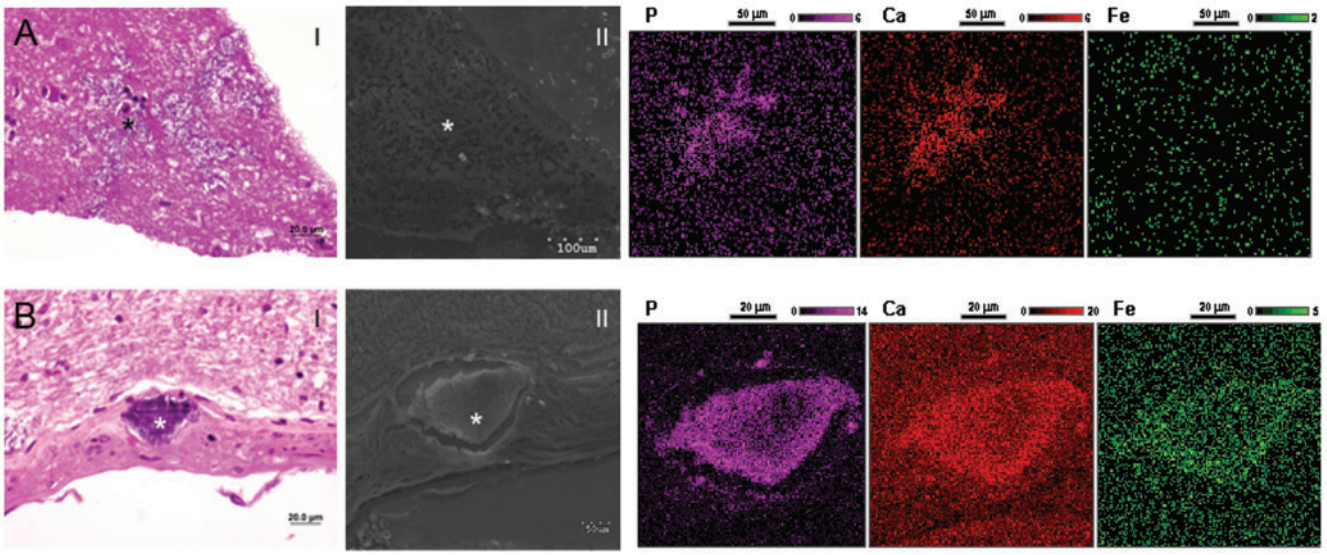

Fig. 6 Scanning electron microscopy with energy dispersive X-ray analysis (SEM-EDXA) of tissue depositions in an SD patient. (**A**) Photomicrograph of the deposition (*) in the putaminal parenchyma on H&E stain (I) and SEM (II) (scale 100 µm). EDXA shows accumulation of phosphorus (P) and calcium (Ca). (**B**) Vessel wall deposition in the putamen (*) shown on H&E stain (I) and SEM (II) (scale 50 µm). EDXA detected collocation of phosphorus (P), calcium (Ca), and iron (Fe).

pyramids to subcortical structures, including the striatum, thalamus, midbrain and brainstem nuclei (Ross, 1980; Manelfe *et al*., 1981; Tredici *et al*., 1982; Davidoff, 1990). In the internal capsule, the CBT and CST fibres are organized somatotopically with the CBT of head and neck representation occupying the genu and the CST of hand and foot representation traversing the posterior third quarter of the posterior limb (Tredici *et al*., 1982; Bogousslavsky and Regli, 1990; Aoki *et al*., 2005; Holodny *et al*., 2005). Focal ischaemic lesions in the genu of the internal capsule have been reported to cause orofacial and laryngeal paresis in stroke patients due to massive disruption of the corticobulbar tract (Manelfe *et al*., 1981; Soisson *et al*., 1982; Tredici *et al*., 1982; Bogousslavsky and Regli, 1990). The microstructural abnormalities in the internal capsule in SD patients reported here are relatively subtle and confined, suggesting the presence of the different pathological process.

The most specific disorganization of CBT/CST in SD was found in the genu of the internal capsule demonstrating right-localized anisotropy decrease, bilateral diffusivity increase and white matter thinning. Although the precise neural correlates of altered anisotropy and diffusivity are not well understood, these measures are thought to be linked to the quality and density of axonal tracts in the brain (Horsfield and Jones, 2002; Le Bihan and van Zijl, 2002). This was confirmed by our *postmortem* findings in an SD patient, which demonstrated reduced axonal course and myelin content in the right genu of the internal capsule, where DTI changes were identified in a larger group of living SD patients. The observed increase in microglial activation in the region of these focal changes may suggest that axonal degeneration could be secondary to a slow demyelination process in this region. Alternatively, the loss of myelin could be secondary to a cell loss within the laryngeal motor cortex and concomitant axonal degeneration. A limitation of this study is the unavailability of the patient's *postmortem* tissue from the laryngeal/orofacial sensorimotor cortex, which rendered us unable to further examine the possible motor cortical involvement that may have been related to white matter changes in the genu of the internal capsule in SD. Detailed interpretation of these findings will require future access to the *postmortem* tissue from the laryngeal motor cortex and internal capsule of both hemispheres for stereological analyses of cortical neuron distribution and axonal density, respectively, in SD patients compared to controls.

Although the DTI study found a highly significant right-lateralized FA abnormalities in SD patients compared to controls, these results were rather unexpected in a disorder, which is task-specific to speech production, usually dominant to the left hemisphere (Binder *et al*., 1995; Desmond *et al*., 1995; Bookheimer *et al*., 1997; Price, 2000; Vernooij *et al*., 2007). However, our finding is in line with a recent fMRI study in patients with ADSD, which has reported symptom-specific functional activation changes localized to the right ventral sensorimotor region during voluntary voice production (Haslinger *et al*., 2005).

Increased diffusivity along the CBT/CST is thought to reflect changes in relative intracellular/extracellular volumes or net loss of structural barriers of diffusion due to cell loss and impaired connectivity within the white matter (Pierpaoli *et al*., 1996; Gass *et al*., 2001; Kantarci *et al*., 2001; Beaulieu, 2002; Sykova, 2004). Mineral accumulations

in the internal capsule of the SD patient found in this study may contribute to water diffusivity changes. Mineral depositions were not observed in our control brain tissue samples, therefore, these abnormalities in the patient's brain may be due to a primary neurological process or a generalized metabolic disorder associated with a disruption in the blood-brain barrier (Casanova and Araque, 2003).

DTI measures were not significantly different between the SD and HV groups in the region of cingulum underlying the anterior cingulate cortex (ACC). The ACC controls voluntary voice initiation and vocal expression of emotional states (Jurgens and von Cramon, 1982; Jurgens, 2002). Although the ACC is reciprocally connected with the laryngeal motor cortex (Simonyan and Jurgens, 2002, 2005), absence of microstructural differences in the white matter underlying the ACC demonstrates a separation of the affected voluntary vocal motor control from unaffected voluntary vocal emotional control in SD patients.

Our study points to the selective abnormalities affecting the voluntary vocal motor control pathway with the abnormalities in the genu of the internal capsule appearing as the most specific disorder-related finding in SD.

Basal ganglia and thalamus

The link between dystonia and basal ganglia dysfunction has been apparent (Berardelli *et al.*, 1998; Hallett, 1998). Basal ganglia balance excitation and inhibition of the thalamo-cortical circuit involved in motor execution. This balance is thought to be altered in task-specific dystonias due to reduced GABAergic metabolism (Levy and Hallett, 2002) and dopaminergic receptor binding (Perlmutter *et al.*, 1997), leading to excessive motor cortical excitation (Hallett, 1998). In a review of 240 cases of lesions in basal ganglia from various causes, Bhatia and Marsden found secondary dystonia to be the most common symptom, occurring in 36% of lesions (Bhatia and Marsden, 1994). Most of these small lesions were located in the lentiform nucleus, particularly in the putamen. Recent neuroimaging studies in other forms of primary dystonia have confirmed the presence of functional and structural changes in the basal ganglia (Black *et al.*, 1998; Eidelberg, 1998; Meunier *et al.*, 2003; Colosimo *et al.*, 2005; Blood *et al.*, 2006; Bonilha *et al.*, 2007).

In this study, diffusivity changes and correlated histopathological abnormalities presented as mineral accumulations of calcium, phosphorus and iron in the parenchyma and vessels of the putamen and globus pallidus were found in SD patients. Equilibrium of calcium and iron distribution is of biological importance for electron exchange and oxidation–reduction reactions. Increases in calcium and iron levels enhance lipid peroxidation and, therefore, can mediate cell membrane damage and degeneration (Casanova and Araque, 2003). Excitotoxic effect of calcium accumulation has been reported in a wide variety of neurological diseases (Casanova and Araque, 2003), including a family with autosomal dominant dystonia-plus syndrome (Wszolek *et al.*, 2006). Iron-induced oxidative processes have been shown to reduce GABAergic inhibition (Zhang *et al.*, 1989) and cause degeneration of the dopaminergic neurons (Sastry and Arendash, 1995). Mineral accumulation in the putamen and globus pallidus found here in SD, therefore, likely underlie the abnormal metabolic processes within the basal ganglia-thalamo-cortical circuitry in SD. Future studies will need to elucidate the relationship between the neurotransmitter and mineral levels in SD and other forms of dystonia. Together with common findings of neuroimaging changes in the basal ganglia and thalamus in other forms of dystonia (Black *et al.*, 1998; Carbon *et al.*, 2004; Colosimo *et al.*, 2005; Blood *et al.*, 2006; Bonilha *et al.*, 2007), our finding of specific histopathological abnormalities in SD underlines a critical involvement of these brain regions in the pathophysiology of primary dystonias (Hallett, 2004).

Cerebellum

We found increased diffusivity in the middle cerebellar peduncle and the deep cerebellar white and grey matter in the patient group, associated with mineral accumulations found in our single SD patient. The cerebellum is involved in the motor control via the ventrolateral thalamus and has a modulatory role in coordination of voice and speech production (Arbib, 1981; Wildgruber *et al.*, 2001; Guenther *et al.*, 2006). Cerebellar dysfunction (Galardi *et al.*, 1996; Ceballos-Baumann *et al.*, 1997; Eidelberg, 1998; Odergren *et al.*, 1998; Hutchinson *et al.*, 2000; Preibisch *et al.*, 2001; Ali *et al.*, 2006) and atrophy (Fletcher *et al.*, 1988; Le Ber *et al.*, 2006) have been reported in a heterogeneous group of patients with dystonia suggesting that this disorder may arise from cerebellar disorganization. This has been supported by studies in rodent models of dystonia showing that primarily cerebellar dysfunction can cause dystonia (Brown and Lorden, 1989; Campbell and Hess, 1998; Richter *et al.*, 1998; Pizoli *et al.*, 2002; Jinnah and Hess, 2006), while cerebellectomy and selective destruction of Purkinje cells can eliminate dystonic symptoms (LeDoux *et al.*, 1993; Campbell *et al.*, 1999). Microstructural abnormalities in the cerebellum and ventral thalamus found in the present study may possibly weaken the cerebello-thalamo-cortical modulatory input in SD and, therefore, play a role in the pathophysiology of dystonia.

Clinical correlations

Measures of water diffusivity were positively correlated with the clinical symptoms of SD, e.g. with the number of voice breaks in sentences. These results together with *postmortem* findings of focal abnormalities in an SD patient treated with botulinum toxin over 10 years until death suggest that microstructural changes may represent primary brain changes contributing to the pathophysiology of this disorder. Discrepancies between our results and recent

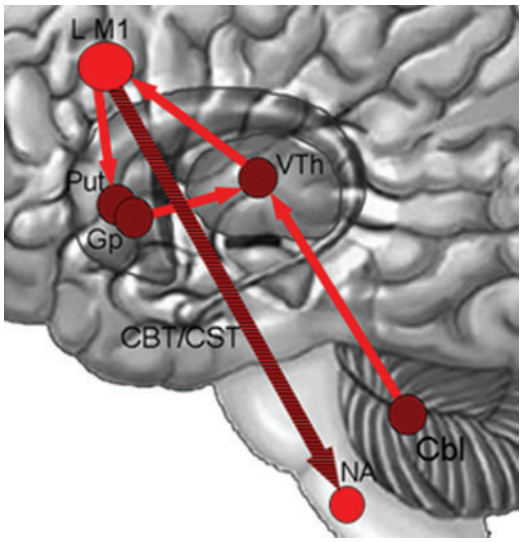

Fig. 7 Simplified schematic illustration of the neural network of voluntary laryngeal control in humans. Direct projections from the laryngeal motor cortex (LMI) to the phonatory motor nuclei (nucleus ambiguus, NA) descend via the corticobulbar/corticospinal tract (CBT/CST). Several connections exist between the LMI and the subcortical motor system. The putamen (Put) receives input from the LMI and projects back to the LMI via the globus pallidus (Gp) and ventral lateral thalamus (VTh) forming striato-pallido-thalamo-cortical loop. Cerebellar motor input (Cbl) to the LMI is via the VTh. Microstructural changes along the CBT/CST as well as in the regions directly or indirectly contributing to the CBT/CST found in this study (dashed areas) may affect voluntary laryngeal control in patients with SD.

DTI findings in four patients with cervical dystonia reporting reversal of white matter changes after botulinum toxin treatment (Blood *et al.*, 2006) may be explained by a larger sample size and more detailed evaluation of the white matter organization in the present study.

It is notable that our study included patients with adductor and abductor SD. Although symptoms of these two types of SD differ, both are characterized by the loss of the *voluntary* control of voice production. This learned behaviour in humans, involving both voluntary adductor and abductor laryngeal movements for speech production, is under control of the laryngeal motor cortex with direct input to the nucleus ambiguus and reticular formation of the brainstem via the CBT (Kuypers, 1958; Jurgens and Ehrenreich, 2007). Therefore, it is unlikely that the differential changes would be found in the white matter tracts between the patients with adductor and abductor SD.

Conclusion

The present study is among the first detailed investigations of the neuropathological basis of SD. Our findings suggest that altered microstructural integrity of the CBT/CST may represent primary neurological changes in SD. Focal microstructural changes along the CBT/CST as well as in the regions directly or indirectly contributing to the CBT/CST are likely to alter the communication between cortical and subcortical brain regions that are essential for voluntary voice control for speech production (Fig. 7). A slow progressive neurodegenerative or metabolic processes in these brain regions may underlie the abnormalities in the microstructural brain organization and, therefore, contribute to the pathophysiology of this disorder. White matter abnormalities in the genu of the internal capsule, where head and neck muscles are represented, are the most *specific* disorder-related findings in SD. On the other hand, DTI changes in the basal ganglia, thalamus and cerebellum in SD represent a common neuroimaging finding in patients with primary dystonias. We substantiated these neuroimaging findings with specific histopathological abnormalities presented as clusters of mineral accumulations in these brain regions in SD, which may contribute to a *common* neuropathological process in the focal dystonias.

Supplementary material

Supplementary material is available at Brain online.

Acknowledgements

We thank Drs Susumu Mori and Xin Li for software support, Drs Noriaki Hattori and S. Lalith Talagala for image acquisition support, Dr Carlo Pierpaoli for advice in data analysis, Dr Pamela R. Kearney for participants' clinical screening, Sandra B. Martin for assistance with patient recruitment and Kimberly Finnegan for rating the voice and speech samples. We are grateful to Viktoria Baker, Laboratory of Pathology, NCI, for histology preparations, and to Dr Mark Raffeld and Cynthia Harris, Molecular Pathology Section, NCI, for immunohistochemistry preparations. Tissue specimens were obtained from the NICHD Brain and Tissue Bank for Developmental Disorders at University of Maryland, Baltimore, MD and from the Human Brain and Spinal Fluid Resource Center, VAMC, Los Angeles, CA, sponsored by NINDS/NIMH, National Multiple Sclerosis Society, VA Greater Los Angeles Healthcare System and Veterans Health Services and Research Administration, Department of Veterans Affairs. This work was supported by the Intramural Program of the National Institute of Neurological Disorders and Stroke.

References

Ali SO, Thomassen M, Schulz GM, Hosey LA, Varga M, Ludlow CL, et al. Alterations in CNS activity induced by botulinum toxin treatment in spasmodic dysphonia: an H215O PET study. J Speech Lang Hear Res 2006; 49: 1127–46.

Aoki S, Iwata NK, Masutani Y, Yoshida M, Abe O, Ugawa Y, et al. Quantitative evaluation of the pyramidal tract segmented by diffusion tensor tractography: feasibility study in patients with amyotrophic lateral sclerosis. Radiat Med 2005; 23: 195–9.

Arbib M. Preceptual structures and distributed motor control. In: Brookhart JM MV, editor. Handbook of physiology. Motor control. Vol. 2. Bethesda: Americal Physiological Society; 1981. pp. 1449–80.

Barkmeier JM, Case JL, Ludlow CL. Identification of symptoms for spasmodic dysphonia and vocal tremor: a comparison of expert and nonexpert judges. J Commun Disord 2001; 34: 21–37.

Basser PJ, Mattiello J, LeBihan D. MR diffusion tensor spectroscopy and imaging. Biophys J 1994; 66: –259–67.

Beaulieu C. The basis of anisotropic water diffusion in the nervous system – a technical review. NMR Biomed 2002; 15: –435–55.

Berardelli A, Rothwell JC, Hallett M, Thompson PD, Manfredi M, Marsden CD. The pathophysiology of primary dystonia. Brain 1998; 121 (Pt 7): 1195–212.

Bhatia KP, Marsden CD. The behavioural and motor consequences of focal lesions of the basal ganglia in man. Brain 1994; 117 (Pt 4): 859–76.

Bielamowicz S, Ludlow CL. Effects of botulinum toxin on pathophysiology in spasmodic dysphonia. Ann Otol Rhinol Laryngol 2000; 109: 194–203.

Binder JR, Rao SM, Hammeke TA, Frost JA, Bandettini PA, Jesmanowicz A, et al. Lateralized human brain language systems demonstrated by task subtraction functional magnetic resonance imaging. Arch Neurol 1995; 52: 593–601.

Black KJ, Ongur D, Perlmutter JS. Putamen volume in idiopathic focal dystonia. Neurology 1998; 51: 819–24.

Bloch CS, Hirano M, Gould WJ. Symptom improvement of spastic dysphonia in response to phonatory tasks. Ann Otol Rhinol Laryngol 1985; 94: 51–4.

Blood AJ, Tuch DS, Makris N, Makhlouf ML, Sudarsky LR, Sharma N. White matter abnormalities in dystonia normalize after botulinum toxin treatment. Neuroreport 2006; 17: 1251–5.

Bogousslavsky J, Regli F. Capsular genu syndrome. Neurology 1990; 40: 1499–502.

Bonilha L, de Vries PM, Vincent DJ, Rorden C, Morgan PS, Hurd MW, et al. Structural white matter abnormalities in patients with idiopathic dystonia. Mov Disord 2007; 22: 1110–6.

Bookheimer SY, Zeffiro TA, Blaxton T, Malow BA, Gaillard WD, Sato S, et al. A direct comparison of PET activation and electrocortical stimulation mapping for language localization. Neurology 1997; 48: 1056–65.

Brown LL, Lorden JF. Regional cerebral glucose utilization reveals widespread abnormalities in the motor system of the rat mutant dystonic. J Neurosci 1989; 9: 4033–41.

Campbell DB, Hess EJ. Cerebellar circuitry is activated during convulsive episodes in the tottering (tg/tg) mutant mouse. Neuroscience 1998; 85: 773–83.

Campbell DB, North JB, Hess EJ. Tottering mouse motor dysfunction is abolished on the Purkinje cell degeneration (pcd) mutant background. Exp Neurol 1999; 160: 268–78.

Carbon M, Kingsley PB, Su S, Smith GS, Spetsieris P, Bressman S, et al. Microstructural white matter changes in carriers of the DYT1 gene mutation. Ann Neurol 2004; 56: 283–6.

Casanova MF, Araque JM. Mineralization of the basal ganglia: implications for neuropsychiatry, pathology and neuroimaging. Psychiatry Res 2003; 121: 59–87.

Ceballos-Baumann AO, Sheean G, Passingham RE, Marsden CD, Brooks DJ. Botulinum toxin does not reverse the cortical dysfunction associated with writer's cramp. A PET study. Brain 1997; 120 (Pt 4): 571–82.

Colosimo C, Pantano P, Calistri V, Totaro P, Fabbrini G, Berardelli A. Diffusion tensor imaging in primary cervical dystonia. J Neurol Neurosurg Psychiatry 2005; 76: 1591–3.

Davidoff RA. The pyramidal tract. Neurology 1990; 40: 332–9.

Desmond JE, Sum JM, Wagner AD, Demb JB, Shear PK, Glover GH, et al. Functional MRI measurement of language lateralization in Wada-tested patients. Brain 1995; 118 (Pt 6): 1411–9.

Edgar JD, Sapienza CM, Bidus K, Ludlow CL. Acoustic measures of symptoms in abductor spasmodic dysphonia. J Voice 2001; 15: 362–72.

Eidelberg D. Functional brain networks in movement disorders. Curr Opin Neurol 1998; 11: 319–26.

Fletcher NA, Stell R, Harding AE, Marsden CD. Degenerative cerebellar ataxia and focal dystonia. Mov Disord 1988; 3: 336–42.

Furutani K, Harada M, Minato M, Morita N, Nishitani H. Regional changes of fractional anisotropy with normal aging using statistical parametric mapping (SPM). J Med Invest 2005; 52: 186–90.

Galardi G, Perani D, Grassi F, Bressi S, Amadio S, Antoni M, et al. Basal ganglia and thalamo-cortical hypermetabolism in patients with spasmodic torticollis. Acta Neurol Scand 1996; 94: 172–6.

Gass A, Niendorf T, Hirsch JG. Acute and chronic changes of the apparent diffusion coefficient in neurological disorders–biophysical mechanisms and possible underlying histopathology. J Neurol Sci 2001; 186 (Suppl 1): S15–23.

Guenther FH, Ghosh SS, Tourville JA. Neural modeling and imaging of the cortical interactions underlying syllable production. Brain Lang 2006; 96: 280–301.

Hallett M. The neurophysiology of dystonia. Arch Neurol 1998; 55: 601–3.

Hallett M. Dystonia: abnormal movements result from loss of inhibition. Adv Neurol 2004; 94: 1–9.

Haslinger B, Erhard P, Dresel C, Castrop F, Roettinger M, Ceballos-Baumann AO. ''Silent event-related'' fMRI reveals reduced sensorimotor activation in laryngeal dystonia. Neurology 2005; 65: 1562–9.

Holodny AI, Gor DM, Watts R, Gutin PH, Ulug AM. Diffusion-tensor MR tractography of somatotopic organization of corticospinal tracts in the internal capsule: initial anatomic results in contradistinction to prior reports. Radiology 2005; 234: 649–53.

Horsfield MA, Jones DK. Applications of diffusion-weighted and diffusion tensor MRI to white matter diseases - a review. NMR Biomed 2002; 15: 570–7.

Hutchinson M, Nakamura T, Moeller JR, Antonini A, Belakhlef A, Dhawan V, et al. The metabolic topography of essential blepharospasm: a focal dystonia with general implications. Neurology 2000; 55: 673–7.

Iwatsubo T, Kuzuhara S, Kanemitsu A, Shimada H, Toyokura Y. Corticofugal projections to the motor nuclei of the brainstem and spinal cord in humans. Neurology 1990; 40: 309–12.

Jiang H, van Zijl PC, Kim J, Pearlson GD, Mori S. DtiStudio: resource program for diffusion tensor computation and fiber bundle tracking. Comput Methods Programs Biomed 2006; 81: 106–16.

Jinnah HA, Hess EJ. A new twist on the anatomy of dystonia: the basal ganglia and the cerebellum? Neurology 2006; 67: 1740–1.

Jurgens U. Neural pathways underlying vocal control. Neurosci Biobehav Rev 2002; 26: 235–58.

Jurgens U, Ehrenreich L. The descending motorcortical pathway to the laryngeal motoneurons in the squirrel monkey. Brain Res 2007; 1148: 90–5.

Jurgens U, von Cramon D. On the role of the anterior cingulate cortex in phonation: a case report. Brain Lang 1982; 15: 234–48.

Kantarci K, Jack CR Jr, Xu YC, Campeau NG, O'Brien PC, Smith GE, et al. Mild cognitive impairment and Alzheimer disease: regional diffusivity of water. Radiology 2001; 219: 101–7.

Karnell MP, Melton SD, Childes JM, Coleman TC, Dailey SA, Hoffman HT. Reliability of clinician-based (GRBAS and CAPE-V) and patient-based (V-RQOL and IPVI) documentation of voice disorders. J Voice 2007; 21: 576–90.

Kulisevsky J, Marti MJ, Ferrer I, Tolosa E. Meige syndrome: neuropathology of a case. Mov Disord 1988; 3: 170–5.

Kuypers HG. Corticobular connexions to the pons and lower brain-stem in man: an anatomical study. Brain 1958; 81: 364–88.

Le Ber I, Clot F, Vercueil L, Camuzat A, Viemont M, Benamar N, et al. Predominant dystonia with marked cerebellar atrophy: a rare phenotype in familial dystonia. Neurology 2006; 67: 1769–73.

Le Bihan D, van Zijl P. From the diffusion coefficient to the diffusion tensor. NMR Biomed 2002; 15: 431–4.

LeDoux MS, Lorden JF, Ervin JM. Cerebellectomy eliminates the motor syndrome of the genetically dystonic rat. Exp Neurol 1993; 120: 302–10.

Levy LM, Hallett M. Impaired brain GABA in focal dystonia. Ann Neurol 2002; 51: 93–101.

Ludlow CL, Schulz GM, Yamashita T, Deleyiannis FW. Abnormalities in long latency responses to superior laryngeal nerve stimulation in

adductor spasmodic dysphonia. Ann Otol Rhinol Laryngol 1995; 104: 928–35.

Manelfe C, Clanet M, Gigaud M, Bonafe A, Guiraud B, Rascol A. Internal capsule: normal anatomy and ischemic changes demonstrated by computed tomography. AJNR. Am J Neuroradiol 1981; 2: 149–55.

McNaught KS, Kapustin A, Jackson T, Jengelley TA, Jnobaptiste R, Shashidharan P, et al. Brainstem pathology in DYT1 primary torsion dystonia. Ann Neurol 2004; 56: 540–7.

Meunier S, Lehericy S, Garnero L, Vidailhet M. Dystonia: lessons from brain mapping. Neuroscientist 2003; 9: 76–81.

Mori S, Wakana, S, van Zijl PCM, Nagae-Poetscher LM. MRI atlas of human white matter. Elsevier Science; Amsterdam, The Netherlands, 2005.

Nash EA, Ludlow CL. Laryngeal muscle activity during speech breaks in adductor spasmodic dysphonia. Laryngoscope 1996; 106: 484–9.

Nichols TE, Holmes AP. Nonparametric permutation tests for functional neuroimaging: a primer with examples. Hum Brain Mapp 2002; 15: 1–25.

Odergren T, Stone-Elander S, Ingvar M. Cerebral and cerebellar activation in correlation to the action-induced dystonia in writer's cramp. Mov Disord 1998; 13: 497–508.

Pajevic S, Pierpaoli C. Color schemes to represent the orientation of anisotropic tissues from diffusion tensor data: application to white matter fiber tract mapping in the human brain. Magn Reson Med 1999; 42: 526–40.

Perlmutter JS, Stambuk MK, Markham J, Black KJ, McGee-Minnich L, Jankovic J, et al. Decreased [18F]spiperone binding in putamen in idiopathic focal dystonia. J Neurosci 1997; 17: 843–50.

Pfefferbaum A, Sullivan EV. Increased brain white matter diffusivity in normal adult aging: relationship to anisotropy and partial voluming. Magn Reson Med 2003; 49: 953–61.

Pierpaoli C, Barnett A, Pajevic S, Chen R, Penix LR, Virta A, et al. Water diffusion changes in Wallerian degeneration and their dependence on white matter architecture. Neuroimage 2001; 13: 1174–85.

Pierpaoli C, Jezzard P, Basser PJ, Barnett A, Di Chiro G. Diffusion tensor MR imaging of the human brain. Radiology 1996; 201: 637–48.

Pizoli CE, Jinnah HA, Billingsley ML, Hess EJ. Abnormal cerebellar signaling induces dystonia in mice. J Neurosci 2002; 22: 7825–33.

Preibisch C, Berg D, Hofmann E, Solymosi L, Naumann M. Cerebral activation patterns in patients with writer's cramp: a functional magnetic resonance imaging study. J Neurol 2001; 248: 10–7.

Price CJ. The anatomy of language: contributions from functional neuroimaging. J Anat 2000; 197 (Pt 3): 335–59.

Richter A, Brotchie JM, Crossman AR, Loscher W. [3H]-2-deoxyglucose uptake study in mutant dystonic hamsters: abnormalities in discrete brain regions of the motor system. Mov Disord 1998; 13: 718–25.

Ross ED. Localization of the pyramidal tract in the internal capsule by whole brain dissection. Neurology 1980; 30: 59–64.

Rueckert D, Sonoda LI, Hayes C, Hill DL, Leach MO, Hawkes DJ. Nonrigid registration using free-form deformations: application to breast MR images. IEEE. Trans Med Imaging 1999; 18: 712–21.

Sapienza CM, Walton S, Murry T. Adductor spasmodic dysphonia and muscular tension dysphonia: acoustic analysis of sustained phonation and reading. J Voice 2000; 14: 502–20.

Sastry S, Arendash GW. Time-dependent changes in iron levels and associated neuronal loss within the substantia nigra following lesions within the neostriatum/globus pallidus complex. Neuroscience 1995; 67: 649–66.

Simonyan K, Jurgens U. Cortico-cortical projections of the motorcortical larynx area in the rhesus monkey. Brain Res 2002; 949: 23–31.

Simonyan K, Jurgens U. Afferent cortical connections of the motor cortical larynx area in the rhesus monkey. Neuroscience 2005; 130: 133–49.

Smith SM. Fast robust automated brain extraction. Hum Brain Mapp 2002; 17: 143–55.

Smith SM, Jenkinson M, Johansen-Berg H, Rueckert D, Nichols TE, Mackay CE, et al. Tract-based spatial statistics: voxelwise analysis of multi-subject diffusion data. Neuroimage 2006; 31: 1487–505.

Soisson T, Cabanis EA, Iba-Zizen MT, Bousser MG, Laplane D, Castaigne P. Pure motor hemiplegia and computed tomography. 19 cases. J Neuroradiol 1982; 9: 304–22.

Sykova E. Extrasynaptic volume transmission and diffusion parameters of the extracellular space. Neuroscience 2004; 129: 861–76.

Tredici G, Pizzini G, Bogliun G, Tagliabue M. The site of motor corticospinal fibres in the internal capsule of man. A computerised tomographic study of restricted lesions. J Anat 1982; 134: 199–208.

Vernooij MW, Smits M, Wielopolski PA, Houston GC, Krestin GP, van der Lugt A. Fiber density asymmetry of the arcuate fasciculus in relation to functional hemispheric language lateralization in both right- and left-handed healthy subjects: a combined fMRI and DTI study. Neuroimage 2007; 35: 1064–76.

Wildgruber D, Ackermann H, Grodd W. Differential contributions of motor cortex, basal ganglia, and cerebellum to speech motor control: effects of syllable repetition rate evaluated by fMRI. Neuroimage 2001; 13: 101–9.

Woods RP, Grafton ST, Holmes CJ, Cherry SR, Mazziotta JC. Automated image registration: I. General methods and intrasubject, intramodality validation. J Comput Assist Tomogr 1998; 22: 139–52.

Wszolek ZK, Baba Y, Mackenzie IR, Uitti RJ, Strongosky AJ, Broderick DF, et al. Autosomal dominant dystonia-plus with cerebral calcifications. Neurology 2006; 67: 620–5.

Zhang ZH, Zuo QH, Wu XR. Effects of lipid peroxidation on GABA uptake and release in iron-induced seizures. Chin Med J 1989; 102: 24–7.

Zweig RM, Hedreen JC. Brain stem pathology in cranial dystonia. Adv Neurol 1988; 49: 395–407.

The human pyramidal syndrome Redux

Fernanda Tovar-Moll[a,b], Jorge Moll[a], Ivanei Edson Bramati[b], Andrea Silveira de Souza[b], Pedro Angelo Andreiuolo[b] and Ricardo de Oliveira-Souza[a,c]

[a]Department of Anatomy, Institute of Biomedical Sciences, Federal University of Rio de Janeiro, [b]Cognitive and Behavioral Neuroscience Unit, Labs-D'Or Hospital Network and [c]Gaffrée e Guinle University Hospital, Rio de Janeiro, Brazil

Correspondence to Fernanda Tovar-Moll and Ricardo de Oliveira-Souza, Cognitive and Behavioral Neuroscience Unit, R. Pinheiro Guimaraes 22, 4° andar, Rio de Janeiro, RJ 22281-080, Brazil
Tel: +55 21 2537 8037; fax: +55 21 2537 8117; e-mail: tovarmollf@gmail.com, rdeoliveira@gmail.com

Received 11 May 2007; accepted 7 June 2007

Experimental studies in nonhuman primates have questioned the selectivity of pyramidal tract damage in giving rise to the classical pyramidal syndrome in humans, characterized by permanent spastic hemiplegia (PSH). According to this view, concomitant injury of extrapyramidal pathways is necessary for the development of both hemiplegia and spasticity. In this study we used conventional magnetic resonance imaging and diffusion tensor imaging tractography to characterize the anatomical correlates of PSH in a patient with a rare and discrete unilateral lesion of the medullary pyramid. Our findings support the hypothesis that damage confined to the medullary pyramid/pyramidal tract is sufficient to produce PSH. In contrast to nonhuman primates, the human 'pyramidal' and 'pyramid' syndromes are equivalent clinico-anatomic concepts. *NeuroReport* 18:1417–1421 © 2007 Lippincott Williams & Wilkins.

Keywords: medullary pyramid, pyramidal tract, spastic hemiplegia, tractography

Introduction

The exact anatomical correlates of permanent spastic hemiplegia (PSH) were hotly debated throughout the twentieth century. The early tenet that PSH resulted from degeneration, focal damage, or dysfunction of the contralateral pyramidal tract (PT) was challenged by experimental evidence [1] that implied that PSH would only occur if extrapyramidal pathways, the collection of descending supraspinal motor pathways that reach the cord following a tegmental course [2], were concomitantly injured [3]. As the medullary pyramids are the only place in the nervous system where the PTs are entirely isolated, lesions therein confined are ideally suited to test the idea that a pyramid lesion suffices to produce PSH. Discrete pyramid lesions in man, however, are rare, and when they do occur, patients usually survive them for years, adding to the scarcity of correlative necropsy material. This study draws upon the new MRI techniques of diffusion tensor imaging (DTI) and tractography to investigate the rare case of a patient with PSH caused by a unilateral and capriciously localized infarct of the left medullary pyramid. Our main goal was to revisit the hypothesis that injury of one pyramid suffices to produce the classical pyramidal syndrome in humans. To illustrate further the specificity of our findings, we studied three additional patients with PSH harboring less selective, more proximal lesions of the motor pathway, as well as four normal healthy volunteers.

Report of case (patient M.P.): unilateral damage to the medullary pyramid

M.P., a 62-year-old man, presented in a wheelchair in December 2001 complaining of right-side weakness which struck him the night before as he went to bed. He was awake and oriented, and could speak, swallow, and move his face normally. His right arm and leg were motionless, but he denied tingling or pins-and-needles sensations. One week later, he could stand up and walk unsupported again. In one month, he had developed a typical hemiplegic attitude, most evident as he stood and walked. On walking, he circumducted the right arm and leg, but did not scuff the toes on the ground. No Romberg sign was observed and the postural adjustments to sudden postural imbalances were normal. Vertical and horizontal pursuit and saccadic eye movements were normal and without nystagmus. The face was symmetric at rest, as well as when he talked and smiled. The tongue was symmetric at rest and on protrusion. Tendon jerks were hyperactive, with ankle clonus and a Hoffmann sign on the right. The plantar reflex was extensor on the right and flexor on the left. His visual fields were full and the corneal reflexes were intact. A characteristic distribution of weakness was noted on arm abduction (4/5), forearm extension (4/5), and hand/fingers flexion (3/5) and extension (0/5). Weakness in the lower limb was observed on thigh flexion (4/5), leg extension (4/5) and flexion (3/5), and in plantar extension (1/5) and dorsiflexion (3/5) of the foot. Spasticity also adopted a characteristic distribution, being most evident in the arm and wrist flexors (5/5), and in the leg flexors and extensors (4/5). Sensation to pinprick, light touch, position sense, and vibration (128 Hz tuning fork) were normal and symmetric all over the body, including the face. His handedness shifted from a premorbid +80 to a current −20 on the Edinburgh Inventory. He scored 28/30 on the mini-mental state examination (MMSE) [4] and 85/100 on the Barthel index, due to bladder incontinence and the inability to climb stairs unaided.

Materials and methods

Patients

In addition to the patient described above (M.P.), three additional patients with PSH and four healthy individuals were included for comparison (pathologic and normal controls). B.P. was densely hemiplegic due to a left ventral pontine infarct, from which she recovered in a few weeks. C.R. and M.C.A. presented with a PSH due to a supracapsular ischemic lesion—in the right corona radiata (C.R.) and in the cortico-subcortical territory of the left middle cerebral artery (M.C.A.) respectively. All participants gave written informed consent before entering the study, which was approved by the LABS-D'Or institutional review board.

Neurobehavioral assessment

Somatic sensibility was probed by a set of tests designed to assess its finer aspects: replication of passive manual attitudes of the contralateral hand with the eyes open and closed [5], thumb localization [6], direction of scratch [7], tactile form perception [8], finger localization [8], Weber's two-point discrimination [9], moving two-point discrimination [10], and determination of sensory thresholds of finger tips [9]. Motor strength, spasticity, and tendon reflexes were graded respectively with the Medical Research Council [11], the modified Ashworth [12], and the National Institute of Neurological Disorders and Stroke (NINDS) scales [13] M.C.A. was unable to cooperate because of global aphasia.

Neuroimaging

Anatomical images were obtained with T1 spin-echo, T2 turbo spin-echo and FLAIR pulse sequences in a 1.5-T Philips-Intera scanner (Eindhoven, The Netherlands). Diffusion-weighted images were acquired with a single-shot, spin-echo echoplanar sequence: TR/TE=4000/110, field-of-view=256 mm^2, matrix=112 × 128, slice thickness=5 mm without gap. Diffusion sensitization gradients were applied in six noncollinear directions, with a b factor of 800 s/mm^2. DTI was transferred and postprocessed using Philips Research Integrated Development Environment software (PRIDE research platform, Fiber Track 4.1, Eindhoven, The Netherlands). Fractional anisotropy (FA) maps color-coded for direction, and fiber-tracking calculations were performed by specifying regions-of-interest (ROIs) on the trajectory of the PT in the cerebral hemisphere and ventral brainstem [14] at (i) the pontomedullary transition, (ii) the middle third of the cerebral peduncle, and (iii) the posterior limb of the internal capsule. Automatic tracking of fibers was performed with a marching algorithm restricting fiber tracking to voxels with a minimum FA of 0.30. Fiber deflection threshold was set to 0.85. In patients, the normal side was also used as a control for the results of tractography.

Statistical analysis

To assess the discrepancy between intraindividual measures of homologous ROIs in each hemisphere we compared the FA values of patients with those of the healthy volunteers. The significance of intraindividual differences for each pair of ROIs was assessed with a modified paired samples t-test [15], adopting a threshold of significance (α) of 0.05, two-tailed. In contrast to earlier statistical techniques, the modified t-test employed here does not overestimate the rarity of differences when control data are derived from small samples. These considerations become especially important in situations where the two measures of interest are highly correlated (in this case, the left and right FA values), an occurrence that often induces clinicians to dismiss discrepancies as 'modest', but which are, in fact, highly abnormal.

Table 1 Patient demographics and clinical characteristics at the acute/subacute phase, and examination at chronic stage

Characteristics	M.P.	B.P.	C.R.	M.C.A.
Sex	Man	Woman	Woman	Man
Age (years)	62	71	71	77
Acute/subacute	R-Hp	L-Hp	R-Hp	L-Hp + global aphasia
Chronic	L-PSH	Recovered	L-PSH	R-PSH

L-Hp, left hemiplegia; L-PSH, left permanent spastic hemiplegia; R-Hp, right hemiplegia; R-PSH, right permanent spastic hemiplegia.

Table 2 Summary of clinical and behavioral findings

Tests	M.P.	B.P.	C.R.	M.C.A.
Sensory exam				
Two-point discrimination threshold (mm)				
Right index finger	3	—	—	—
Left index finger	3	—	—	—
Moving two-point discrimination threshold (mm)				
Right index finger	2	—	—	—
Left index finger	2	—	—	—
Direction of scratch test				
Face (cheek)				
Right (0–10)	10/10	10/10	10/10	—
Left (0–10)	10/10	10/10	10/10	—
Hand (palmar surface)				
Right (0–10)	10/10	10/10	10/10	—
Left (0–10)	10/10	10/10	10/10	—
Tactile form perception				
Left hand (0–10)	10/10	10/10	10/10	—
Right hand (0–10)	08/10	08/10	8/10	—
Finger localization test				
Single fingers				
Left hand (0–10)	10/10	10/10	10/10	—
Right hand (0–10)	10/10	10/10	10/10	—
Pairs of fingers				
Left hand (0–10)	10/10	9/10	9/10	—
Right hand (0–10)	10/10	9/10	9/10	—
Sen. Ind. fingertip (g) (0.008–0.08)				
Left	0.080	—	—	—
Right	0.080	—	—	—
Thumb localizing				
Left (0–3)	3	3	—	—
Right (0–3)	3	3	—	—
MMSE (0–30)	28	30	29	0
Barthel index (0–100)	85	95	30	30
Ed. Hand. Invent. (−100/+100)				
Premorbid	80	100	100	100
Current	−20	100	100	−100

Ed. Hand. Invent. (−100/+100), Edinburgh Handedness Inventory (range: −100/+100); MMSE, mini-mental state examination; Sen. Ind. fingertip (g) (0.008–0.08), Sensory thresholds in index fingertip (g) (normal range: 0.008–0.080).

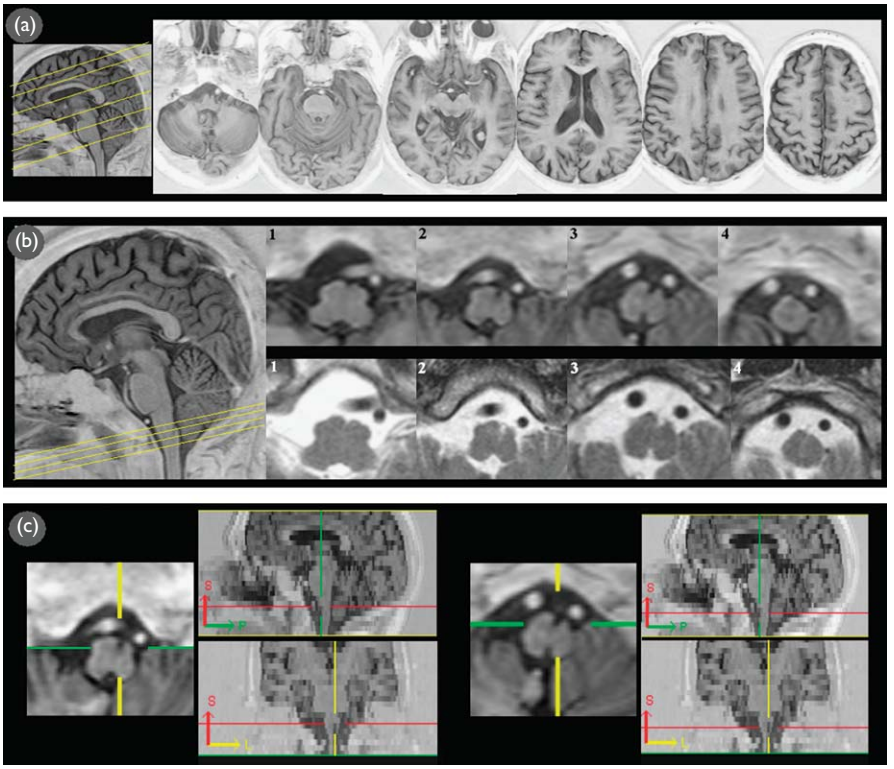

Fig. 1 (a) T1-weighted, inversion-recovery (TIW-IR) MRI images of M.P. at different levels across the lower brainstem and cerebral hemispheres. No significant abnormalities were observed at these levels. (b) Zoomed views of medullary pyramid lesion of M.P. The sagittal image shows the location of transverse cuts across the medulla oblongata (TIW-IR and T2-weighted images are displayed in the superior and inferior rows respectively, from dorsal to ventral levels). A small infarct at the level of the left medullary pyramid can be clearly observed as a wedge-shaped hypointensity in TIW images and hyperintensity in T2W images (slices 2 and 3). Note that slices 1 and 4, located 5 mm above and below the lesion, do not show abnormalities. (c) Reformatted TIW-IR images of the medullary pyramid lesion of M.P. Note the fusiform shape of the lesion, best appreciated in the coronal views.

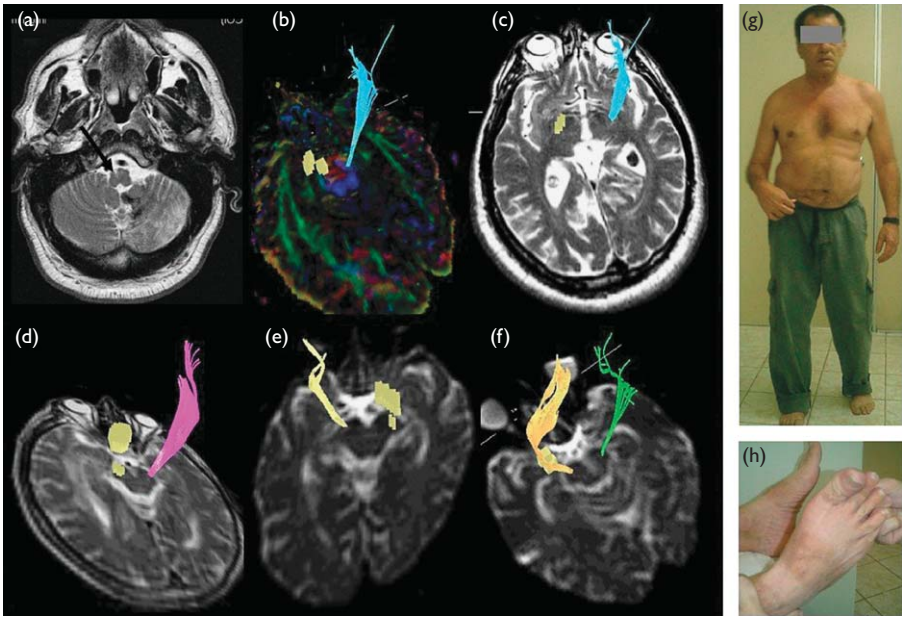

Fig. 2 (a) The left medullary pyramid infarct is shown on an axial T2 weighted image (T2WI) in M.P.; (b–f) fiber-tracking results from the three regions-of-interest approach. (b, c) Normal appearance of the reconstructed right PT and its absence in the left hemisphere in color-coded FA map (b) and T2WI (c) of M.P. (d) Intact PT in the right hemisphere and its absence in the left hemisphere in M.C.A. (e) Normal appearance of the reconstructed left PT and its absence in the right hemisphere in C.R. (f) Normal appearance of the reconstructed left PT and decrease in bulk on the right PT in B.P. (g and h) Typical Wernicke–Mann hemiplegic attitude during walking and right extensor plantar reflex in M.P. PT, pyramidal tract.

Results

Clinical and behavioral findings

The main clinical and behavioral findings are summarized in Tables 1 and 2.

Neuroanatomical findings

M.P. had a T1-hypointense/T2-hyperintense spindle-shaped lesion in the left ventromedial medulla well above the pyramidal decussation. The lesion was confined to the pyramid, with its major length paralleling the longitudinal axis of the brainstem, leaving the tegmentum and the medial lemnisci intact (Figs 1 and 2a). It corresponded to the type-2 infarction of Katoh and Kawamoto's classification [16], indicating that the anatomical boundaries of the medullary pyramid had not been exceeded. Such infarcts usually result from occlusion of a median perforating branch of the vertebral artery [17]. B.P. had an infarct occupying the lower third of the right basis pontis that rendered her hemiplegic for a few weeks. The infarct fell within the territory of the anterolateral pontine arteries, which supply the ventrolateral pontine base, including the lateral portions of the PT [18]. C.R. and M.C.A developed a disabling PSH from which there was little recovery: in C.R. a small infarct was seen in the corona radiata underneath the right precentral cortex, whereas M.C.A. suffered an extensive infarct of probable embolic origin occupying the superficial and deep territories of the left middle cerebral artery.

Diffusion tensor imaging and tractography findings

In comparison with the normal side, FA was decreased at and below the site of damage in all patients (Table 3). This corresponds respectively to local effects (at lesion level) and to Wallerian degeneration [19]. FA values rostral to the injury were normal in both patients with ventrocaudal brainstem lesions (M.P. and B.P.). The intact PT was reconstructed from the medullary pyramid to the subcortical rolandic region in all patients. On the injured side, the PT was not visible in the three patients with PSH (Fig. 2b–e). In B.P., who recovered from hemiplegia, the PT on the side of injury was clearly seen, although diminished in bulk (Fig. 1f). Figure 1g and h depict the patient's spastic hemiplegia and the extensor plantar reflex.

Table 3 Fractional anisotropy values along the pyramidal tract of patients and healthy controls

	Ponto-medullary (left/right)	Cerebral peduncle (left/right)	Internal capsule (left/right)
Controls			
1	0.47/0.51	0.72/0.68	0.60/0.61
2	0.58/0.59	0.78/0.75	0.64/0.62
3	0.55/0.57	0.75/0.75	0.60/0.56
4	0.56/0.59	0.82/0.80	0.71/0.68
Patients			
MP	0.46*/0.69	0.57/0.60	0.61/0.59
BP	0.58/0.21*	0.66/0.64	0.70/0.70
CR	0.54/0.39*	0.66/0.45*	0.60/0.49*
MCA	0.26*/0.52	0.48*/0.75	0.25*/0.68

Regions-of-interest (ROIs) placed in left and right cerebral hemisphere and ventral brainstem at: (i) the ponto-medullary transition, (ii) the middle third of the cerebral peduncle, and (iii) the posterior limb of the internal capsule.
*$P \leq 0.001$, two-tailed (following the modified paired samples *t*-test procedure of Crawford *et al.*, 1998) [15].

Discussion

This study investigates a patient with a rare, selective lesion to the left medullary pyramid who developed PSH. MRI and tractography confirmed the damage to the PT and the preservation of neighboring structures. The discreteness of the pyramid lesion was further attested by the sparing of somatic sensibility (medial lemnisci), by the preservation of facial (corticofacial fibers) and lingual (hypoglossal nucleus and nerve) motility, as well as by the absence of vertical nystagmus (medial longitudinal fasciculus). The neuroimaging findings in the additional patients with PSH (M.P., C.R., and M.C.A.) showed patterns compatible with a more widespread, less selective Wallerian degeneration of cortico-spinal and cortico-bulbar tracts. Moreover, the remaining PT fibers caudal to the pons observed in patient B.P. probably accounted for her good recovery [20,21]. In conclusion, our findings substantiate *post-mortem* observations that, in contrast to the nonhuman primate, a unilateral infarct confined to the medullary pyramid suffices to produce contralateral PSH in humans [22–25].

Acknowledgements

The authors are indebted to Mr José Ricardo Pinheiro and Mr Jorge Baçal (Section of Rare Documents and Works, Instituto Oswaldo Cruz Library, Rio de Janeiro) for the retrieved classical journal articles and books.

References

1. Denny-Brown D. *The cerebral control of movement*. Springfield, Illinois: Charles C. Thomas; 1966.
2. Prus J. Die Leitungsbahnen und Pathogenese der Rindenepilepsie. *Wien klin Wschr* 1898; **11**:857–863 (translated by MD Willner and MA Kennard: On the pathways and pathogenesis of cortical epilepsy. *Res Publ Ass Nerv Ment Dis* 1948; **27**:129–145).
3. Wiesendanger M. Pyramidal tract function and the clinical 'pyramidal syndrome'. *Human Neurobiol* 1984; **2**:227–234.
4. Brucki S, Nitrini R, Caramelli P, Bertolucci PHF, Okamoto IH. Suggestions for utilization of the mini-mental state examination in Brazil. *Arq Neuropsiquiatr* 2003; **61**:777–781.
5. Dejerine J. *Semeiology of nervous system affections [in French]*. Paris: Masson et Cie; 1914.
6. Hirayama K, Fukutate T, Kawamura M. Thumb localizing test: examination for disturbance of articular localization. *Clin Neurol (Tokyo)* 1986; **26**:448–454 (abstracted in English).
7. Hankey GJ, Edis RH. The utility of testing tactile perception of direction of scratch as a sensitive clinical sign of posterior column dysfunction in spinal cord disorders. *J Neurol Neurosurg Psychiatry* 1989; **52**:395–398.
8. Benton AL, Sivan AB, deS Hamsher K, Varney N, Spreen O. *Contributions to neuropsychological assessment. A clinical manual*. 2nd ed. Oxford: Oxford University Press; 1994.
9. Spreen O, Strauss E. *A compendium of neuropsychological tests. Administration, norms, and commentary*. 2nd ed. New York: Oxford University Press; 1998.
10. Dellon AL. The moving two-point discrimination test: clinical evaluation of the quickly adapting fiber/receptor system. *J Hand Surg* 1978; **3**: 474–481.
11. Manschot S, van Passel L, Buskens E, Algra A, van Gijn J. Mayo and NINDS scales for assessment of tendon reflexes: between observer agreement and implications for communication. *J Neurol Neurosurg Psychiatry* 1998; **64**:253–255.
12. Bohannon RW, Smith MB. Interrater reliability of a modified Ashworth Scale of muscle spasticity. *Phys Ther* 1986; **67**:206–207.
13. Hallett M. NINDS myotatic reflex scale. *Neurology* 1993; **43**:2723.

14. Ross ED. Localization of the pyramidal tract in the internal capsule by whole brain dissection. *Neurology* 1980; **30**:59–64.
15. Crawford JR, Howell DC, Garthwaite PH. Payne and Jones revisited: estimating the abnormality of test score differences using a modified paired samples *t* test. *J Clin Exp Neuropsychol* 1998; **20**:898–905.
16. Katoh M, Kawamoto T. Bilateral medullary infarction. *J Clin Neurosci* 2000; **7**:543–545.
17. Caplan LR. Intracranial branch atheromatous disease: a neglected, understudied, and underused concept. *Neurology* 1989; **39**:1246–1250.
18. Bassetti C, Bogousslavsky J, Barth A, Regli F. Isolated infarcts of the pons. *Neurology* 1996; **46**:165–175.
19. Thomalla G, Glauche V, Weiller C, Röther J. Time course of Wallerian degeneration after ischemic stroke revealed by diffusion tensor imaging. *J Neurol Neurosurg Psychiatry* 2005; **75**:266–268.
20. Aguilar MJ. Recovery of motor function after unilateral infarction of the basis pontis. *Am J Phys Med* 1969; **48**:279–288.
21. Fisher CM. Pure spastic paralysis of corticospinal origin. *Can J Neurol Sci* 1977; **4**:251–258.
22. Brown WJ, Fang HCH. Spastic hemiplegia in man. Lack of flaccidity in lesion of the pyramidal tract. *Neurology* 1961; **11**:829–835.
23. Fisher CM. Concerning the mechanism of recovery in stroke hemiplegia. *Can J Neurol Sci* 1992; **19**:57–63.
24. Ropper AH, Fisher CM, Kleinman GM. Pyramidal infarction in the medulla: a cause of pure motor hemiplegia sparing the face. *Neurology* 1979; **29**:91–95.
25. Oliveira-Souza R. Motor hemiplegia and the cerebral organization of movement in man. II. The myth of the human extrapyramidal system. *Arq Neuropsiquiatr* 1989; **47**:8–15.

Cerebral Cortex Advance Access published April 20, 2006

Cerebral Cortex
doi:10.1093/cercor/bhj178

Neuroplasticity in Human Callosal Dysgenesis: A Diffusion Tensor Imaging Study

Fernanda Tovar-Moll[1,2], Jorge Moll[2], Ricardo de Oliveira-Souza[2], Ivanei Bramati[2], Pedro A. Andreiuolo[2] and Roberto Lent[1]

[1]Department of Anatomy, Institute of Biomedical Sciences, Federal University of Rio de Janeiro, Brazil and [2]Cognitive and Behavioral Neuroscience Unit, Labs-D'Or Hospitals Network, Rio de Janeiro, Brazil

Callosal dysgenesis (CD) is observed in many neurodevelopmental conditions, but its subjacent mechanisms are unknown, despite extensive research on animals. Here we employ magnetic resonance diffusion tensor imaging and tractography in human CD to reveal the aberrant circuitry of these brains. We searched particularly for evidence of plasticity. Four main findings are described—1) in the presence of a callosal remnant or a hypoplastic corpus callosum (CC), fibers therein largely connect the expected neocortical regions; 2) callosal remnants and hypoplastic CCs display a fiber topography similar to normal; 3) at least 2 long abnormal tracts are formed in patients with defective CC: the well-known Probst bundle (PB) and a so far unknown sigmoid, asymmetrical aberrant bundle connecting the frontal lobe with the contralateral occipitoparietal cortex; and 4) whereas the PB is topographically organized and has an ipsilateral U-connectivity, the sigmoid bundle is a long, heterotopic commissural tract. These observations suggest that when the developing human brain is confronted with factors that hamper CC fibers to cross the midline, some properties of the miswired fibers are maintained (such as side-by-side topography), whereas others are dramatically changed, leading to the formation of grossly abnormal white matter tracts.

Keywords: callosal agenesis, callosal development, corpus callosum, cortex development, cortical commissures, DTI

Introduction

Plasticity has been recognized as a fundamental and universal property of the nervous tissue, capable of providing changes to its structure and function in response to environmental challenges, from invertebrates to mammals including humans. Plastic changes can vary widely, from subtle modulations of synaptic transmission (Blitz and others 2004; Nordeen KW and Nordeen EJ 2004) to gross displacements of functional areas in the brain (Elbert and others 2002), as much as the environmental changes that provoke them, which can vary from subtle sensory events to large, destructive lesions of the nervous system. In general, it is believed that younger mammals are more susceptible to structural reorganization of a compensatory nature (Kennard 1942), such as neuronal proliferation, axonal (re)growth, and circuit reconstruction (Clowry and others 2004; Maffei and others 2004; Feller and Scanziani 2005), whereas older animals have their plastic possibilities restricted to the synaptic level (Froemke and others 2005), although there are documented exceptions to this "Kennard principle" (Schneider 1979; Arnold and others 2005; Tailby and others 2005).

Clinicopathological observations suggest that the immature human brain is capable of major structural and functional reorganization, as exemplified by the excellent recovery of children subjected to extensive removal of one hemisphere as the last therapeutic resource to control epilepsy that is otherwise intractable (Bernasconi and others 2000; Villablanca and Hovda 2000). Some children born without a corpus callosum (CC) may represent another example of this remarkable plastic property of the brain as they lack the interhemispheric disconnection syndrome that is typical of split-brain adults (Sperry 1970).

Because the CC is the major commissural fiber bundle in the human brain, investigating the reorganization of white matter in different forms of isolated callosal dysgenesis (CD) provides a unique window to understand human neuroplasticity. CD can appear as 1) a partial defect of the CC (e.g., lack of the body and splenium, with the presence of a rostral remnant), 2) hypoplasia (homogeneous reduction of the callosal size), or 3) a complete lack of the commissure (agenesis). The first description of CD was made by Reil (1812), and the first evidence for plastic reorganization of callosal fibers was provided by Probst (1901), who recognized the aberrant longitudinal bundle of fibers that was named after him (Probst bundle [PB]). CD can present as an isolated abnormality, or may come associated with other lesions or malformations. The result is a wide spectrum of clinical features (Lassonde and others 2003), from a complete lack of recognizable symptoms to severe mental retardation, language deficits, and motor impairment. CD has been described in association with more than 50 different metabolic and genetic disorders of the central nervous system (Richards and others 2004), although its molecular and cellular causes remain largely unknown.

Whereas earlier cases were only identified postmortem, with the introduction of computerized tomography (CT) and magnetic resonance imaging (MRI), most cases are now diagnosed directly in vivo (CT: Meyer, Röricht, and Woiciechowsky 1998; MRI: Kuker and others 2003). In virtually all the cases documented by neuroimaging techniques, the PBs are the only morphological indication that plasticity of cortical circuits may have occurred during development, despite the fact that their functional role, either compensatory or maladaptive, has not been revealed so far. The trajectory of some of the Probst fibers was studied in animal models (Ozaki and others 1987, 1989; Ozaki and Shimada 1988), but the precise topography and function of these fibers in humans remain unknown.

Until very recently, noninvasive neuroimaging techniques (including conventional MRI) had very limited power to characterize white matter structures in humans. In the past decade, new magnetic resonance (MR) pulse sequences had a major and increasing impact on the assessment and management of many neurological diseases. More recently, the development of diffusion tensor imaging (DTI) allowed the estimation of vector fields describing the directional diffusivity of water molecules

in the living human brain. DTI describes the anisotropic properties of water diffusion on a voxel basis, thus revealing important details of fiber tract orientation. Diffusion tensor can thus be used to reconstruct the trajectories of major fiber systems in 3-dimensional spaces (Shrager and Basser 1998; Basser and others 2000). Computer graphics–based renderings of these reconstructed "fiber tracts" have been termed MR "tractography." The rapid progress of MR hardware technology (powerful and stable gradients) together with important advances in pulse sequence designs has pushed DTI into the clinical neuroscience arena. DTI scanning is now feasible in most clinical conditions, both in adults and in children (Albayram and others 2002).

A recent DTI/tractography short study of 4 cases of CD (Lee and others 2004) was able to show abnormalities in white matter structure in this condition. These preliminary findings encourage a more thorough and detailed use of DTI for the investigation of specific patterns of white matter developmental changes in CD. Here we employ DTI/tractography to characterize the white matter structural reorganization in patients with different types of CD in vivo, showing that developmental plasticity in humans may produce major reorganization of great tracts in the brain. We aimed at 1) comparing the topographic arrangement of PBs and their putative connectivity with those of the CC of normal subjects, 2) evaluating the trajectory and connectivity patterns of callosal fibers that cross through the remnant callosum in partial dysgenesis, and 3) searching for evidence of additional aberrant circuits.

Our results provide evidence that when the developing human brain is confronted with factors that hamper CC fibers to cross the midline, some properties of the miswired fibers are maintained (such as side-by-side topography), whereas others are dramatically changed, leading to the formation of grossly abnormal white matter tracts.

Materials and Methods

Patients

Eleven patients aged from 1 to 33 years and with different types of CD were analyzed: 3 with callosal agenesis (complete lack of the CC), 3 with callosal hypoplasia, and 5 with partial CD. None had contraindications for MRI. An experienced neurologist performed clinical evaluations. Patients' characteristics are summarized in Figure 1. Ten individuals with no evidence of neurological disease served as normal controls. Written informed consent was obtained from the patients or their parents. All procedures were approved by the Ethics Committee of our institution and performed according to international regulations (Declaration of Helsinki 2000).

Neuroimaging

Anatomical images were obtained with a 1.5-T Philips-Intera scanner, using the following pulse sequences: spin-echo T_1 weighted (time repetition [TR]/echo time [TE]/matrix/field of view [FOV] = 550 ms/20 ms/256 × 256/240 mm), turbo spin-echo T_2 weighted (TR/TE/matrix/FOV = 3500 ms/90 ms/256 × 256/256 mm), inversion recovery T_1 weighted (TR/TE/time to inversion [TI]/matrix/FOV = 3000 ms/30 ms/300 ms/256 × 256/256 mm), and fluid-attenuated inversion recovery (TR/TE/TI/matrix/FOV = 9000 ms/100 ms/2300 ms/256 × 256/256 mm), all with a slice thickness of 5 mm without gap.

	Case1 (ISL)	Case2 (THSR)	Case3 (VHSH)	Case4 (ARS)	Case5 (DPV)	Case6 (TCSR)	Case7 (ALF)	Case8 (CFS)	Case9 (KCA)	Case10 (SOL)	Case11 (MGS)
Gender	F	M	M	M	M	F	M	F	M	F	F
Age (years)	25	4	6	33	10	8	2	1	7	7	5
Psycho-motor develop-mental abnormal-ities	Aphasia Moderate mental retardation	Mild mental retardation	Mild mental retardation	None	Autism	None	Moderate to severe flaccid para-paresis	Psycho-motor retardation	None	Severe mental retardation	Severe mental retardation
Type of dysgenesis	Partial/genu remnant	Partial/genu remnant	Hypoplasia	Hypoplasia	Hypoplasia	Total agenesis	Partial/genu and dorsum remnants	Total agenesis	Partial/genu remnant	Total agenesis	Partial/genu remnant
Probst bundles	Present	Present	Undissociable from cingulate	Not identified	Undissociable from cingulate	Present	Undissociable from cingulate	Present	Not identified	Present	Present
Cingulate gyrus	Inverted	Inverted	Apparently normal	Apparently normal	Inverted	Inverted	Not inverted, enlarged	Inverted	Inverted posteriorly	Inverted	Inverted
Lateral ventricles	Parallel Colpo-cephalus	Parallel Colpo-cephalus	Slight Colpo-cephalus	Slight Colpo-cephalus	Parallel Colpo-cephalus	Parallel Colpo-cephalus	Hydro-cephalus	Colpo-cephalus	Communicant	Hydro-cephalus	Hydro-cephalus
Other brain abnormal-ities	None	None	None	None	None	None	None	Micro-cephalus	Lobar holopros-encephalus	Micro-cephalus Dandy-Walker	Microcephalus Dandy-Walker
Extracranial abnormal-ities	None	None	None	None	None	None	None	None	None	Facial dysmorphism	Facial dysmorphism
Anatomical Images	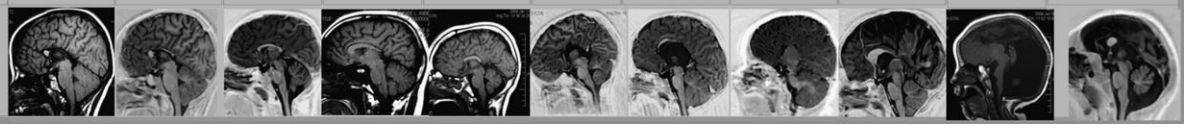										

Figure 1. Clinical characteristics and MRI findings in studied patients.

Diffusion-weighted images were acquired in axial and sagittal planes with single-shot, spin-echo echo-planar sequences—1) axial: TR/TE = 4000/110 ms, FOV = 256 mm, matrix = 112 × 128, slice thickness = 5 mm without gap and 2) sagittal: TR/TE = 4491/121 ms, FOV = 256 mm, matrix = 112 × 128, slice thickness = 5 mm without gap. Diffusion sensitization gradients were applied in 6 noncollinear directions (*x*, *y*, *z*, *xy*, *yz*, *xz*), with a *b* factor of 800 s/mm^2. Diffusion tensor data were transferred and postprocessed using a software written in Interactive Data Language, Philips Research Integrated Development Environment software (PRIDE research platform, Fiber Track 4.1). The diffusion tensor data set for each voxel was generated including eigenvalues and eigenvectors using multivariate fitting. Fractional anisotropy (FA) maps and color-coded FA maps for fiber direction were produced according to procedures described in detail by Pajevic and Pierpaoli (1999). Fiber tracking (tractography) was performed using a technique known as the Fiber Assignment by Continuous Tracking (Mori and others 1999; Xue and others 1999). For the purpose of the present paper, the white matter was identified in the anatomical images and then in the color-coded FA maps. Both the anatomical images and the FA color-coded maps were used to guide the proper placement of 2-dimensional regions-of-interest (ROIs) in order to reconstruct the 3-dimensional fiber bundles. Fiber tracking was accomplished by manually specifying ROIs over the trajectory of 1) the callosal remnant, 2) the PB, 3) the cingulate bundle, and 4) additional white matter locations emerging from this analysis. We further employed multiple ROIs in different locations both ipsi- and contralaterally in patients and controls to exclude "skipping-tract" artifacts (Pierpaoli and others 2001; Mori and van Zijl 2002; Lazar and Alexander 2003; Huang and others 2004). Equivalent ROIs were specified for control subjects. For precise localization, all the ROIs were placed on the color-coded FA maps and on the corresponding axial, coronal, and sagittal anatomical images. Automatic tracking of fibers was performed with a marching algorithm, restricting fiber tracking to voxels with a minimum FA of 0.30. Fiber deflection threshold was set to 0.85 (corresponding to 45° for the angle between 2 "eigenvectors" in contiguous voxels). These procedures were repeated independently by 2 investigators.

Placement of ROIs

To trace the fibers crossing at the CC, a polygonal ROI was drawn in the midsagittal plane of each control subject, encompassing the entire CC. In order to detect a rostrocaudal topography of the callosal fibers, 5 equally spaced ROIs with equivalent areas were placed along the CC in the midsagittal plane of each control subject (Fig. 3, Panel *1A*). To investigate the existence of a dorsoventral callosal topography, 5 triplets of contiguous ROIs were defined dorsoventrally, as shown in Figure 3, Panel *1B*. A similar strategy was used to uncover fiber topography in callosal hypoplasia. In order to determine the connectivity of the callosal remnant in each patient with partial CD, single irregular polygonal ROIs were drawn encompassing the entire remnant area at the midsagittal plane (Fig. 3, Panel *2A*). PBs were identified in the anatomical images and in the color-coded FA maps of 5 patients. Directional color-coded FA images in a coronal plane 6 mm posterior to the anterior commissure were used as references to place the ROIs designed to trace both PBs of each patient. A similar procedure was used to trace the cingulate bundles in both patients and control groups. To confirm the asymmetry of the aberrant bundles that were found crossing through the callosal remnants, 2 ROIs were positioned in different places of their trajectory in the contralateral hemisphere (Fig. 5, Panel *1*), and the FA threshold was decreased as low as 0.05, along with a lower deflection threshold of 0.60. Using the same procedure in the control subjects (Fig. 5, Panel *2*) and observing that no tracts could be reconstructed, it was confirmed that the presence of asymmetrical aberrant bundles could not be attributed to reconstruction artifacts.

To characterize the topographic organization of the PB, each bundle was divided into 4 quadrants (as shown in Fig. 4, Panel *2D*) at the coronal plane in the color-coded FA maps. Each quadrant was treated as a separate ROI for tracing fibers in an equivalent number of seed points. In one patient (Case 5, Fig. *2B*), PBs were identified but could not be discerned from the adjacent cingulate bundles based on anatomical or color-coded FA map. A single thickened bundle was observed in each hemisphere, possibly containing both cingulate and PB fibers. These thick bundles were then arbitrarily divided into lateral and medial regions at the coronal plane in the color-coded FA map. In each region, an equivalent number of seed points were placed to trace the fibers, transversally to the medial and lateral regions.

Because there is controversial evidence concerning the occurrence of plasticity in the anterior commissure of CD animals and humans, we tried to place ROIs in this structure at the sagittal plane to clarify this issue. However, technical limitations of the DTI acquisition (slice thickness and resolution) precluded reliable assessment of the anterior commissure in the present study.

Results

Conventional Imaging

Conventional MRI (i.e., anatomical images) showed the typical anatomical features of CD, including parallel, enlarged lateral ventricles, downward displacement of the cingulate gyrus, radial sulci at the medial brain surface, and PBs. The main clinical characteristics and conventional MRI findings of all patients are listed in Figure 1, and the basic anatomical types are exemplified in Figure 2.

Fiber Organization of Normal CC

Anatomical and recent DTI fiber-tracking studies have shown a rostrocaudal topographic organization of callosal fibers in normal individuals (de Lacoste and others 1985; Xu and others 2002; Abe and others 2004). However, the fiber organization of callosal remnants in CD is largely unknown. Our findings in normal individuals confirmed the rostrocaudal topographic organization of normal CC fibers as described in the previous studies, with frontal fibers crossing through the genu, parietal fibers mostly through the body, and occipital fibers through the splenium (Fig. 3, Panel *1A,C,D*). We also demonstrated an evident dorsoventral fiber distribution pattern within the normal CC: fibers derived from medial cortical sectors cross dorsally in the CC, whereas those originated in dorsolateral sectors of the cortex were positioned ventrally in the CC (Fig. 3, Panel *1B,E–G*).

Topographic Organization in Callosal Remnants and Hypoplastic Tracts

Radiologists and pathologists usually assume that callosal remnants situated rostrally correspond to the genu, whereas caudal remnants correspond to the splenium. However, this assumption remains unproven, and remnants might simply represent other segments of the CC, mechanically displaced under abnormal conditions. Moreover, the connectivity pattern established by fibers that make up the CC remnants could be accounted for by at least 2 alternative possibilities: either they would contain "compressed" tracts with an expanded connectivity encompassing large extents of cortex or their fibers would keep their connection fields restricted to specific sectors of the cortex as occurs in the normal CC. We found that fibers of rostral remnants connect the rostral prefrontal cortex of both hemispheres (Fig. 3, Panel *2A–D*), confirming that they indeed represent the genu in these patients, rather than fibers with enlarged projection fields. A "tail" of fibers projecting backward at the left side can be observed consistently in many of these cases (arrow in Fig. 3, Panel *2*) and will be described below.

Another important issue concerns the possible preservation of topography within the remnant or within a hypoplastic callosum. Do the fibers therein conserve their overall topographic relations as if they were comprised within a normal callosum? We found a consistent rostrocaudal and dorsoventral distribution

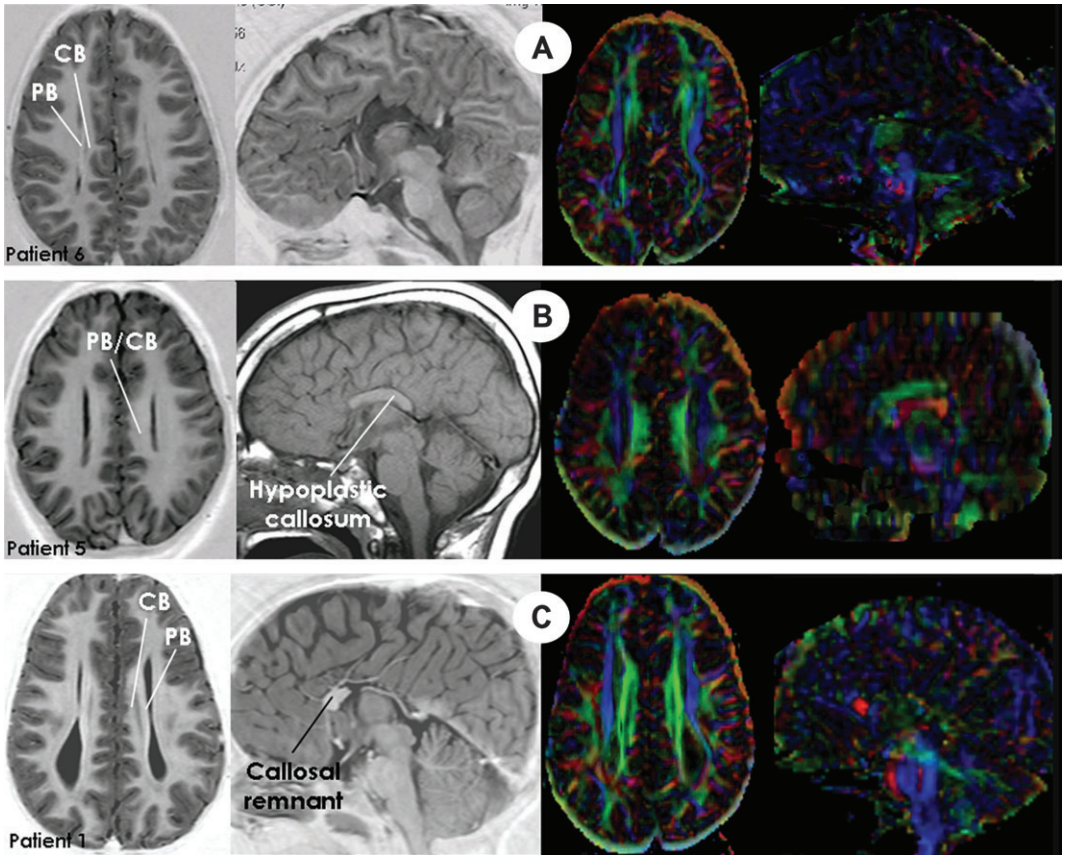

Figure 2. Types of CD. T_1-weighted images and color-coded FA maps: callosal agenesis (*A*), callosal hypoplasia (*B*), and partial CD with remnant (*C*). CB, cingulate bundle.

of fibers in all patients with either partial CD or hypoplasia that agrees with the topography seen in the normal individuals (Fig. 4, Panel *1A–C*). This finding indicates that the topographic rules orienting the rostrocaudal arrangement of the remaining callosal fibers are preserved despite the developmental defects that hindered commissuration of a greater number of fibers.

Developmental Plasticity of Cortical Fibers in CD

Aberrant fibers forming the PBs were traced in 5 subjects, 2 of them with CC agenesis and 3 with partial dysgenesis. We first posed the question whether the fibers within the PB displayed a pattern of connectivity in any way similar to the normal callosal fibers. Second, we wanted to know whether Probst fibers conserved a topographic organization consistent with the callosal fibers that formed it. We found that Probst fibers leave the bundle at successive rostrocaudal levels and deflect dorsally or ventrally toward the cortical gray matter (Fig. 4, Panel *1F–H,2A–C*, fibers in purple), creating a multiple U-system of longitudinal connections in the cortex, similar to the pattern described in acallosal mice by Wahlsten and his collaborators (Ozaki and others 1987, 1989; Ozaki and Shimada 1988). This multiple U-arrangement differed clearly from the long, rostrocaudal pattern typical of the cingulate bundle (shown in yellow in Fig. 4, Panel *1F–H,2A–C*).

In addition, by employing a set of small ROIs positioned within the PB (Fig. 4, Panel *2D*), we were able to demonstrate that it presented a consistent, topographic, and spatial organization of fiber trajectories (Fig. 4, Panel *2E–F*) that was maintained within the PB as well as in the cortical white matter after leaving the bundle. Thus, PB fibers positioned ventrally exhibited a longer, longitudinal trajectory and connected the parietooccipital regions with more anterior sectors of the frontal lobe, whereas those situated dorsally in the PB were more arched, U-shaped, and projecting to dorsal cortical sectors in the same hemisphere.

The PB could not be individualized in some of the patients with callosal hypoplasia (Case 5, Fig. 1). Instead, a single thick, longitudinal bundle was observed in each hemisphere in the conventional anatomical images and also in the FA and color-coded FA maps (Fig. 2*B*). We wondered whether this thick bundle contained both the cingulum and the PB and whether the corresponding fibers were segregated or mixed therein. These issues were addressed by arbitrarily dividing this thick bundle into lateral and medial sectors and placing an equivalent number of seed points in each sector (Fig. 4, Panel *1D*). Fibers with trajectories matching those described above for the PB and the cingulum were identified, indicating that these 2 bundles were adjacent in these patient (Fig. 4, Panel *1F–H*), although a morphological septum between them was not apparent, as in all other cases. We could note that the lateral fibers exhibited the U-arrangement of the PB as described above and that the medial fibers showed trajectories that are more longitudinal and ventral, thus compatible with the cingulate bundles.

A Hitherto Undescribed Aberrant Tract in CD

The neurological literature attributes a large variability of symptoms to patients with CD, from mental retardation to mild intelligence quotient subnormality and from aphasia to

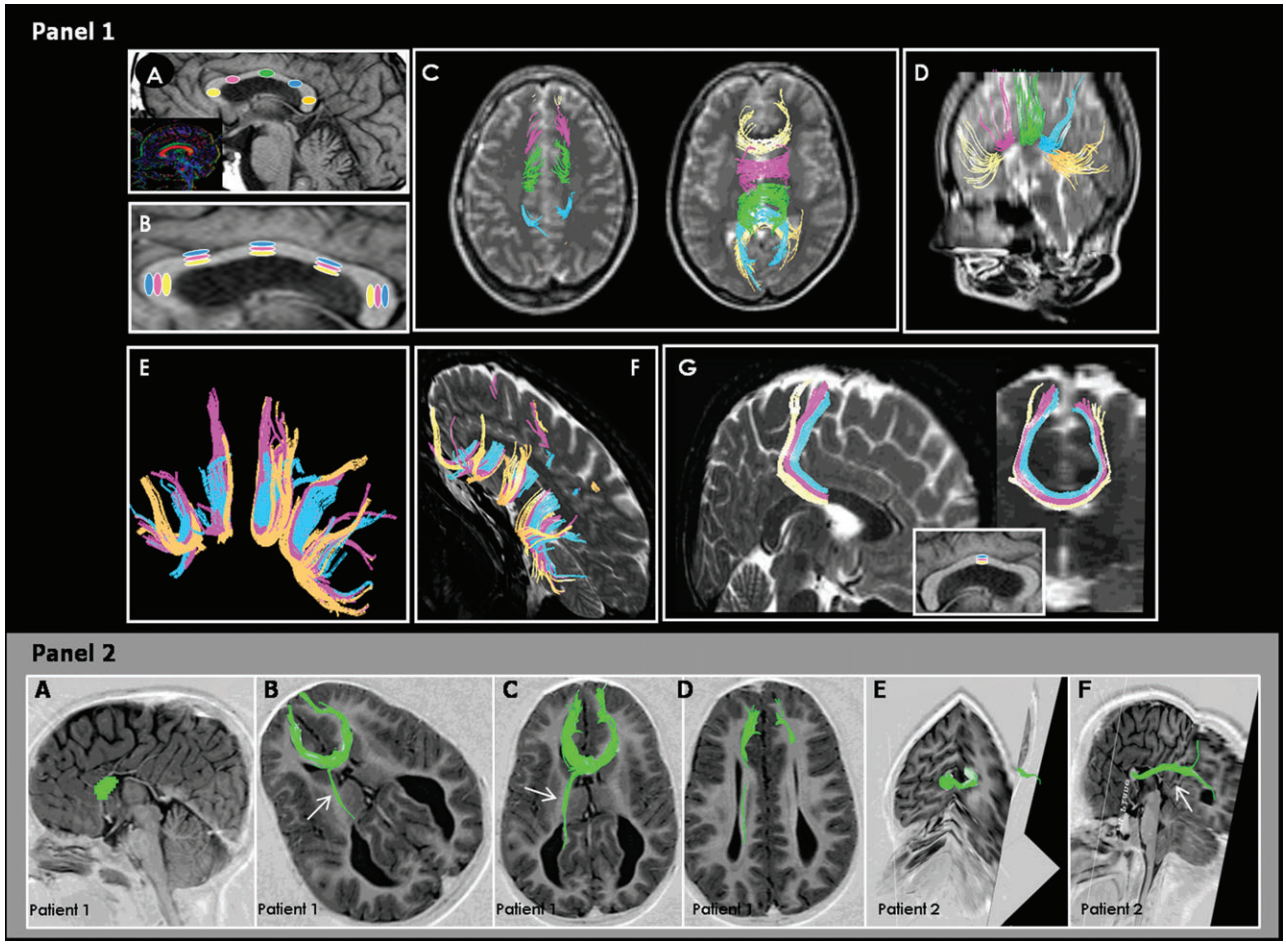

Figure 3. Panel *1*: Topographic arrangement of normal callosal fibers. (*A*) and (*B*) represent differently color-coded ROIs, positioned in rostrocaudal and dorsoventral succession, respectively, in order to seed the corresponding callosal fibers as shown in (*C–G*). The inset in (*A*) shows the FA map for the same control brain. (*C*) shows transverse sections with the corresponding rostrocaudal callosal sectors with fibers heading medially (dorsal section at the left) and crossing the midline (ventral section at the right). These fibers are shown from a lateral perspective in (*D*). (*E*) and (*F*) show the dorsoventral organization of callosal fibers resulting from the ROIs placement as shown in (*B*). (*G*) shows the mediolateral cortical topography for one selected triplet of ROIs (inset) positioned dorsoventrally in the CC, in a slightly tilted sagittal plane (at the left) and a coronal plane (at the right). Panel *2*: Connections of the callosal remnant in 2 cases of partial dysgenesis. (*A*) shows an ROI (in green) encompassing the entire rostral remnant of the CC, and (*B–D*) represent transverse sections (ventral to dorsal, *B–D*), showing that most callosal fibers that cross through the remnant are genual, connecting the prefrontal cortex of both hemispheres. (*E*) and (*F*) represent another case of similar morphology. Note that an aberrant caudal fascicle (arrows) emerges from the callosal tract to course in a caudal direction parallel to the PB, medially to the lateral ventricles.

hyperactivity (Lassonde and others 2003). This extensive variability suggests that a number of largely unknown neuroplastic events may take place in dyscallosal brains. We had observed a caudal tail of fibers when tracing the connections of the callosal remnant (see Fig. 3, Panel *2*) and hypothesized that this could be an aberrant callosal tract that could be distinguished from PB. We tested this hypothesis 1) by placing of a single ROI at the genual callosal remnant, at the midsagittal plane, and 2) by using a combination of 2 strategically positioned ROIs, one at the callosal remnant and the other more laterally, in the coronal plane, approximately 2–4 cm posterior to the anterior commissure (Fig. 5, Panel *1B,E–F*). These analyses revealed a so far unknown asymmetric, abnormal tract in 4 CD patients (Fig. 3, Panel *2* and Fig. 5, Panel *1B–D*). This tract followed a sigmoid trajectory beneath the PB, connecting the left parietooccipital region with the contralateral frontal pole, through the genual remnant and PB (patients 1 and 2) or through the hypoplastic body (patients 4 and 7). The "sigmoid aberrant bundle" was asymmetrical (Fig. 5, Panel *1*) because it consistently connected the right prefrontal cortex with the left occipital cortex but was absent (patients 1, 2, and 7) or very small in the mirror-symmetric configuration in one case with hypoplastic CC (patient 4). To exclude the possibility of an artifact ("kissing" or "skipping" fibers), we placed an equivalent ROI in the callosal genu of 10 normal controls (Fig. 5, Panel *2A–C*). Only the regular, homotopic callosal connections were reconstructed (Fig. 5, Panel *2D*), even when very low FA threshold (0.05) was adopted. Using the 2-ROI procedure, similar thresholds and even larger ROIs at the coronal plane, no tracts linking the callosal genu and parietooccipital regions were identified. We concluded that the sigmoid aberrant bundle is a real anatomical entity formed in CD subjects, suggesting that the brain of these subjects can undergo extensive rewiring, including the formation of long, massive, aberrant tracts connecting cortical regions located far apart.

Discussion

The CC is the major commissural fiber bundle in the human brain. In adults, its damage or surgical transection leads to the

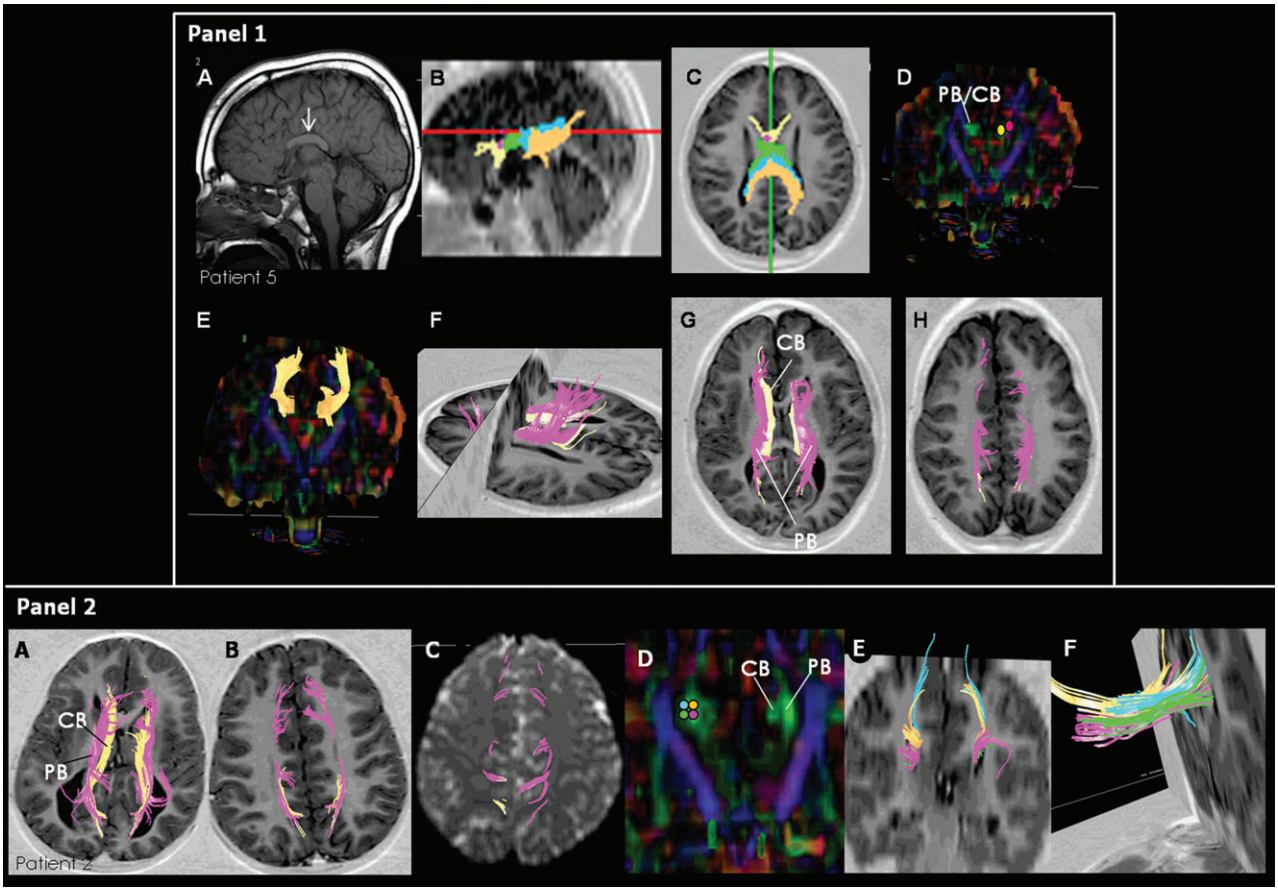

Figure 4. Panel *1*: Fiber connectivity of a case with callosal hypoplasia. (*A*) shows the hypoplastic CC in the sagittal plane (arrow). (*B*) and (*C*) show that the topographic arrangement of callosal fibers is maintained in the hypoplastic CC. The red line in (*B*) represents the transverse plane in (*C*), and the green line in (*C*) shows the sagittal plane in (*B*). (*D*) is a directional FA color-coded map at the coronal plane, showing that the PB cannot be distinguished from the cingulate bundle (CB). Two ROIs are shown at the right, used to separate PB from CB. (*E*) shows the directional FA map at the coronal plane and the position of 2 large, bilateral ROIs for tractography, illustrating the trajectory of the thick, "mixed" PB/CB tracts. (*F–H*) show the separation of PB from CB in the transverse plane, achieved by positioning small ROIs medially (yellow in *D*) and laterally (purple). The U-connectivity of the PB can now be clearly identified (*H*), as well as the more longitudinal and ventrally situated fibers of the CB (*F*, *G*). Panel *2*: Topographic arrangement of the Probst fibers in a CD case with remnant. (*A–C*) show the PBs (in purple), segregated from the CBs (in yellow), shown in transverse sections. Note that Probst fibers leave the bundle toward the cortex in different regions along their longitudinal course (*A*), projecting mainly to mesial cortical areas (*B*, *C*). (*D*) represents a directional FA map at the coronal plane, with the PBs and CBs coded in green. Four ROIs were placed in the left PB, color coded in different hues. (*E*) and (*F*) show that fibers within the PB exhibit a topographic organization in both the dorsoventral and the mediolateral axes. (*E*) is a coronal section, tilted in (*F*) around a vertical axis, for better visualization.

classical interhemispheric disconnection syndrome (Sperry 1970), which is usually not observed when the CC is congenitally absent (Lassonde and others 1991). However, patients with CD even without other anatomical anomalies can show variable clinical presentations, ranging from no symptoms at all to severe cognitive impairment (Lassonde and others 2003). Remarkably, this clinical variability is poorly correlated with gross anatomical features, suggesting the existence of major changes at a finer level. Although CD was extensively explored in animals, most studies in humans have been limited to postmortem anatomical descriptions or conventional MRI. DTI/tractography now provides a powerful tool to characterize finer changes in white matter structure in vivo and, as observed in our cases, indicates the occurrence of plastic events leading to the formation of aberrant tracts in the brain.

We have reported 4 basic findings in patients with CD—1) when there is a rostral callosal remnant, fibers therein do not expand their target territory in the neocortex; instead, they connect the rostral regions of the frontal lobes as genual fibers normally would; a similar conclusion holds for cases with a hypoplastic CC; 2) callosal remnants and hypoplastic CC display a fiber topography reminiscent of normal CC; 3) at least 2 long abnormal tracts are formed in patients with defective CC: the long-time known PB and a sigmoid, asymmetrical aberrant bundle connecting the right frontal lobe with the contralateral occipitoparietal cortex; and 4) the PB maintains a topographic organization, albeit ipsilateral, as callosal fibers would normally do contralaterally; the sigmoid bundle, on the other hand, is a heterotopic commissural tract about which no topographic or functional information is available. These observations suggest that when the human brain is confronted with factors that hamper CC fibers to cross the midline normally during development, some properties of the miswired fibers are maintained (such as a side-by-side topographic organization), whereas others are dramatically changed, leading to the formation of grossly aberrant white matter tracts.

The Developmental Framework for Callosal Plasticity

During development, callosal axons grow over long distances to reach their final targets. Their first task after emerging from the somata is to grow toward the white matter, what they seem to do following polarity cues intrinsic to the neuron (Polleux and

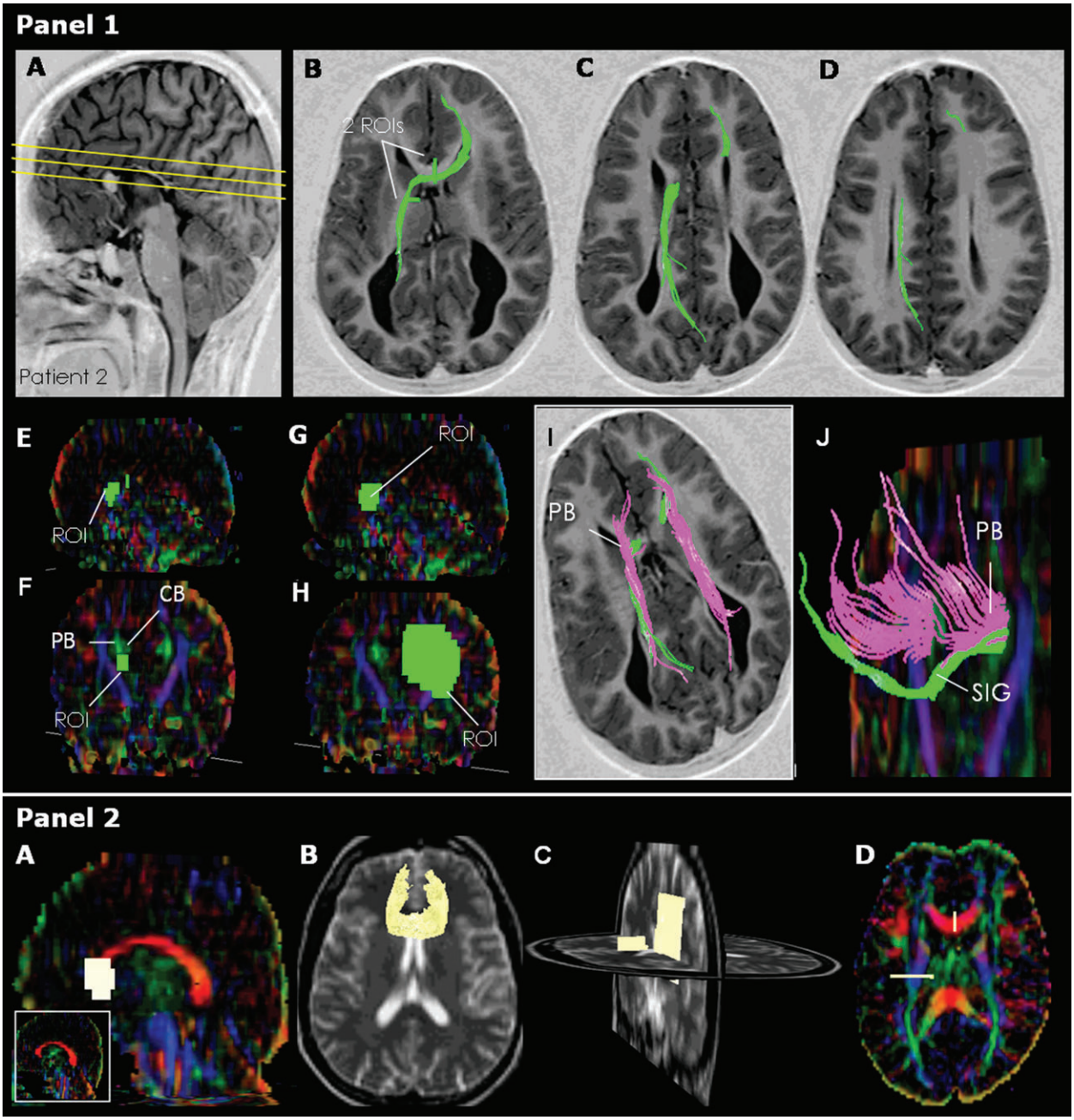

Figure 5. Panel *1*: The aberrant sigmoid bundle (SIG) in a CD case. (*A*) shows the transverse planes illustrated in (*B–D*) from ventral to dorsal. The aberrant SIG was seeded by the 2 ROIs in (*B*) and is shown to connect the right frontal pole with the left parietooccipital cortex by way of the anterior callosal remnant. The bundle seems to overlap the ventricle because it is slightly curved upward out of the background plane. The 2 effective ROIs in (*B*) are also shown over the FA sagittal (*E*) and coronal (*F*) maps. Larger ROIs positioned at mirror-symmetric locations with FA threshold as low as 0.05 (*G*, *H*) fail to reconstruct a contralateral bundle, demonstrating its asymmetric nature and discarding the possibility of a skipping-tract artifact. Panels (*I*) and (*J*) show that the SIG (in green) is segregated from the PB (in purple). (*I*) is a transverse plane, whereas (*J*) is a coronal plane slightly tilted around a vertical axis. Panel *2*: Connectivity of genual fibers in a control case, showing no caudal fibers emerging from the CC. (*A*) shows a color-coded FA map in the sagittal plane, with an ROI placed at the genu. The inset shows the same map without the genual ROI. (*B*) shows the corresponding reconstruction of callosal fibers crossing the genu and connecting the frontal lobes of both hemispheres. (*C*) shows a lateral perspective of the 2 ROIs shown on a transverse FA map in (*D*), one ROI placed at the genu (represented sagittally in *C*, orthogonal to a transverse background plane) and another in the white matter caudally (coronal plane, slightly tilted around a vertical axis). Both ROIs were set to a low FA threshold of 0.05. However, as demonstrated in (*B*), callosal fibers cross the genu and connect the frontal lobes of both hemispheres as expected, but no fibers connecting these 2 ROIs were reconstructed in any of the normal brains.

others 1998), and extrinsic gradients of diffusible molecules (semaphorins, ephrins, netrin) that attract them toward the ventricular layer and then make them deflect or bifurcate subventricularly taking a medial direction (Serafini and others 1996; Bagnard and others 1998; Hu and others 2003; Uziel and others 2003). Close to the midline, the prospective callosal axons enter a tunnel of glial cells that secrete repulsive molecules (e.g., Slit-2), channeling them toward the opposite hemisphere (Shu and Richards 2001; Richards 2002; Richards and others 2004; Lent and others 2005). Actual pathfinding in search of the midline seems to be performed only by pioneering axons originating in the cingulate cortex (Koester and O'Leary

1994; Rash and Richards 2001; but see Ozaki and Wahlsten 1998), whereas the bulk of axons are presumed to simply follow the pioneers. At the opposite hemisphere, little is known about the guidance cues and growing mechanisms of callosal axons, except that they overshoot the homotopic targets, leaving a branch that arborizes at the right point, and then eliminate somehow the overshooting fiber (Hedin-Pereira and others 1999). The establishment of a mature pattern of callosal projections involves the transient growth of supernumerary axons and arbors that are later selectively eliminated (for a recent review, see Innocenti and Price 2005).

These developmental mechanisms have only indirectly been demonstrated in humans, as suggested by the formation of midline cellular and extracellular matrix structures involved in axonal guidance (Lent and others 2005) and a perinatal reduction of cross-sectional callosal area that might indicate the massive axonal elimination shown to occur in animals (Clarke and others 1989). Recent MRI measures have added evidence to this latter suggestion, both in the callosal tract (Keshavan and others 2002) and in the cortical tissue (Thompson and others 2000).

Classical descriptions have proposed a rostrocaudal gradient of formation of the callosal tract beginning at approximately 11 weeks postovulatory (Rakic and Yakovlev 1968). According to this view, a rostral locus of commissuration would form first at the prospective position of the genu, followed by the rostrocaudal addition of axons to form the body and splenium and an inverse sequence to form the callosal rostrum. However, other authors have suggested that the embryonic CC has a bicentric origin, with a rostral sector forming at the lamina rostralis and a more caudal region appearing simultaneously over the hippocampal commissure (Kier and Truwit 1996, 1997). The fact that genual fibers (i.e., fibers located rostrally in the CC and projecting to prefrontal cortical territories) are the most common callosal remnants in CD tends to favor the former hypothesis, although there are reported cases in which remnants are located more posteriorly (reviewed by Richards and others 2004). Thus, it can be concluded that the pathological disturbance in CD cases with genual remnants spares the rostral pioneer fibers and, therefore, presumably does not interfere with the guidance mechanisms provided to the pioneers by the midline cellular and matrix structures. Along the same lines, the subsequent rostral and caudal addition of callosal fibers is obstructed by the pathological insult.

An Interplay between Rigidity and Plasticity in CD

Despite indirect data, none of the above mechanisms have been unequivocally shown to be impaired in CD. However, the available evidence seems to indicate that callosal neurons survive in CD cases, projecting axons to normal and abnormal targets. This is substantiated by the existence of remnant and aberrant tracts that presumably contain callosal fibers. Therefore, the hodological information derived from DTI data can be used to draw important conclusions concerning the balance between plasticity and rigidity (or lack of plasticity) in CD. The fact that a hypoplastic CC exists in some cases, whereas a small remnant is placed rostrally in others, poses the question whether the fibers within these smaller tracts would conserve their specific connectivity (rigidity) or enlarge their territory (plasticity) to occupy the sites left vacant by impaired callosal fibers. We found the first hypothesis to be true as most fibers in the rostral remnants connect the frontal lobes in a very specific, focused manner (compare Fig. 3, Panel *2* with Fig. 5, Panel *2*) and do not invade other territories, except in some particular situations (see below). Similar findings have been reported in mice with congenital deficiencies of the CC (Olavarria and others 1988).

A second important observation concerns the maintenance of a topographic arrangement by fibers within callosal remnants (Fig. 4, Panel *1B–C*) and the PB (Fig. 4, Panel *2*). In this case, if rules for topography were completely disrupted by the pathological processes, we would not find such a topographic order within these tracts. Topography in the normal CC has been shown in animals (Barbas and Pandya 1984; Cipolloni and Pandya 1985; Rockland and Pandya 1986; Olavarria and others 1988; Nakamura and Kanaseki 1989; Matsunami and others 1994) and in humans (Xu and others 2002; Abe and others 2004; see also de Lacoste and others 1985). In general (Fig. 3, Panel *1*), frontal regions become connected through the genu, parietal regions through the body, and occipital regions through the splenium. Also, dorsomedial cortical fibers cross dorsally within the CC, whereas more lateral axons occupy the ventral sectors of the callosal tract. A topographic order was also seen within the PB (Fig. 4, Panel *2*), suggesting that fibers therein use cues to sort themselves that do not depend on the mechanisms impaired by the developmental disturbances of CD. Given the normal pattern of projections of rostral callosal remnants, the frontal poles of the hemispheres are appropriately interconnected, and it should be expected that at least the corresponding frontal functions are spared in these cases.

An example of plastic rewiring of callosal connections derives from the robust aberrant tracts that form in many CD cases: the well-known PB (Probst 1901) and the sigmoid bundle described here for the first time. The PB has been extensively studied in mutant mice (Ozaki and others 1987, 1989; Ozaki and Shimada 1988; Ozaki and Wahlsten 1993) and in surgically ablated hamsters (Lent 1982, 1983), employing tract-tracing techniques. In humans, PB is consistently observed in cases of CD (Lassonde and others 2003) and may even be found in individuals with a normal CC (Hori and Stan 2004). In rodents, Probst fibers usually display tortuous trajectories, leaving and returning to the bundle and eventually crossing the midline through the septum bordering the ventricular surface (Lent 1982, 1983). Many of these longitudinal fibers form U-shaped connections in the medial sectors of the ipsilateral cortex. In addition, a topographic organization was discerned within the PB, according to the cortical region of origin of the fibers (Ozaki and Shimada 1988). Most authors assume that PB is composed of callosal fibers whose way across the midline was blocked during development. The topographic similarities between normal callosal target regions and the ipsilateral connections established by Probst fibers in animals and, according to our data, in humans strongly support this assumption. The preservation of fiber order in both callosal remnants and the longitudinal aberrant bundle comes in line with the idea that topography is a prespecified property of some fiber systems, the CC among them. In this context, it has been shown that callosal axons are topographically organized from the outset (Innocenti and Clarke 1984). We, therefore, conclude that in CD, the pathological insult at the origin of this condition does not target the cues for fiber ordering in the callosum, even though their trajectories become entirely abnormal.

The sigmoid bundle, on the other hand, is hard to uncover using descriptive anatomical techniques, as it courses within

the normal-looking white matter of CD patients after crossing the remnant or hypoplastic callosum. Postmortem tract-tracing techniques have not been employed in these patients as they would require an improbable association of the congenital defect with acquired cortical lesions followed by short survival plus the availability of the brains for studies with silver impregnation of degenerating fibers. DTI/tractography, however, has proven to be capable of revealing this "hidden" tract. We are confident to exclude the possibility that this bundle be artifactual because 1) it consistently connects the right frontal lobe with the left occipital cortex and does not appear contralaterally (except in one case, as described), despite our efforts to place mirror-symmetric ROIs with low FA thresholds to reveal a contralateral bundle (Fig. 5, Panel *1*), and 2) it was never seen in the 10 control brains studied with similar ROIs as in the patients (Fig. 5, Panel *2*).

As aberrant bundles in CD cases contain fibers that emerge from living neurons, they are presumed to be functional. Whether their function is compensatory or maladaptive, however, is a matter for speculation because a direct approach of their functional performance has not been available so far. One would imagine that the PB, being so consistent among patients, would serve a compensatory rather than a maladaptive role (Lassonde and others 1988, 1991; Sauerwein and Lassonde 1994; Lessard and others 2002), at least in acallosal individuals who lead a normal life without cognitive impairment (Meyer, Röricht, and Niehaus 1998). Therefore, it would not respond for the great variability of symptoms of CD patients. Clarification of this assumption, however, will have to await functional investigations using electrophysiological techniques, as well as clinicoradiological and neuropsychological investigations in larger samples of patients with CD.

The opposite hypothesis could hold in the case of the sigmoid aberrant tract found in 37% (4 of 11) of our cases. No similar structure such as this has been described so far either in animals or in humans, except for a brief mention by Lee and others (2004, 2005) of an occipital branch of fibers exiting from the callosal remnant in one of their cases. Remarkably, these 4 patients had the most severe impairments: 3 of them had moderate mental retardation and 1 had severe motor impairment. We, therefore, hypothesize that this highly asymmetric, aberrant circuit may somehow be related to the disabilities of these patients.

In conclusion, the search for aberrant projections in CD, as well as in other developmental disorders, by using imaging techniques can potentially be combined with electrophysiological methods in a way to address the functional relevance of neuroplastic changes and to better account for the variable and broad clinical presentations that are often observed. In addition, it might be possible to distinguish between plastic changes that cause functional disabilities and symptoms and those that are compensatory and beneficial to patients.

Notes

This work is part of the PhD thesis of FT-M submitted to the Programa de Ciências Morfológicas, Instituto de Ciências Biomédicas and was supported by the Conselho de Desenvolvimento Científico e Tecnológico (CNPq # 471623/2003-2) and the Centro de Educação Continuada em Medicina, Rede D'Or Hospitals. We thank Drs Leonardo C. Azevedo and Elaine L. Gerk for providing access to the patients of Hospital Fernandes Figueira, Fiocruz, Brazil, Prof. Linda Richards for comments on the text, and Dr Maria Beatriz A.M. Gonzaga for patients' sedation support during image acquisition. We also thank all patients and health volunteers for their collaboration in the study. *Conflict of Interest*: None declared.

Address correspondence to Dr Fernanda Tovar-Moll, Neuroimmunology Branch, National Institutes of Neurological Diseases and Stroke/National Institutes of Health, 10 Center Drive, Building 10, Room 5B08, Bethesda, MD 20892, USA. Email: tovarmof@ninds.nih.gov.

References

Abe O, Masutani Y, Aoki S, Yamasue H, Yamada H, Kasai K, Mori H, Hayashi N, Masumoto T, Ohtomo K. 2004. Topography of the human corpus callosum using diffusion tensor tractography. J Comput Assisted Tomogr 28:533–539.

Albayram S, Melhem ER, Mori S, Zinreich SJ, Barkovich AJ, Kinsman SL. 2002. Holoprosencephaly in children: diffusion tensor MR imaging of white matter tracts of the brainstem—initial experience. Radiology 223:645–651.

Arnold SE, Talbot K, Hahn CG. 2005. Neurodevelopment, neuroplasticity, and new genes for schizophrenia. Prog Brain Res 147:319–345.

Bagnard D, Lohrum M, Uziel D, Puschel AW, Bolz J. 1998. Semaphorins act as attractive and repulsive guidance signals during the development of cortical projections. Development 125:5043–5053.

Barbas H, Pandya DN. 1984. Topography of commissural fibers of the prefrontal cortex in the rhesus monkey. Exp Brain Res 55:187–191.

Basser PJ, Pajevic S, Pierpaoli C, Duda J, Aldroubi A. 2000. In vivo fiber tractography using DT-MRI data. Magn Reson Med 44:625–632.

Bernasconi A, Bernasconi N, Lassonde M, Toussaint PJ, Meyer E, Reutens DC, Gotman J, Andermann F, Villemure JG. 2000. Sensorimotor organization in patients who have undergone hemispherectomy: a study with (15)O-water PET and somatosensory evoked potentials. Neuroreport 28:3085–3090.

Blitz DM, Foster KA, Regehr WG. 2004. Short-term synaptic plasticity: a comparison of two synapses. Nat Rev Neurosci 5:630–640.

Cipolloni PB, Pandya DN. 1985. Topography and trajectories of commissural fibers of the superior temporal region in the rhesus monkey. Exp Brain Res 57:381–389.

Clarke S, Kraftsik R, Van der Loos H, Innocenti GM. 1989. Forms and measures of adult and developing human corpus callosum: is there sexual dimorphism? J Comp Neurol 280:213–230.

Clowry GJ, Davies BM, Upile NS, Gibson CL, Bradley PM. 2004. Spinal cord plasticity in response to unilateral inhibition of the rat motor cortex during development: changes to gene expression, muscle afferents and the ipsilateral corticospinal projection. Eur J Neurosci 20:2555–2566.

Declaration of Helsinki. 2000. World medical association declaration of Helsinki: ethical principles for medical research involving human subjects. JAMA 284:3043–3045.

de Lacoste MC, Kirkpatrick JB, Ross ED. 1985. Topography of the human corpus callosum. J Neuropathol Exp Neurol 44:578–591.

Elbert T, Sterr A, Rockstroh B, Pantev C, Muller MM, Taub E. 2002. Expansion of the tonotopic area in the auditory cortex of the blind. J Neurosci 22:9941–9944.

Feller MB, Scanziani M. 2005. A precritical period plasticity in visual cortex. Curr Opin Neurobiol 15:94–100.

Froemke RC, Poo MM, Dan Y. 2005. Spike-timing-dependent synaptic plasticity depends on dendritic location. Nature 434:221–225.

Hedin-Pereira C, Lent R, Jhaveri S. 1999. Morphogenesis of callosal axons in hamsters. Cereb Cortex 9:50–64

Hori A, Stan AC. 2004. Supracallosal longitudinal fiber bundle: heterotopic cingulum, dorsal fornix or Probst bundle? Neuropathology 24:56–59.

Hu Z, Yue X, Shi G, Yue Y, Crockett DP, Blair-Flynn J, Reuhl K, Tessarolo L, Zhou R. 2003. Corpus callosum deficiency in transgenic mice expressing a truncated Ephrin-A receptor. J Neurosci 23:10963–10970.

Huang H, Zhang J, Van Zijl PCM, Mori S. 2004. Analysis of noise effects on DTI-based tractography using the brute-force and multi-ROI approach. Magn Reson Med 52:559–565.

Innocenti GM, Clarke S. 1984. The organization of immature callosal connections. J Comp Neurol 230:287–309.

Innocenti GM, Price DJ. 2005. Exuberance in the development of cortical networks. Nat Rev Neurosci 6:955–965.
Kennard MA. 1942. Cortical reorganization of motor function: studies on a series of monkeys of various ages from infancy to maturity. Arch Neurol Psychiatry 48:227–240.
Keshavan MS, Diwadkar DA, DeBellis M, Dick E, Kotwal R, Rosenberg DR, Sweeney JA, Minshew N, Pettegrew JW. 2002. Development of the corpus callosum in childhood, adolescence and early adulthood. Life Sci 70:1909–1922.
Kier EL, Truwit CL. 1996. The normal and abnormal genu of the corpus callosum: an evolutionary, embryologic, anatomic, and MR analysis. AJNR (Am J Neuroradiol) 17:1631–1641.
Kier EL, Truwit CL. 1997. The lamina rostralis: modification of concepts concerning the anatomy, embryology, and MR appearance of the rostrum of the corpus callosum. AJNR (Am J Neuroradiol) 18: 715–722.
Koester SE, O'Leary DD. 1994. Axons of early generated neurons in cingulate cortex pioneer the corpus callosum. J Neurosci 14: 6608–6620.
Kuker W, Mayrhofer H, Mader I, Nagele T, Krageloh-Mann I. 2003. Malformations of the midline commissures: MRI findings in different forms of callosal dysgenesis. Eur Radiol 13:598–604.
Lassonde M, Sauerwein H, Chicoine AJ, Geoffroy G. 1991. Absence of disconnexion syndrome in callosal agenesis and early callosotomy: brain reorganization or lack of structural specificity during ontogeny? Neuropsychologia 29:481–495.
Lassonde M, Sauerwein H, McCabe N, Laurencelle L, Geoffroy G. 1988. Extent and limits of cerebral adjustment to early section or congenital absence of the corpus callosum. Behav Brain Res 30:165–181.
Lassonde MC, Sauerwein HC, Lepore F. 2003. Agenesis of the corpus callosum. In: Zaidel E, Iacoboni M, editors. The parallel brain. Cambridge, MA: MIT Press. p 357–369.
Lazar M, Alexander AL. 2003. An error analysis of white matter tractography methods: synthetic diffusion tensor field simulations. Neuroimage 20:1140–1153.
Lee SK, Ki DI, Kim DI, Kim DJ, Kim HD, Kim DS, Mori S. 2005. Diffusion-tensor MR imaging and fiber tractography: a new method of describing aberrant fiber connections in developmental CNS anomalies. Radiographics 25:53–65.
Lee SK, Mori S, Kim DJ, Kim SY, Kim DI. 2004. Diffusion tensor MR imaging visualizes the altered hemispheric fiber connection in callosal dysgenesis. AJNR (Am J Neuroradiol) 25:25–28.
Lent R. 1982. Neuroanatomical effects of neonatal transection of the corpus callosum in hamsters. J Comp Neurol 223:548–555.
Lent R. 1983. Cortico-cortical connections reorganize in hamsters after neonatal transection of the callosal bridge. Dev Brain Res 11: 137–142.
Lent R, Uziel D, Baudrimont M, Fallet C. 2005. Cellular and molecular tunnels surrounding the forebrain commissures of human fetuses. J Comp Neurol 483:375–382.
Lessard N, Lepore F, Villemagne J, Lassonde M. 2002. Sound localization in callosal agenesis and early callosotomy subjects: brain reorganization and/or compensatory strategies. Brain 125: 1039–1053.
Maffei A, Nelson SB, Turrigiano GG. 2004. Selective reconfiguration of layer 4 visual cortical circuitry by visual deprivation. Nat Neurosci 7:1353–1359.
Matsunami K, Kawashima T, Ueki S, Fujita M, Konishi T. 1994. Topography of commissural fibers in the corpus callosum of the cat: a study using WGA-HRP method. Neurosci Res 20:137–148.
Meyer BU, Röricht S, Niehaus L. 1998. Morphology of acallosal brains as assessed by MRI in six patients leading a normal life. J Neurol 245:106–110.
Meyer BU, Röricht S, Woiciechowsky C. 1998. Topography of fibers in the human corpus callosum mediating interhemispheric inhibition between the motor cortices. Ann Neurol 43:360–369.
Mori S, Crain BJ, Chacko VP, van Zijl PCM. 1999. Three-dimensional tracking of axonal projections in the brain by magnetic resonance imaging. Ann Neurol 45:265–269.
Mori S, van Zijl PC. 2002. Fiber tracking: principles and strategies—a technical review. NMR Biomed 15:468–480
Nakamura H, Kanaseki T. 1989. Topography of the corpus callosum in the cat. Brain Res 485:171–175.
Nordeen KW, Nordeen EJ. 2004. Synaptic and molecular mechanisms regulating plasticity during early learning. Ann N Y Acad Sci 1016: 416–437.
Olavarria J, Serra-Oller MM, Yee KT, Van Sluyters RC. 1988. Topography of interhemispheric connections in neocortex of mice with congenital deficiencies of the callosal commissure. J Comp Neurol 270:575–590.
Ozaki HS, Iwahashi K, Shimada M. 1989. Ipsilateral corticocortical projections of fibers which course within Probst's longitudinal bundle seen in the brains of mice with congenital absence of the corpus callosum: a study with the horseradish peroxidase technique. Brain Res 493:66–73.
Ozaki HS, Murakami TH, Toyoshima T, Shimada M. 1987. The fibers which leave the Probst longitudinal bundle seen in the brain of an acallosal mouse: a study with the horseradish peroxidase technique. Brain Res 400:239–246.
Ozaki HS, Shimada M. 1988. The fibers which course within the Probst's longitudinal bundle seen in the brain of a congenitally acallosal mouse: a study with the horseradish peroxidase technique. Brain Res 441:5–14.
Ozaki HS, Wahlsten D. 1993. Cortical axon trajectories and growth cone morphologies in fetuses of acallosal mouse strains. J Comp Neurol 336:595–604.
Ozaki HS, Wahlsten D. 1998. Timing and origin of the first cortical axons to project through the corpus callosum and the subsequent emergence of callosal projection cells in mouse. J Comp Neurol 400:197–206.
Pajevic S, Pierpaoli C. 1999. Color schemes to represent the orientation of anisotropic tissues from diffusion tensor data: application to white matter fiber tract mapping in the human brain. Magn Reson Med 42:526–540.
Pierpaoli C, Barnett A, Pajevic S, Chen R, Penix LR, Virta A, Basser P. 2001. Water diffusion changes in Wallerian degeneration and their dependence on white matter architecture. Neuroimage 13: 1174–1185
Polleux F, Giger RJ, Ginty DD, Kolodkin AL, Ghosh A. 1998. Patterning of cortical efferent projections by semaphorin-neuropilin interactions. Science 282:1904–1906
Probst M. 1901. Ueber den Bau des balkenlosen Grosshirns, sowie uber Mikrogirie und Heterotopie der grauen substanz. Arch Psychiatr Nervenkr 34:709–786.
Rakic P, Yakovlev PI. 1968. Development of the corpus callosum and the cavum septi in man. J Comp Neurol 132:45–72.
Rash BG, Richards LJ. 2001. A role for cingulate pioneering axons in the development of the corpus callosum. J Comp Neurol 434: 147–157
Reil JC. 1812. Mangel des mittleren und freyen Theils des Balkens im Menschengehirn. Arch Physiol 11:314–344.
Richards LJ. 2002. Axonal pathfinding mechanisms at the cortical midline and in the development of the corpus callosum. Braz J Med Biol Res 35:1431–1439.
Richards LJ, Plachez C, Ren T. 2004. Mechanisms regulating the development of the corpus callosum and its agenesis in mouse and human. Clin Genet 66:276–289.
Rockland KS, Pandya DN. 1986. Topography of occipital lobe commissural connections in the rhesus monkey. Brain Res 365:174–178.
Sauerwein HC, Lassonde M. 1994. Cognitive and sensory-motor functioning in the absence of the corpus callosum: neuropsychological studies in callosal agenesis and callosotomized patients. Behav Brain Res 64:229–240.
Schneider GE. 1979. Is it really better to have your brain lesion early? A revision of the "Kennard principle". Neuropsychologia 17:557–583.
Serafini T, Colamarino SA, Leonardo ED, Wang H, Beddington R, Skarnes WC, Tessier-Lavigne M. 1996. Netrin-1 is required for commissural axon guidance in the developing vertebrate nervous system. Cell 87:1001–1004.

Shrager RI, Basser PJ. 1998. Anisotropically weighted MRI. Magn Reson Med 40:160–165.
Shu T, Richards LJ. 2001. Cortical axon guidance by the glial wedge during the development of the corpus callosum. J Neurosci 21:2749–2758.
Sperry RW. 1970. Perception in the absence of the neocortical commissures. In: Association for Research of Nervous and Mental Disease, Percept Disor 48:123–138.
Tailby C, Wright LL, Metha AB, Calford MB. 2005. Activity-dependent maintenance and growth of dendrites in adult cortex. Proc Natl Acad Sci USA 102:4631–4636.
Thompson PM, Giedd JN, Woods RP, MacDonald D, Evans AC, Toga AW. 2000. Growth patterns in the developing brain detected by using continuum mechanical tensor maps. Nature 404:190–193.
Uziel D, Garcez PP, Henrique NP, Furtado DA, Lent R. 2003. Transiently bifurcated callosal axons during cortical development in mice. Soc Neurosci Abstr 35.10.
Villablanca JR, Hovda DA. 2000. Developmental neuroplasticity in a model of cerebral hemispherectomy and stroke. Neuroscience 95:625–637.
Xu D, Mori S, Solaiyappan M, van Zijl PC, Davatzikos C. 2002. A framework for callosal fiber distribution analysis. Neuroimage 17:1131–1143.
Xue R, van Zijl PCM, Crain BJ, Solaiyappan M, Mori S. 1999. In vivo three dimensional reconstruction of rat brain axonal projections by diffusion tensor imaging. Magn Reson Med 42:1123–1127.

Livros Grátis

(http://www.livrosgratis.com.br)

Milhares de Livros para Download:

Baixar livros de Literatura
Baixar livros de Literatura de Cordel
Baixar livros de Literatura Infantil
Baixar livros de Matemática
Baixar livros de Medicina
Baixar livros de Medicina Veterinária
Baixar livros de Meio Ambiente
Baixar livros de Meteorologia
Baixar Monografias e TCC
Baixar livros Multidisciplinar
Baixar livros de Música
Baixar livros de Psicologia
Baixar livros de Química
Baixar livros de Saúde Coletiva
Baixar livros de Serviço Social
Baixar livros de Sociologia
Baixar livros de Teologia
Baixar livros de Trabalho
Baixar livros de Turismo